Universidade do Minho
Escola de Engenharia

José do Egipto Ferreira Antunes

Hair Modulation and Transdermal Delivery: Optimization through Molecular Dynamics simulations

dezembro de 2018

FCT
Fundação para a Ciência e a Tecnologia
MINISTÉRIO DA EDUCAÇÃO E CIÊNCIA

POPH QUALIFICAR É CRESCER.
QUADRO DE REFERÊNCIA ESTRATÉGICO NACIONAL PORTUGAL 2007.2013
Governo da República Portuguesa
UNIÃO EUROPEIA Fundo Social Europeu

José do Egipto Ferreira Antunes Hair Modulation and Transdermal Delivery: Optimization through Molecular Dynamics simulations UMinho|2018

Universidade do Minho
Escola de Engenharia

José do Egipto Ferreira Antunes

Hair Modulation and Transdermal Delivery: Optimization through Molecular Dynamics simulations

Tese de Doutoramento em Engenharia Química e Biológica

Trabalho efetuado sob a orientação do
Professor Doutor Artur Cavaco-Paulo

dezembro de 2018

DECLARAÇÃO

Nome:
José do Egipto Ferreira Antunes

Endereço eletrónico egipto@ceb.uminho.pt

Título da Tese de Doutoramento:
Hair Modulation and Transdermal Delivery: Optimization through Molecular Dynamics simulations

Orientadores:
Professor Doutor Artur Cavaco-Paulo

Ano de conclusão: 2018

Designação do Doutoramento:
Programa Doutoral em Engenharia Química e Biológica

Universidade do Minho, 17/12/2018

Assinatura: José do Egipto Ferreira Antunes

STATEMENT OF INTEGRITY

I hereby declare having conducted my thesis with integrity. I confirm that I have not used plagiarism or any form of falsification of results in the process of the thesis elaboration. I further declare that I have fully acknowledged the Code of Ethical Conduct of the University of Minho.

University of Minho, 17/12/2018

Full name: José do Egipto Ferreira Antunes

Signature: José do Egipto Ferreira Antunes

"Science is a way of
thinking much more than
it is a body of knowledge"
Carl Sagan

The research presented in this document was done within the Bioprocess and Bionanotechnology Research Group, Centre of Biological Engineering, University of Minho, Braga, Portugal. Part of this work was funded by the Portuguese Foundation for Science and Technology (FCT) through the Ph.D. grant SFRH/BD/122952/2016.

Agradecimentos

Esta tese, como qualquer outra, nunca poderia ser concluída sem a ajuda de muitos intervenientes, e cabe-me nesta secção agradecer aqueles que mais contribuíram para a sua realização.

Costumo ser contido mas sincero, e tendo isto em consideração gostaria de começar por agradecer ao meu orientador, o Professor Doutor Artur Cavaco-Paulo pelas oportunidades que me tem dado na ciência, por ter acreditado no meu potencial e me ter acolhido no seu grupo de trabalho.

Agradeço também ao Doutor Nuno Azoia, que foi também meu mentor em grande parte desta tese, bem como na minha introdução ao mundo da química computacional.

Agradeço a todo o grupo de investigação Bioprocessos e Bionanotecnologia, a todos os que ainda fazem parte do mesmo, bem como a todos com quem me cruzei. Agradeço em especial à Célia Cruz por todo o trabalho experimental da área do cabelo, ao Vadim Volkov pelo seu companheirismo e ajuda técnica, à Tarsila Castro pela entreajuda na área computacional e pelas revisões técnicas, bem como ao Bruno Fernandes e à Vanessa Ferreira pela companhia e boa disposição ao longo dos anos.

Gostaria de agradecer também a todo o pessoal da Universidade do Minho que tenha de uma forma ou de outra me ajudado, bem como à própria instituição por me fornecer em conjunto com o meu orientador todas as condições técnicas necessárias à realização desta tese. Agradeço ao Departamento de Informática, mais precisamente ao seu centro computacional pelo uso do supercomputador "SEARCH".

Agradeço também à FCT pelo financiamento concedido a parte desta tese.

Não poderia deixar de fora o meu agradecimento especial aos meus amigos pessoais, e muito menos á minha família, em especial aos meus pais, que muito lutaram para me providenciar uma vida digna, com elevados valores morais e sem descurar a cultura e educação, sem a sua força e seu caracter nunca estaria onde estou hoje.

Por fim um agradecimento especial à Telma Silva, pelo seu amor, dedicação e compreensão, mesmo em momentos mais difíceis em que cedia ao *stress* e cansaço. É mais um pilar na minha vida, sempre presente para me apoiar.

A todos um sincero e sentido muito obrigado!

Abstract

Hair Modulation and Transdermal Delivery: Optimization through Molecular Dynamics simulations

Hair is a symbol of beauty and a key element in the self-image of humans. Much time, effort and money are applied in the hair care, and the aggressive cosmetic market strongly invests in the research and development of new hair products with several claims.

Nowadays much is known about the hair, from its morphological characteristics, to the genetics behind its stages of grow and rest, however many aspects also remains unknown. The precise determination of the keratin intermediary filaments arrangement in the hair structure is one important issue needing more study. A better understanding of this assembling and the way how it is affected by external elements can greatly improve the research in the hair field, and the developing of new products and applications.

The transdermal delivery of drugs is an exciting area, since avoids several disadvantages of oral, pulmonary and intravenous routes. However the skin is an impermeable barrier, challenging the delivery of the drug by this route. Several new systems/formulations and techniques have been studied to increase the rate and the number of drugs delivered topically. The stratum corneum is the outermost layer of the skin, and is pointed as the major limiting to its translocation by the drugs. So, this skin layer is actually target of intense research, but seems not enough to the establishment of widely transdermal delivery systems.

Molecular dynamics simulations, with its inherent advantages and with the ability to study, at the atomic level, the mechanisms behind the keratin assembling in the hair, as well the interaction between skin lipids and molecules in transdermal delivery, can quickly boost the knowledge in these areas.

This project aims to study the impact in the hair of the interaction between compounds or formulations with its fiber contain to modulate the hair, and aims to optimize the transdermal drug delivery, using molecular dynamics simulations. The development of robust molecular dynamics models of these phenomena to allow the proposed studies is the key of this thesis.

Resumo

Modulação Capilar e Entrega Transdérmica: Otimização através de Simulações de Dinâmica Molecular

O cabelo é um símbolo de beleza e um elemento chave na imagem dos humanos. Muito tempo, esforço e dinheiro são despendidos no tratamento capilar, e o mercado agressivo da cosmética investe fortemente na pesquisa e desenvolvimento de novos produtos para o cabelo com várias reivindicações.

Nos dias de hoje muito se sabe sobre o cabelo, desde as suas características morfológicas à genética por de trás das suas fases de crescimento e estagnação, no entanto muitos aspetos continuam desconhecidos. A determinação precisa da estruturação dos filamentos intermediários de queratina no cabelo é exemplo de um tema que necessita mais estudo. Uma melhor compreensão desta estruturação e de como ela é afetada por elementos externos pode melhorar significativamente a investigação na área capilar e o desenvolvimento de novos produtos e aplicações.

A entrega transdérmica de drogas é uma área interessante, uma vez que evita muitas desvantagens da entrega de drogas por via oral, pulmonar e intravenosa. A pele é no entanto uma barreira impermeável, desafiando a entrega de drogas por esta rota. Vários sistemas, formulações e técnicas têm sido estudadas para aumentar a taxa e o número de drogas entregues por via da pele. A camada mais externa da pele, o estrato córneo, é apontado como o maior responsável pelo seu limitado atravessamento por drogas. Assim essa camada é alvo de intenso estudo, embora não pareça ser suficiente para o aparecimento de sistemas de amplo espectro para entrega transdérmica.

As simulações por dinâmica molecular podem rapidamente aumentar o conhecimento nestas áreas, devido às suas vantagens inerentes e à possibilidade do estudo a nível atómico de mecanismos responsáveis pela estruturação do cabelo, bem como do estudo da interação de moléculas com os lípidos da pele.

Esta tese tem como objetivos o estudo da interação do cabelo com compostos ou formulações para modulação capilar, bem como otimizar a entrega transdérmica de drogas, usando em ambos os casos simulações de dinâmica molecular. O desenvolvimento de modelos robustos de dinâmica molecular desses processos, para permitir os estudos propostos é o fator chave desta tese.

Index

List of abbreviations

BIDOUB model: model of lipid matrix with four adjacent layers

CER: ceramide

CER EOS: also named ceramide 1, is a combination of a ester-linked ω-hydroxy acid with a Sphingosine

CER NP: also named ceramide 3, is a combination of Nonhydroxy fatty acid and Phytosphingosine

CER NS: also named ceramide 2, is a combination of Nonhydroxy fatty acid and Sphingosine

CG: coarse-grained resolution

CHOL: cholesterol

CHOLO: cholesterol-oleate

CHOLS: cholesterol-sulfate

DOUB model: model of lipid matrix with two adjacent layers

DMSO: dimethylsulfoxide

FFA: free faty-acid

FG: fine-grained resolution

HB: Hydrogen bonds

IFS: intermediate filaments

LM: lipid matrix

Old LM: old model of lipid matrix

MD: molecular dynamics

NPT: ensemble with number of particles, pressure and temperature constant

NRD: Nile-Red

NVT: ensemble with number of particles, volume and temperature constant

PLA: polylactic acid

PLX: poloxamer

PMF: potential of mean force

PT: keratin protofibril

RDF: radial distribution function

RG: the radius of gyration

RMSD: root mean square deviation

SAS: solvent accessible surface area

SC: stratum corneum

SPD: pulmonary associated surfactant protein D

SQ: squalene

TD: transdermal delivery

TG: triglycerides

WE: wax esters

YM: Young's Modulus

List of figures

Chapter I

Chapter II

Chapter III

Chapter IV

List of tables

Chapter I

Chapter IV

List of equations

Chapter II

Thesis Motivation and Outline

The hair and the skin are elements of the utmost importance for humans. Their role in defining our self-image and acting as barriers to the external environment is obvious. However the importance of these biological systems is broad, they protect us to environmental aggressions, they provide clues about our health, they help in the body homeostasis regulation and they allow the sensing of the world. These shared functions show that although structurally different the hair and the skin have much in common. Even structurally the hair and skin share properties, such as having dead cells filled with keratin proteins.

In this thesis we wanted to develop computational models, to be used in molecular dynamics simulations, which correctly mimic the behavior of hair and skin structures at molecular level. The two structures were choose because they share the lack of consensus about its structure at molecular level, and because many applied research is performed with these subjects for cosmetic or health purposes, existing a strong experimental background in this field in our research group. So the results of this thesis can improve fundamental and applied research in these areas, helping in the understanding of the molecular structure of these elements, as well improving compounds to be applied in the hair or skin with ability to modulate their properties or to drug delivery.

This document is divided in four chapters which are based in four research articles, the first two already published and the others in submission process.

In **Chapter I** is described the molecular dynamics model development of a truncated protofibril that is a structure of the hair fiber. The results of interaction simulations between

the model and alcoholic formulations correlated well with experimental assays with hair and the same formulations, and can explain the uptake increase of one peptide by the hair.

In the **Chapter II** is described the change of the resolution of the previous model and the conducting of mechanical tests simulations with the new model. The results of these simulations agree with laboratorial mechanical tests performed with hair strands and show the improvement of hair mechanical properties by one peptide.

In the **Chapter III** we did an extensive review of the skin barrier studies which apply molecular dynamics simulations. The models and results of many works were discussed as well the power, the limitations and the future perspectives of this computational methodology use in the skin barrier study.

In the **Chapter V** we developed a molecular dynamics model of stratum corneum lipid matrix, with unusual configuration of ceramides, according the more recent studies about the molecular structure of the stratum corneum. A model of sebum oil was also developed and several interaction simulations, as well steered simulations, were performed to reveal some insights about the skin barrier properties.

Lastly, in the **Final Remarks**, we briefly discuss the thesis outcomes, if the objectives were achieved, the possible improvements and the future perspectives.

Chapter I

Hair Keratin Molecular Dynamics Studies.

Development of hair keratin model and study of formulations impact in the hair fiber.

This chapter is based on the following publication:

Egipto Antunes, Célia F. Cruz, Nuno Azoia, Artur Cavaco-Paulo. The effects of solvent composition on the affinity of a peptide towards hair keratin: experimental and molecular dynamics data. *RSC Advances*, 2015, 5, 12365–12371.

DOI: 10.1039/C4RA13901A

Chapter I abstract:

The study of the interaction between hair filaments and formulations or peptides is of utmost importance in fields like cosmetic research. Keratin intermediate filaments structure is not fully described, limiting the molecular dynamics (MD) studies in this field although its high potential to improve the area. We developed a computational model of a truncated protofibril, simulated its behavior in alcoholic based formulations and with one peptide. The simulations showed a strong interaction between the benzyl alcohol molecules of the formulations and the model, leading to the disorganization of the keratin chains, which regress with the removal of the alcohol molecules. This behavior can explain the increase of peptide uptake in hair shafts evidenced in fluorescence microscopy pictures. The model developed is valid to computationally reproduce the interaction between hair and alcoholic formulations and provide a robust base for new MD studies about hair properties. It is shown that the MD simulations can improve hair cosmetic research, improving the uptake of a compound of interest.

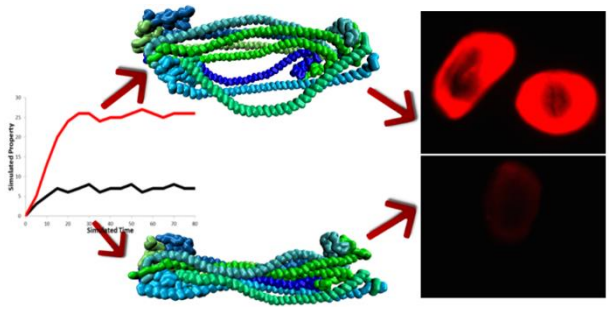

Figure I: Graphical abstract of the Chapter I.

Introduction

Hair is a proteinaceous biomaterial with a complex structure, serving to protect the body against environmental factors such as cold or heat, the sunlight and wetness.

The hair fiber is usually divided into three zones: the cuticle (outermost zone, Figure 1G), the cortex (surrounded by the cuticle), and in the center zone of thicker hairs, the medulla (Figure 1F). The cuticle corresponds to a stratified layer of thin and flat overlapping cells, like the fish scales, and acts as a chemical and physical barrier, protecting the inner zones. The medulla is constituted by hollow cells with amorphous material and air spaces.[1]

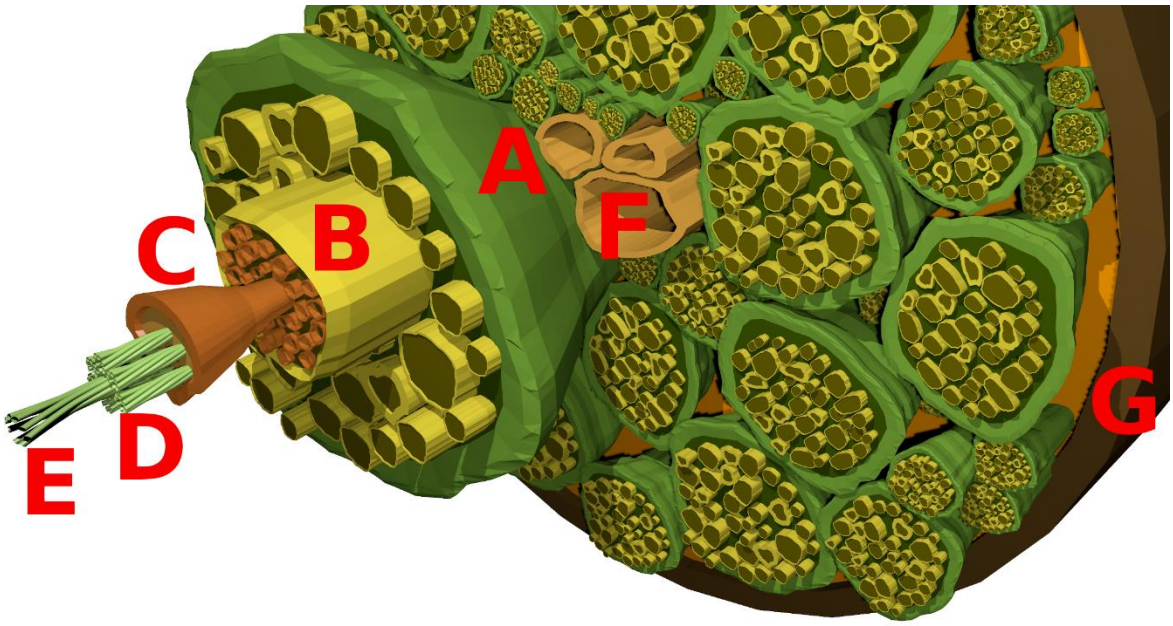

Figure 1: Schematic 3D representation of one cut hair shaft. (A): Cell membrane complex; (B): macrofibril; (C): matrix; (D): microfibrils or intermediate filaments; (E): protofibril; (F): hollow medulla cells; (G): hair cuticle. The representation is not at scale.

The cortex has long, cylindrical assembled cortical cells surrounded by the cell membrane complex (Figure 1A). Macrofibrils (Figure 1B) and intermacrofibrilar material compose the cortical cells. The macrofibrils can be further divided into microfibrils (Figure

1D) and a surrounding matrix (Figure 1C) composed by associated proteins, cytoplasmatic and nuclear remains of keratinocytes. The microfibrils are also known as intermediate filaments, and are composed by 4 protofibrils (Figure 1E), which have 2 protofilaments, each one with two dimers of α-helix coiled-coil keratins. The Figure 1 illustrates the hierarchical structure of the hair fiber.

In the intermediate filaments assembly, the α-helix coiled-coil dimer of keratin is made with one keratin of type I (acidic keratins) and one of type II (basic or neutral keratins), forming a heterodimer, since this assembly is much more stable than a homodimer.[2] Each α-keratin has four coiled-coil domains (denominated as 1A, 1B, 2A and 2B), three linker domains (L1, L12, and L2), and the head and tail terminal domains. This structure is shared with all intermediate filaments such as vimentin, desmin and lamins, and is represented in Figure 2.

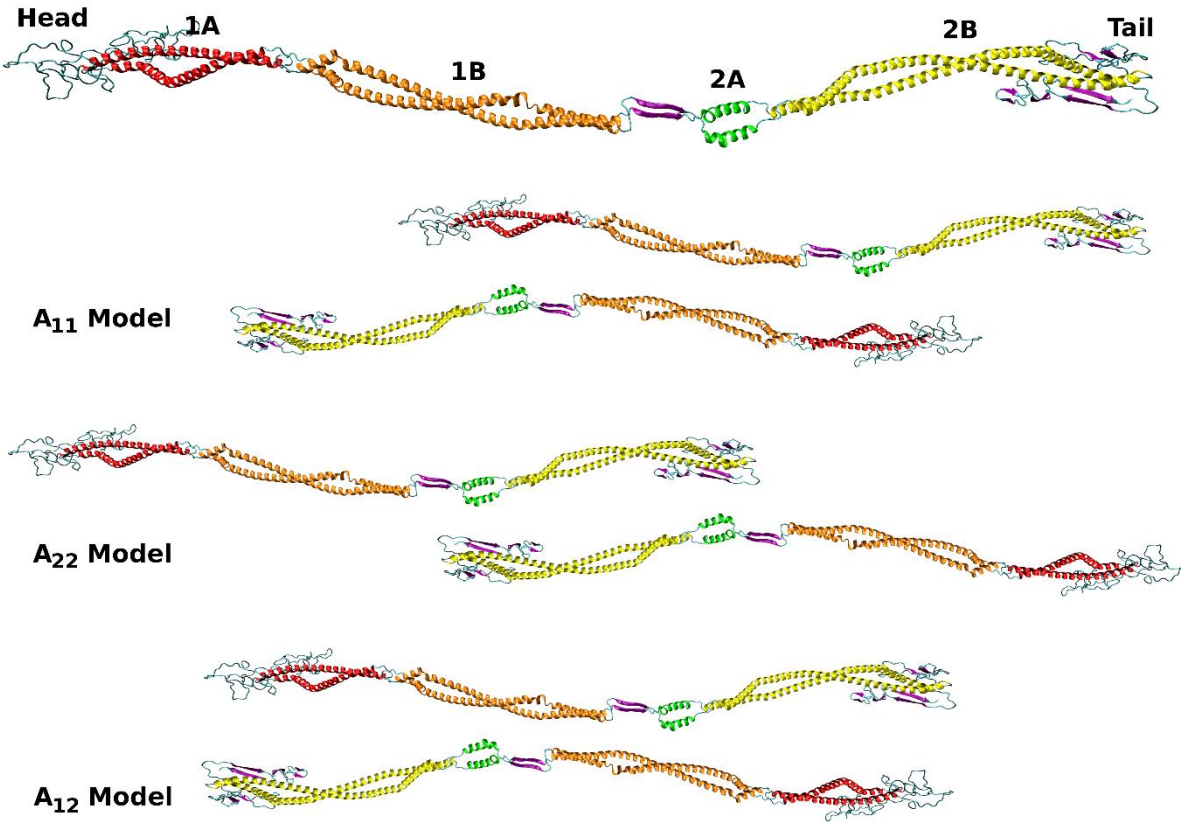

Figure 2: **Top:** Representation of one vimentin intermediate filament dimer, with its domains discriminated. **Bottom:** Representation of three models of intermediary filaments dimers pairing. The pictures were rendered using the structure obtained by Zhao Qin and colleagues.[3]

The assembly of the keratin dimer is made by pairing each domain of one α-keratin with the same domain of the adjacent α-keratin (see Figure 2 Top), while the assembly of one protofilament (two dimers) is anti-parallel. It is not completely clear how the protofilament assembly is made, and there are three main modes of pairing described, namely the A_{11}, A_{12} and the A_{22} (see Figure 2).[4] The A_{11} mode is defined by the antiparallel overlap of 1B segments, the A_{22} mode by the antiparallel overlap of 2B segments and the A_{12} mode by the antiparallel overlap of intermediate filaments dimers. The higher assemblies in octamers (protofibrils), micro and macrofibrils of the IFs, are not fully characterized, at the molecular level, mainly in the hair IFs. The few literature about this thematic, incised more in the vimentin IFs due the existence of crystallographic models for these filaments, or in the skin keratins due to the skin diseases that affect many humans,[5-8] however these filaments are different from hair IFs.

There are 54 elements of the human keratin family (skin and hair keratins), 28 of type I and 26 of type II. It was found that keratin 31, 33a, 34, 38b, 81, 85 and 86 are the most abundant keratins in the hair[9] and, for example, Keratin 31 is mostly expressed in lower and mid cortex, while keratins 34 and 86 are mostly expressed in mid and upper cortex.[10-12] It seems that the pairing of the protofilament is not predefined in terms of the keratins elements, allowing competition between the keratins and different pairs can be found.[12]

Molecular dynamics (MD) has been applied with success in the study of complex biomaterials, providing unique and detailed molecular information inaccessible by others techniques. The systems studied by MD are increasing in number, diversity and complexity, from single proteins in water,[13] to cell membranes[14,15] or even stratum corneum.[16-18]

Despite all potential of MD simulations, this technique has only been applied in the study of hair in a few works.[19-22] The MD has a great potential to boost some aspects in the hair products development research, speeding up the process while saving resources and money. Previously our group studied the affinity between fragments of pulmonary associated surfactant protein D (SPD) and α-keratin, in formulations containing benzyl alcohol, propylene glycol and ethanol.[19] SPD is a surfactant protein synthetized in the lung and due to the ability of these kind of peptides to interact with hair lipids they have been study as helper agents in the recovery of damaged hair.[19,23,24] Here we are extending the scope of this

previous work by building a bigger computational model of a hair and changing formulations composition. The new model describe a truncated protofibril (8 keratins), assembling the 2B domains of keratin 34 and keratin 86, as a simplified model of one hair shaft. This model was subject to several MD simulations with different formulations. The SPD fragment chosen was the one with less affinity to keratin in the previous work, to facilitate the evaluation of differences in peptide affinity due to the formulations. The simulations results were compared with experimental tests performed with real hair. We intent to show that the affinity of peptides can be increased by formulations composition and that this property, together with the stronger interactions of the formulations with the hair, can be assessed by MD simulations.

Materials and methods

All simulations were performed with the GROMACS 4.0.7[25] software package, using the MARTINI[26] force field. The MARTINI force-field, being a coarse-grained force-field, has a possible drawback when dealing with proteins, namely the rigidity of its secondary structure, thus not allowing the modeling of secondary structure changes. However, there are many examples of studies of proteinaceous systems with this force field with great success, since the secondary structure rigidity only limits studies, focusing on properties or phenomena, strongly dependent on the protein structure.[27–29]

In all simulations the procedure was the same, namely we begun with the energy minimization of the systems for 500 steps with steepest descent method. Then the systems were subject to a short simulation (3 ns), in the canonical ensemble or NVT (number of molecules, volume and temperature constants), to relax the structures and generate velocities according to a temperature of 300 K. The production simulations were performed with the isothermal–isobaric ensemble or NPT (number of molecules, pressure and temperature constants), with simulation times ranging from 65 to 510 ns. Berendsen coupling was used to maintain the temperature at 300 K with a relaxation time of 0.7 ps, and also a Berendsen coupling to maintain the pressure at 1 atm, with a time constant of 3 ps and a compressibility

of 3x10-5 bar-1.[30] The simulation box was dodecahedric, the integration time step of 30 fs and the Lincs algorithm was used as bond constrainer.[31] To the nonbonded interactions, cut offs and shifts at 12 Å were applied, with a decrease of the van der Waals forces between 9 and 12 Å, and a decrease of electrostatic forces throughout the whole interaction distance.

Keratin protofibril model building

The majority of the hair weight corresponds to the keratin fiber, but a complete macrofibril, or even the smaller microfibril reach sizes far beyond the usual system sizes simulated in MD. However the hair has a hierarchical structure, in which smaller units will assemble into bigger structures and these assemble again into even bigger structures, giving the macroscopic properties of the material.[21,32] Considering this we built a computational model of a truncated protofibril, assembling 8 truncated α-keratins. The truncated zone corresponds to α-keratins 2B domain from the L2 link to C tail, and the assembly of the 4 dimers is based in the A_{22} model, with dimer to dimer anti-parallel pairing. Pymol software[33] was used to create the 3D all-atom structure of one keratin 34 (type I) and of one keratin 86 (type II), using its peptide sequence from UniProt database. The choice of the keratin chains was based in the fact that both belong to the group of the most expressed keratins in hair, and both are present on the hair cortex, increasing the probability of this pair be representative of hair cortex content. The A_{22} model was chosen because there is not a consensus about the model that better describe the two dimer pairing, and this model allows the end to end pairing of the different chains turning the full structure more compact. These structures were converted to coarse-grained models, and were duplicated and joined together to build the dimer, the tetramer and finally the octamer. The resulting model of one truncated protofibril of hair keratin was chosen taking into account the physical assembling properties presented in MD simulations, comparing with the existing studies about hair keratins and intermediate filaments assembling.[3,6,34] A more detailed description of the full process is presented in Chapter I attachments.

Interactions Simulations

The hair model thus obtained was then used in the simulations of the interaction of several formulations with the hair fiber. The formulations tested were based on the one used in the previous work of our group,[19] and are composed by ethanol, benzyl alcohol, propylene

glycol and water. The original formulation (OF) had a composition (v/v) of 10, 0.5, 1.5 and 88, respectively. The computational formulations used in this work do not include explicit propylene glycol due to limitations with its parametrization to the MARTINI force field. In this force field four water molecules are modeled by one polar bead, P4 type, and the parametrization of the propylene glycol molecule would lead to one polar bead similar to the four water model. The ethanol parametrization is available, together with other solvents in the MARTINI website (http://md.chem.rug.nl/cgmartini/), and this molecule is modeled by a P1 bead. For benzyl alcohol there is no parametrization available, so we modeled the molecule, based on the available benzene parametrization, as three SC5 beads, corresponding to the benzene like ring, and one P1 bead corresponding to the OH alcohol group. More details about this alcohol parametrization are described in Chapter I attachments.

The concentration of benzyl alcohol ranged between 0.5 and 3 % (v/v), since the benzyl alcohol solubility limit in water is 3.5 g/100 mL at 20 ºC and 4.29 g/mL at 25 ºC, and solutions with 4 % of this alcohol present some turbidity (see Figures 9 and 10 in Chapter I attachments).

The behavior of the hair model in the formulations was simulated for 510 ns, with the same protocol described above. After the simulations the systems evolution and the final structure of the protofibrils were evaluated either visually or statistically, measuring properties such as the radial distribution function (RDF), the root mean square deviation (RMSD), the radius of gyration (RG) and the solvent accessible surface area (SAS).

Besides the experimental tests, described in the next section, we also assess the effect of BE3, and B3 formulations in the interaction of one SPD fragment (QAAFSQ) with the hair through MD. This peptide corresponds to a small fragment of a glycoprotein synthesized by alveolar type II cells and by nonciliated bronchiolar epithelial cells[35] and was chosen because the previous work had demonstrated low affinity with keratin dimer.[19] Thus it is expected that the increase of affinity of this peptide with hair will be easier to demonstrate. We create one system for each formulation, with 4 replicas each, containing the hair model and 6 peptides. The behavior of the systems was simulated for 510 ns, and in the end the formulations were removed from the simulation box, water was added and the behavior of the aqueous systems was simulated for another 510 ns.

We also performed some preparatory simulations of the protofibril and the BE3 formulation using the gromos 43A1-S3 force field[36] with the same methodology of the coarse grained simulations This united atom force field provides atomic detail to the system however turns the system huge and more computing demanding. The results of these simulations were similar to the coarse grained simulations (see Chapter I attachments, Figure 11), but we only obtained computing performances of 0.4 ns/24 h against 50 ns/24 h in the coarse grained simulations. Once the lack of atomic detail seems do not affect the properties studied in the coarse grained simulations (the results of united atoms and coarse grained simulations are similar), and these simulations are much less computing demanding (allowing simulate longer time scales), we advance in the work with only the coarse grained simulations.

Experimental Tests

The interaction simulations were compared with experimental tests in human hair. Virgin Asian hair tresses were provided by International Hair Importers & Products (New York). Before use, the hair fibers were washed with running water and commercial shampoo. The hair tresses undergone eight cycles of bleaching because in our research group we intend to develop products to help in damaged hair recovering, and the bleaching although very common in hair styling is a very aggressive treatment to the hair. In each cycle, the hair was incubated with 10 % H_2O_2 (v/v) in Na_2CO_3/$NaHCO_3$ pH 9.0, for 1 hour at 50 ºC. Between cycles, the hair was washed with running water and commercial shampoo. Afterwards, the different formulations, whose compositions are described in Table 1 were tested in the bleached hair fibers.

In order to ease the analysis of the formulation effect, we use the engineered SPD fragment covalently linked, in the N-terminus, to the fluorescent dye 5(6)-carboxytetramethylrhodamine, succinimidyl ester (or 5-TAMRA). This peptide was synthesized by JPT Peptide Technologies GmbH (Berlin, Germany). After treatment, cross sections of the hair fibers samples were analyzed by fluorescence microscopy. The hair fibers were initially embedded in an epoxy resin and 15 mm transversal cuts were obtained using a microtome (Leitz). The samples were analyzed using an inverted fluorescence microscope Leica DMIL at a magnification 20x. The most representative images were chosen.

***Table 1*:** Description of the different aqueous formulations content used in this work. The percentage is relative to the solvent volume. BE: formulations containing benzyl alcohol and ethanol; B: formulations containing benzyl alcohol.

	Benzyl alcohol	**Ethanol**	**Propylene glycol**
Label	**Vol. (%)**		
OF	0.5	10	1.5
BE0.5	0.5	10	0
BE1	1	10	0
BE1.5	1.5	10	0
BE2	2	10	0
BE2.5	2.5	10	0
BE3	3	10	0
B1.5	1.5	0	0
B2	2	0	0
B2.5	2.5	0	0
B3	3	0	0

Results and Discussion

The non-existence of an entire crystallographic model of the keratin intermediate filaments is likely the major responsible for the low number of MD studies focusing the hair. To overcome this limitation, models of keratin and of the larger structures resulting of its assembling, such as dimers or protofilaments, can be designed and developed with more or less complexity and detail, and this approach was done on the few studies available.[19-22]

We joined 4 dimers of truncated keratin 34-keratin 86 chains (from the L2 link to C tail) and simulate its assembling in water, to build a truncated protofibril model (see Chapter I attachments for more information). The assembled keratinaceous octamer in the end of these simulations presented structural properties similar to the literature description of the intermediate filaments. Since the precise determination of protofibril atomic structure is out of the scope of this work, we move ahead for the interaction simulations.

The time evolution of the system BE4 is depicted in the Figure 3. It is clear the destabilization of the fiber, which is promoted by the formulation, since the initial protofibril structure is stable in water. It is also clear the tendency of the benzyl alcohol molecules to be located near the hair model, interacting with its keratins. Both effects are also evident in all other systems, with and without ethanol, and the destabilization seems to increase with the benzyl alcohol concentration (see Figure 7 and 8 in Chapter I attachments).

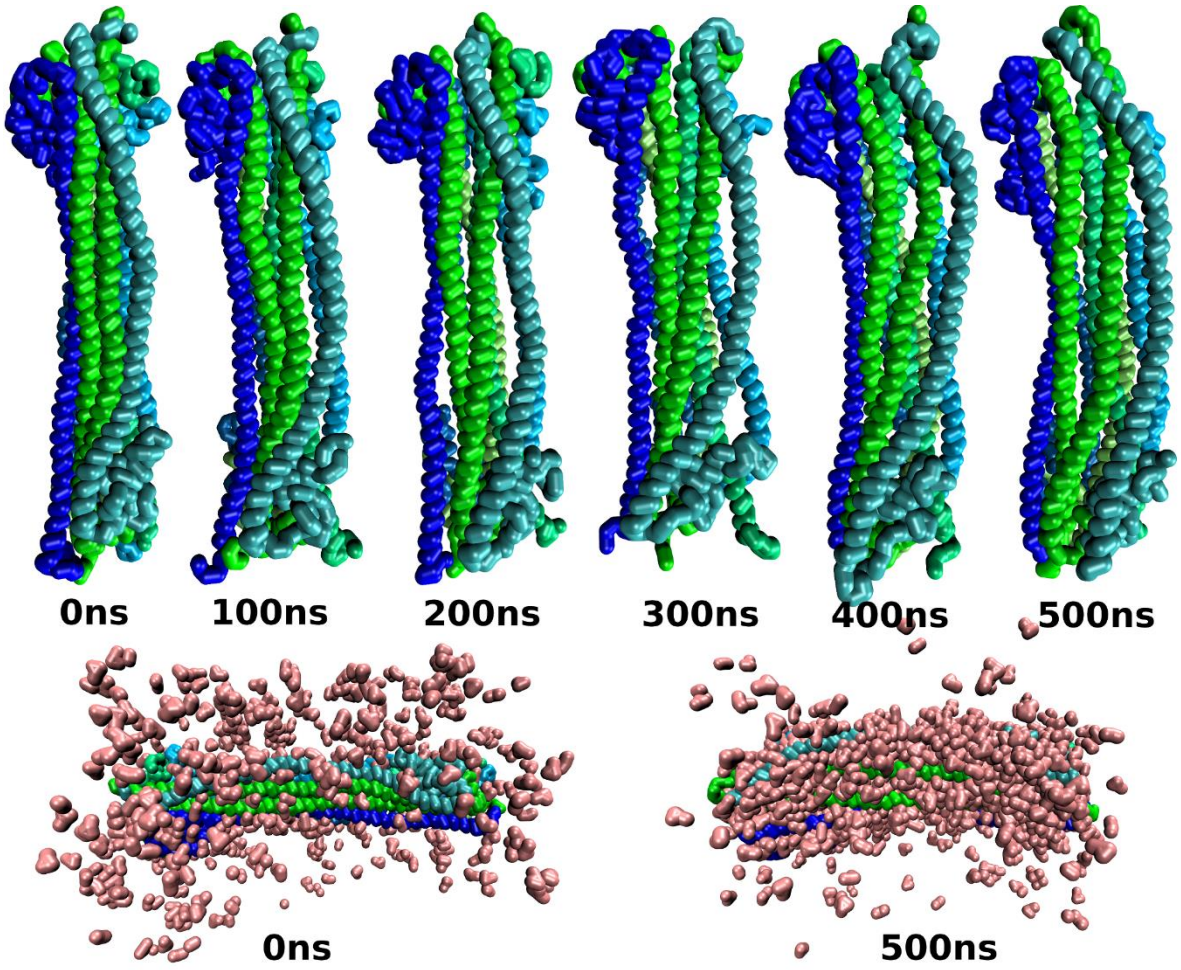

Figure 3: **Top:** Time evolution of the hair model (truncated protofibril) incubated in the formulation BE3. The solvent molecules were omitted for clarity. **Bottom:** initial and final states of the same system showing the tendency of benzyl alcohol molecules (pink).

The RDF analysis confirms the benzyl alcohol tendency to be located near the hair model. This analysis defines the ratio between the local and average concentration of the

target molecules, at a given distance. The value 1 indicates a random distribution of the molecules, and higher values indicate a tendency of the molecules to be located at such distance. The RDF analysis of systems BE2 and B2 is presented in the Figure 4. All the other systems presented similar RDF distribution pattern (in Chapter I attachments are present the RDF graphics for all formulations).

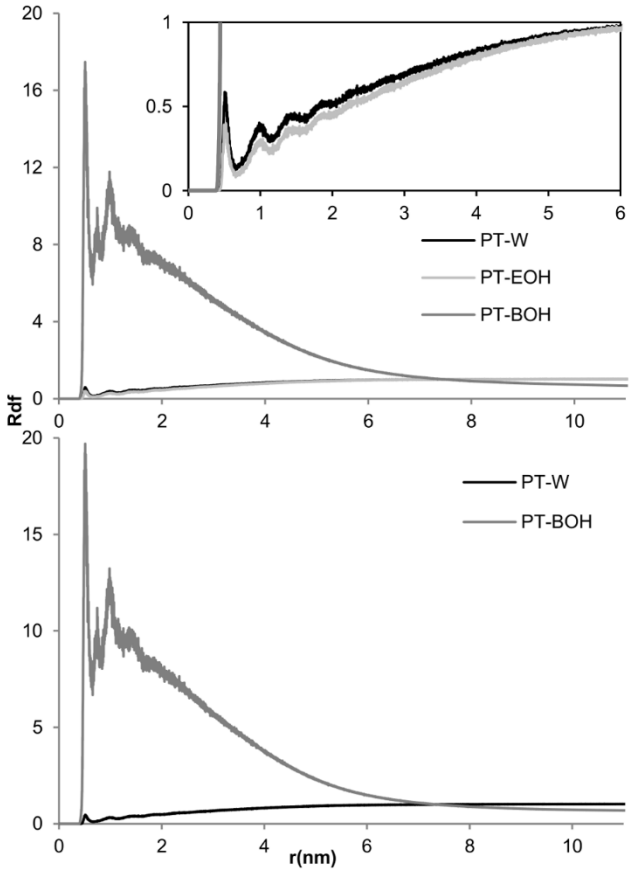

Figure 4: Graphical representation of the Radial Distribution Function (RDF) values of the systems with 2 % of benzyl alcohol, with (Top) and without (Bottom) ethanol molecules. PT-W, PT-EOH, PT-BOH: RDF values between the protofibril and water; ethanol and benzy alcohol, respectively.

It is clear that the RDFs values for benzyl alcohol molecules are very high at small distances, with some initial peaks corresponding to solvation layers, decreasing for bigger distances. For higher distances the RDF values are lower than 1, confirming that the benzyl alcohol molecules tend to be located near to the hair, as it was shown in Figure 3. The ethanol and water behavior are remarkably distinct to benzyl alcohol, while similar to each other; the RDFs values in both cases are lower than 1, increasing towards this value as the distance increase. The absence of ethanol does not change the RDF behavior of both water and benzyl alcohol.

The degree of destabilization observed in the simulations appears to increase with the concentration of the benzyl alcohol in the systems. However it is hard to visually evaluate the differences between systems with lower variation of benzyl alcohol concentration, problem that is overcome by the structural analysis of the hair model in the system. The RMSD indicates the spatial deviation of the hair structure from its starting

conformation. The average values from the final 110 ns of simulation in the different systems are presented in the Table 2.

The systems presented an overall increase of RMSD values with the increase of benzyl alcohol content, and there are no significant differences between the systems with or without ethanol. The RMSD values show a substantial spatial deviation of the protofibril initial structure, which seems to be linked to the benzyl alcohol concentration. However the evaluation of RMSD values cannot be directly linked to the destabilization observed in the simulations because movements like torsions, rotations, and stretching also contribute to the RMSD values but do not lead to the lateral dissociation observed in the simulations.

Table 2: Root Mean Square Deviation (RMSD) average values of the last 110 ns of each simulation and the respectively standard deviation.

RMSD (nm)					
BE0.5	**BE1**	**BE1.5**	**BE2**	**BE2.5**	**BE3**
0.83 ±0.04	1.03 ±0.03	1.10 ±0.04	1.25 ±0.03	1.26 ±0.02	1.19 ±0.04
		B1.5	**B2**	**B2.5**	**B3**
		0.98 ±0.02	1.30 ±0.04	1.19 ±0.03	1.15 ±0.03

To better understand the effect of the formulations in the stability of the hair model, the RG and SAS values were evaluated. These values are presented in the Figure 5. The SAS analysis provides information about the area of the hair model that is accessible to the solvent, being related with the hair model destabilization because the lateral dissociation of the keratins increases the area of the proteinaceous material accessible to the solvent. On the other hand, in MD studies, the RG measures the compaction of the structure of proteins. We measured the RG relative to the transversal axis of the cylindrical protofibril, and the values were normalized, which allows the evaluation of the lateral disassembling of the keratins chains since it follows this axis.

The RG and SAS values showed a global tendency to increase with the increase of benzyl alcohol concentration. As in the RMSD analysis, are bigger the differences between the RG and SAS values in the lower and higher benzyl alcohol concentration than between the RG and SAS values in formulations with or without ethanol.

The fluorescence microscopy pictures in the Figure 5 clearly showed an increase of fluorescence in the hair. The pictures showed one interesting feature - the hair treated with formulations containing ethanol presented much lower fluorescence in the inner zones of hair cortex.

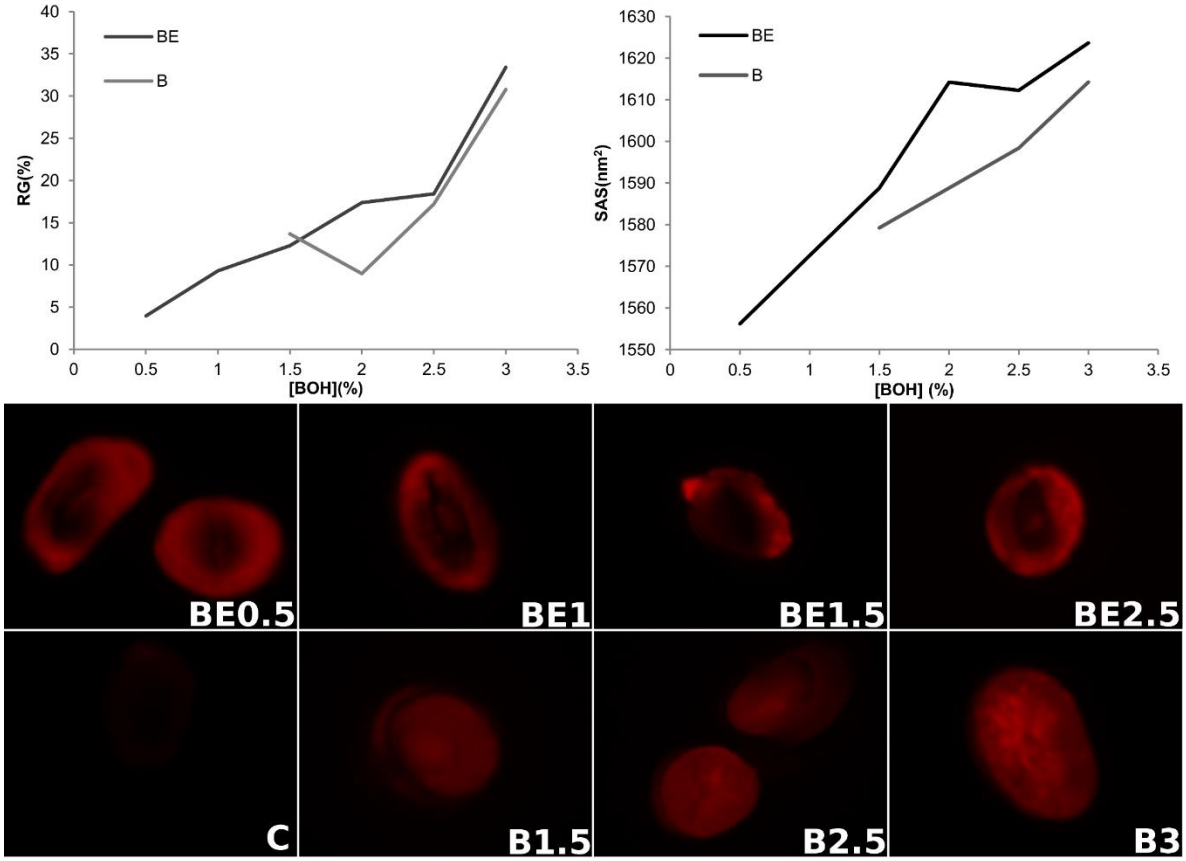

Figure 5: **Top:** Graphical representation of the Radius of Gyration (RG) and Solvent Accessible Surface area (SAS). **Bottom:** Snapshots of transversal cuts of bleached hair shafts, treated with the different formulations and with the QAAFSQ-TAMRA peptide (C: control).

At this point it is clear that the formulations composition will affect the stability of the keratins assembly in the hair shaft, and that this destabilization is able to ease the penetration of the peptide into the hair.

In order to evaluate, at a molecular level, the interaction of the peptide with the hair model some simulations were performed. Some snapshots of the evolution of one system composed by the hair model and 6 SPD fragments, during 1020ns, are presented in Figure 6. In the first half of the simulation the proteinaceous material was dissolved in the BE3 formulation and the second half only in water.

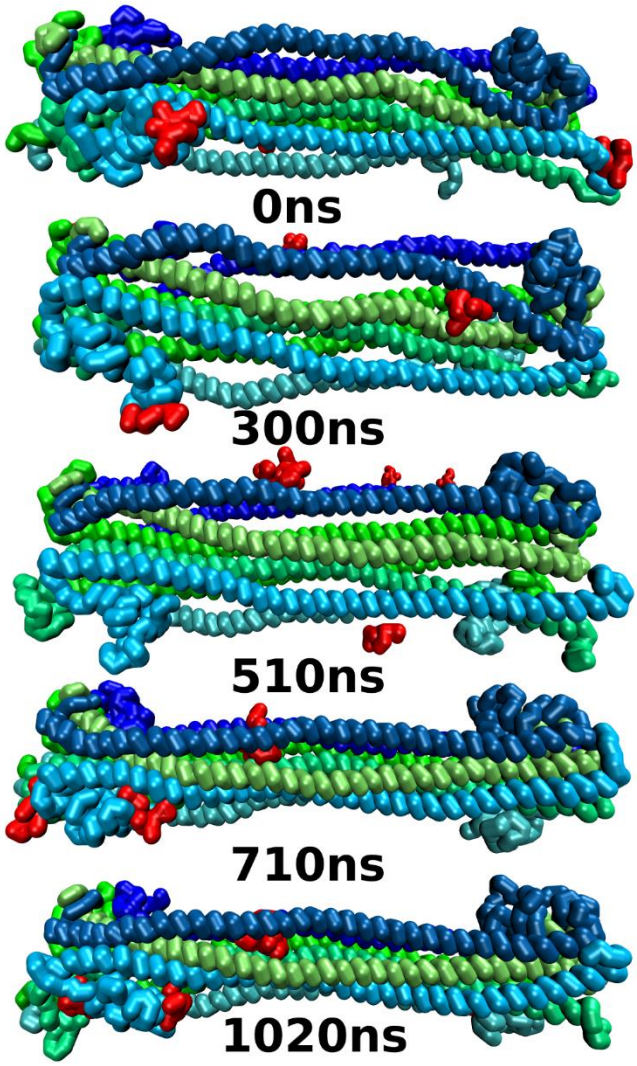

Figure 6: Snapshots of the simulation of the hair model and 6 peptides of QAAFSQ (in red) in the BE3 formulation until 510 ns. The BE3 formulation was removed at this point and the system was filled with water, extending the simulation for another 510 ns.

Once again the formulations promote the destabilization of the keratin assembly, allowing the penetration of the peptide into the interior of the fiber. Nonetheless the interaction of the peptide with the keratins is not very strong while the formulation is present, but when the formulations are removed, what is equivalent to washing the hair after the incubation with the formulations, the peptide stays attached to the fiber. What seems to be clear is that the formulations do not increase the affinity of the peptide towards the hair. Instead, the formulations are able to facilitate the penetration of the peptide into the fiber, increasing the amount of peptide that penetrates the fiber and interacts with the keratins. This behavior is in agreement with the fluorescence pictures, showing how the peptide can be absorbed by the hair. The same simulations were made for the formulations B3 (results not showed), and the behavior was similar, the lateral expansion of the keratins in hair model was bigger when the formulations do not contain ethanol, and this can be the cause of the difference in fluorescence patterns showed in the microscopy studies. Bigger expansions can lead to more peptide being trapped in the hair fibers, while allowing the peptide to penetrate deeper into the hair shaft.

The small solubility range of benzyl alcohol in aqueous solutions limited the number of different formulations is this work. This is a limitation of the experimental procedure, were we are using aqueous solutions to mimic cosmetic formulations. We also made simulations with higher concentration of benzyl alcohol (see Chapter I Figures 1 and 2), that were excluded from the work because the impossibility to compare with fluoresce tests, due to the solubility problems. However, in the cosmetic field the formulations used in commercial products are not solutions, but are instead gels, lotions, shampoos, among others, where the concentration of benzyl alcohol could be higher than its solubility in water. With the simulations it is possible to overcome solubility problems like this one, turning the screening of new formulations easier than in other models, like the ones using aqueous solutions.

Conclusions

The computational model built in this work proved to be a good approach to provide information about the way how formulations can change the affinity of peptides, or other compounds, towards hair fibers. The simulations showed a strong interaction between molecules of benzyl alcohol and the keratins, leading to a destabilization of the hair model structure which increases with the benzyl alcohol concentration. The fluorescence microscopy experiment showed that the absorption in the hair fiber of the SPD fragment is improved with the increase of benzyl alcohol in the formulations, and this can be explained by the mechanisms observed in the simulations. The theoretical and experimental data are in good agreement, showing that the built model is valid to describe the interactions between formulations and hair.

With the MD simulations we were able to select formulations with better performance in the enhancement of peptide absorption by the hair. But the hair model built allows the study of many other features and phenomena, as long as its inherent peculiarities are taken into account. This can be of great interest to researchers in fields of applied research, such as cosmetic applications, to fundamental research.

Acknowledgments

We acknowledge the access to the Minho University GRIUM cluster.

References

[1]. R. Dawber, Hair: Its structure and response to cosmetic preparations, *Clin. Dermatol.*, 1996, 14, 105–112.

[2]. M. Hatzfeld, The coiled coil of in vitro assembled keratin filaments is a heterodimer of type I and II keratins: use of site-specific mutagenesis and recombinant protein expression, *J. Cell Biol.*, 1990, 110, 1199–1210.

[3]. Z. Qin, L. Kreplak, and M. J. Buehler, Hierarchical structure controls nanomechanical properties of vimentin intermediate filaments, *PLoS One*, 2009, 4, e7294.

[4]. S. V Strelkov, H. Herrmann, and U. Aebi, Molecular architecture of intermediate filaments, *Bioessays*, 2003, 25, 243–51.

[5]. H. Herrmann, M. Häner, M. Brettel, N. O. Ku, and U. Aebi, Characterization of distinct early assembly units of different intermediate filament proteins, *J. Mol. Biol.*, 1999, 286, 1403–20.

[6]. C.-H. Lee, M.-S. Kim, B. M. Chung, D. J. Leahy, and P. a Coulombe, Structural basis for heteromeric assembly and perinuclear organization of keratin filaments, *Nat. Struct. Mol. Biol.*, 2012, 19, 707–15.

[7]. L. Norlén, S. Masich, K. N. Goldie, and A. Hoenger, Structural analysis of vimentin and keratin intermediate filaments by cryo-electron tomography, *Exp. Cell Res.*, 2007, 313, 2217–27.

[8]. U. Aebi, W. E. Fowler, P. Rew, and T. T. Sun, The fibrillar substructure of keratin filaments unraveled, *J. Cell Biol.*, 1983, 97, 1131–43.

[9]. N. R. Barthélemy, A. Bednarczyk, C. Schaeffer-Reiss, D. Jullien, A. Van Dorsselaer, and N. Cavusoglu, Proteomic tools for the investigation of human hair structural proteins and evidence of weakness sites on hair keratin coil segments, *Anal. Biochem*, 2012, 421, 43–55.

[10]. J. Schweizer, L. Langbein, M. a Rogers, and H. Winter, Hair follicle-specific keratins and their diseases, *Exp. Cell Res.*, 2007, 313, 2010–20.

[11]. L. Langbein, The Catalog of Human Hair Keratins I, *J. Biol. Chem*, 1999, 274, 19874–19884.

[12]. L. Langbein, M. a Rogers, H. Winter, S. Praetzel, and J. Schweizer, The Catalog of Human Hair Keratins II, *J. Biol. Chem.*, 2001, 276, 35123–32.

[13]. A. C. Lorenzo and E. R. Caffarena, Elastic properties, Young's modulus determination and structural stability of the tropocollagen molecule: a computational study by steered molecular dynamics, *J. Biomech.*, 2005, 38, 1527–33.

[14]. A. P. Demchenko and S. O. Yesylevskyy, Nanoscopic description of biomembrane electrostatics: results of molecular dynamics simulations and fluorescence probing, *Chem. Phys. Lipids*, 2009, 160, 63–84.

[15]. E. Antunes, N. G. Azoia, T. Matamá, A. C. Gomes, and A. Cavaco-Paulo, The activity of LE10 peptide on biological membranes using molecular dynamics, in vitro and in vivo studies, *Colloids surfaces B Biointerfaces*, 2013, 106, 240–7.

[16]. C. Das, M. G. Noro, and P. D. Olmsted, Simulation Studies of Stratum Corneum Lipid Mixtures, *Biophys. J.*, 2009, 97, 1941–51.

[17]. M. I. Hoopes, M. G. Noro, M. L. Longo, and R. Faller, Bilayer Structure and Lipid Dynamics in a Model Stratum Corneum with Oleic Acid, *J. Phys. Chem. B*, 2011, 115, 3164–71.

[18]. M. Martins, N. G. Azoia, A. Ribeiro, U. Shimanovich, C. Silva, and A. Cavaco-Paulo, In vitro and computational studies of transdermal perfusion of nanoformulations containing a large molecular weight protein, *Colloids Surf. B. Biointerfaces*, 2013, 108, 271–8.

[19]. N. G. Azoia, M. M. Fernandes, N. M. Micaêlo, C. M. Soares, and A. Cavaco-Paulo, Molecular modeling of hair keratin/peptide complex: Using MM-PBSA calculations to describe experimental binding results, *Proteins Struct. Funct. Bioinforma.*, 2012, 80, 1409–1417.

[20]. C. Danciulescu, B. Nick, and F.-J. Wortmann, Structural Stability of Wild Type and Mutated α-Keratin Fragments: Molecular Dynamics and Free Energy Calculations, *Biomacromolecules*, 2004, 5, 2165–75.

[21]. C.-C. Chou and M. J. Buehler, Structure and Mechanical Properties of Human Trichocyte Keratin Intermediate Filament Protein, *Biomacromolecules*, 2012, 13, 3522–32.

[22]. D. W. Cheong, F. C. H. Lim, and L. Zhang, Insights into the Structure of Covalently Bound Fatty Acid Monolayers on a Simplified Model of the Hair Epicuticle from Molecular Dynamics Simulations, *Langmuir*, 2012, 28, 13008–17.

[23]. Fernandes, M.; Cavaco-Paulo, A. Protein Disulphide Isomerase-Mediated Grafting of Cysteine-Containing Peptides onto over-Bleached Hair. *Biocatal. Biotransformation* 2012, 30, 10–19.

[24]. Fernandes, M. M.; Cavaco-Paulo, A. Protein Disulphide Isomerase-Assisted Functionalization of Proteinaceous Substrates. *Biocatal. Biotransformation* 2012, 30, 111–124.

[25]. Hess, B.; Kutzner, C.; Spoel, D. van der; Lindahl, E. GROMACS 4: Algorithms for Highly Efficient, Load-Balanced, and Scalable Molecular Simulation. *J. Chem. Theory Comput.* 2008, 4, 435–447.

[26]. Marrink, S. J.; Risselada, H. J.; Yefimov, S.; Tieleman, D. P.; Vries, A. H. de The MARTINI Force Field: Coarse Grained Model for Biomolecular Simulations. *J. Phys. Chem. B* 2007, 111, 7812–24.

[27]. Hall, B. A.; Armitage, J. P.; Sansom, M. S. P. Mechanism of Bacterial Signal Transduction Revealed by Molecular Dynamics of Tsr Dimers and Trimers of Dimers in Lipid Vesicles. *PLoS Comput. Biol.* 2012, 8, e1002685.

[28]. Risselada, H. J.; Marelli, G.; Fuhrmans, M.; Smirnova, Y. G.; Grubmüller, H.; Marrink, S. J.; Müller, M. Line-Tension Controlled Mechanism for Influenza Fusion. *PLoS One* 2012, 7, e38302.

[29]. Risselada, H. J.; Kutzner, C.; Grubmüller, H. Caught in the Act: Visualization of SNARE-Mediated Fusion Events in Molecular Detail. *Chembiochem* 2011, 12, 1049–55.

[30]. Berendsen, H. J. C.; Postma, J. P. M.; Gunsteren, W. F. van; DiNola, A.; Haak, J. R. Molecular Dynamics with Coupling to an External Bath. *J. Chem. Phys.* 1984, 81, 3684.

[31]. Hess, B.; Bekker, H.; Berendsen, H. J. C.; Fraaije, J. G. E. M. LINCS: A Linear Constraint Solver for Molecular Simulations. *J. Comput. Chem.* 1997, 18, 1463–1472.

[32]. C. Popescu and H. Höcker, Hair—the most sophisticated biological composite material, *Chem. Soc. Rev*., 2007, 36, 1282–91.

[33]. Schrodinger LLC The PyMOL Molecular Graphics System, Version 1.1, 2010.

[34]. Strelkov, S. V; Herrmann, H.; Geisler, N.; Wedig, T.; Zimbelmann, R.; Aebi, U.; Burkhard, P. Conserved Segments 1A and 2B of the Intermediate Filament Dimer: Their Atomic Structures and Role in Filament Assembly. *EMBO J.* 2002, 21, 1255–66.

[35]. Persson, A.; Chang, D.; Rust, K.; Moxley, M.; Longmore, W.; Crouch, E. Purification and Biochemical Characterization of CP4 (SP-D), a Collagenous Surfactant-Associated Protein. *Biochemistry* 1989, 28, 6361–6367.

[36]. S.-W. Chiu, S. A. Pandit, H. L. Scott, and E. Jakobsson, An Improved United Atom Force Field for Simulation of Mixed Lipid Bilayers, *J. Phys. Chem. B*, 2009, 113, 2748–63.

Chapter I Attachments

Keratin protofibril model building.

The majority of the hair weight corresponds to the keratin fiber. However a complete macrofibril or the smaller microfibril reach sizes far beyond the usual systems sizes simulated in molecular dynamics, even with coarse-grained force fields like MARTINI. Considering this, we build a computational model of a truncated protofibril assembling 8 truncated α keratin. The truncated zone corresponds of α-keratins 2B domain from the L2 link to C tail, and the assembling of the 4 dimers is based in the A_{22} model, with dimer to dimer anti-parallel pairing. The size of the model, approximately 20 nm of length, was expected to be big enough to reproduce hair keratins properties at a reasonable simulation time. Each of the four dimer are composed for one K34 (type I) and one K86 (type II), since, according the literature, these keratins belong to the group of most expressed keratins in hair, and are presented in the cortex, the most representative zone of the hair. As stated in the Introduction section of main document, there are no atomistic models of entire keratins, so we build one computational model of each of the two chosen keratins with Pymol software,[1] from the L2 domain to the C terminal of the chain. The chains were defined, in the software, as having α-helix structure with the exception of the L2 and C terminal domains that have no defined secondary structure. The aminoacid sequence of the K34 and K86 was accessed from UniProt database entry O76011 (http://www.uniprot.org/uniprot/O76011) and O43790 (http://www.uniprot.org/uniprot/O43790), respectively. These all-atoms models were converted to coarse-grained models by the Martinize script (available at http://cgmartini.nl), and for each keratin type six replicas were made, and each one was simulated for 65 ns (three replicas in water and three in vacuum of each K34 and K86). The short simulation allows the relaxation of the aminoacid sequence, and a more favorable spatial conformation of the keratins chains. All the replicas showed the same behavior, namely the compaction of the L2 and C tail, forming globular zones at the terminal zones of keratins monomer models, and the 2B domains presented lesser compaction maintaining a coiled structure as expected. In the next step we manually put one K34 and K86 side to side pairing its domains, in water and

vacuum to simulate its assembling. Since the behavior of the monomers in the first simulations was similar in all replicas, were tested different combinations, using the resulting conformations of the previous replicas, resulting in three systems of K34/K86 dimer in water (DW1, DW2 and DW3), and three in vacuum (DV1, DV2, and DV3) all with small conformations variations. In this case we choose to build six systems that are very similar to be equivalent to experiment replicas, but with small differences in the spatial conformation that allows a larger sampling of this property. The systems were simulated for 150ns and in this case there are few differences between systems at the end. The systems with the monomers in vacuum, DV1, DV2, and DV3 were excluded from the next simulations due to the structures presented in the end of simulations, in which the coiled domains of the two monomers are not fully aligned, leading to conformations incompatibles with the A_{22} assembling model. The DW1, DW2 and DW3 systems presented similar structure, at the end of the 150ns simulated. The L2 and C domains of each keratin in all systems interact with the same domain of the adjacent keratin, forming globular zones in the truncated dimer terminations. The globular zones do not presented a tendency to any particular structure, and differ between the three systems. In both systems the 2B domain maintained its coiled structure, and interacted with each other, approximating both keratin chains. In the DW3 system the assembly of the C domains was lightly different, resulting in a separation of C termination domains comparing with the DW1 and DW2 systems. In the available molecular models of other IFs like vimentin,[2] or of skin keratins,[3] the 2B domains have two points where the helix chains of each keratin turn around the other, and in the middle the chains are more separated (see Figure 2 in the Introduction section). In our non-excluded simulations there are also to points of more close contact and the separation in the middle zone, however due to a lesser turn of one keratin around the other the contacts and separation are lesser evident, and in the DW3 system there was also a separation between the C domains. These differences can be due the fixed secondary structure of the proteins in the MARTINI force field, (can lead to a lesser flexible keratin chain, avoiding bigger turns in the chain) or due to the truncation of the model (can add degrees off freedom). Since the evaluation of molecular structure of keratins protofibrils are out of the scope of this study we considered the dimers models reliable for the study propose.

After the dimer assembling simulations we joined together four dimers in order to build a truncated model of keratin protofibril (PT). We build 8 systems, (4 different systems each one with one replica), using the structure's from previous simulations in water. The systems PT1, PT2, PT3 and its replicas (PT1R, PT2R and PT3R) are composed for 4 equal dimers from the previous DW1, DW2 and DW3, respectively. The remaining system and its replica, PT4 and PT4R, have two dimers from the DW2 and two from DW3 systems. It is important to remember that although the systems are being treated as different, the difference is only relative to its spatial conformations, since all systems have the same constitution (dimers of K34 and K86). Once again in the next simulations are sample several starting points but with little differences to be possible compare the final conformations.

After joining the dimers, the systems were hydrated and its behavior in water was simulated by about 500 ns. The simulations showed the approximation between the dimers, resulting, in most cases, in the interaction of the 4 dimers that composed the systems forming a core structure. In the systems PT1, PT1R, PT2, PT2R and PT4R the attachment of the four dimers was full, and take between 45 to 70 ns. However the systems PT3 and PT3R presented, at the end of 500 ns, structures not fully compact with some of its keratins chains away of the core structure, in its central domains. The system PT4 also presented some separation between some chains, but at lower level. Although the compactness of the final structures was similar between the replicas, the spatial arrangement of the keratins chains, and the shape of the PT were different. The truncated octamer of the systems PT1, PT2R e PT4R presented a cylindrical shape, and the systems PT1R, PT2 and PT4, in turn, arranged its dimers in an elliptical cylinder shape, as well the systems PT3 and PT3R but these with a broader center. The evaluation of these simulations results is a challenge task due to the poor knowledge at molecular level of the IFs assembling. However we chose the PT structure from the system PT4R to proceed with the interaction simulations, due to more compactness and cylindrical shape presented, similar to the models described in literature for vimentin and intermediate filaments.[2-4]

Some considerations:

The PT structural conformations presented in the several simulated systems were different, even between replicas. The time evolution of the dimers attachment and posterior rearrangement of its chains showed that the way the dimers are placed in the systems and the dimer structure itself (that resulted from the dimer assembling simulations), are factors that affect the final structure of the PT model. This is because all the PT systems, in which its keratins chains are not full joined together, had the dimer for the DW3 system that presented a separation between the C domains of the two keratins chains, which seems difficult the full join of the keratins chains in the PT assembling. However this is not the principal influence in the assembling of the dimers, once even between replicas the final structures are different, and the PT4R system, for example, have DW3 dimers but do not present separation in the C domain zone. Take this is consideration, the system PT4R was considered reliable to model the hair keratin behavior in MD simulations.

Attachments References

[1]. Schrodinger LLC The PyMOL Molecular Graphics System, Version 1.1, 2010.

[2]. Strelkov, S. V; Herrmann, H.; Geisler, N.; Wedig, T.; Zimbelmann, R.; Aebi, U.; Burkhard, Conserved segments 1A and 2B of the intermediate filament dimer: their atomic structures and role in filament assembly, P. *EMBO J.*, 2002, 21, 1255–66.

[3]. Lee, C.-H.; Kim, M.-S.; Chung, B. M.; Leahy, D. J.; Coulombe, P., Structural basis for heteromeric assembly and perinuclear organization of keratin filaments, *Nat. Struct. Mol. Biol.*, 2012, 19, 707–15.

[4] Qin, Z.; Kreplak, L.; Buehler, M. J., Hierarchical structure controls nanomechanical properties of vimentin intermediate filaments, *PLoS One*, 2009, 4, e7294.

[5] Marrink, S. J.; Risselada, H. J.; Yefimov, S.; Tieleman, D. P.; de Vries, A. H., The MARTINI force field: coarse grained model for biomolecular simulations, *J. Phys. Chem. B*, 2007, 111, 7812–24.

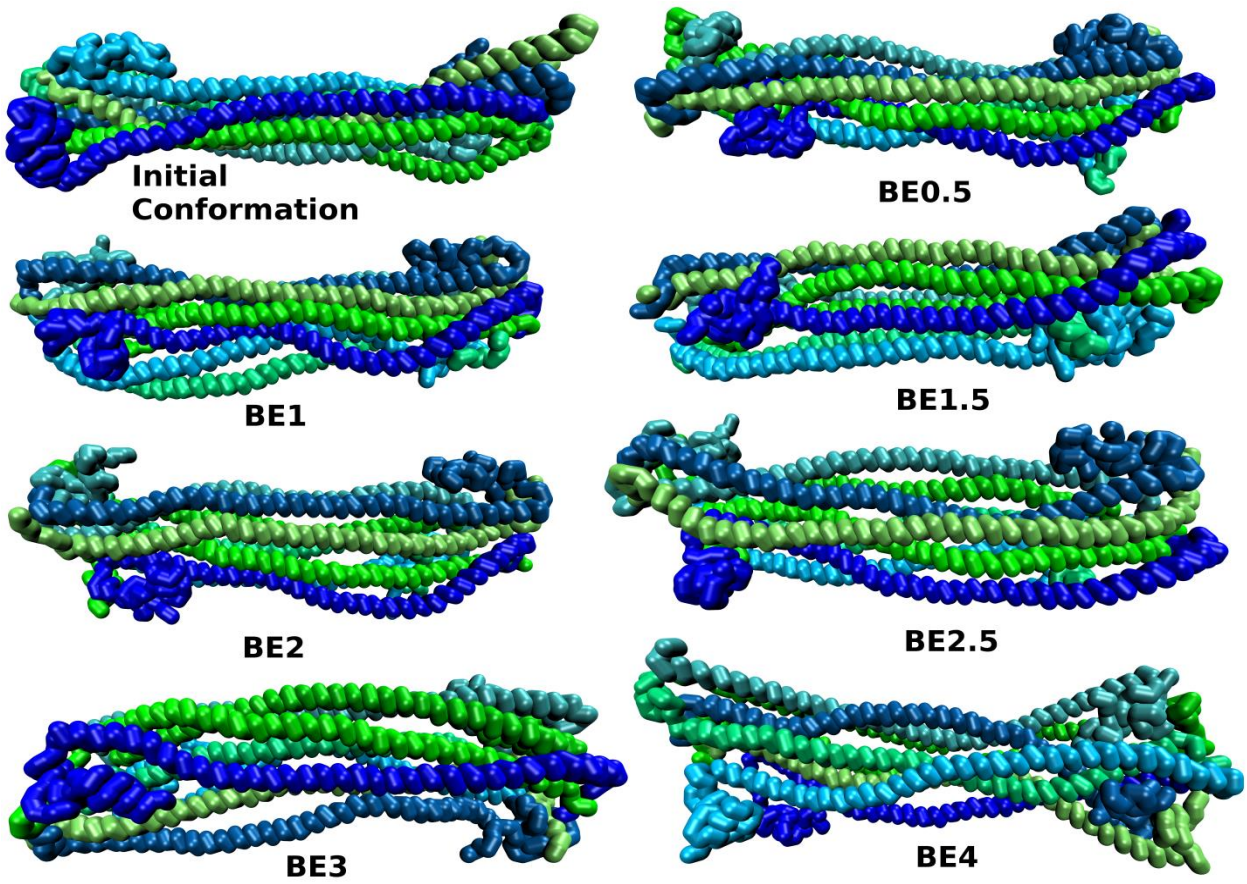

Figure 7: Initial (up at left) and final (510ns) conformations of the systems in the simulations containing ethanol.

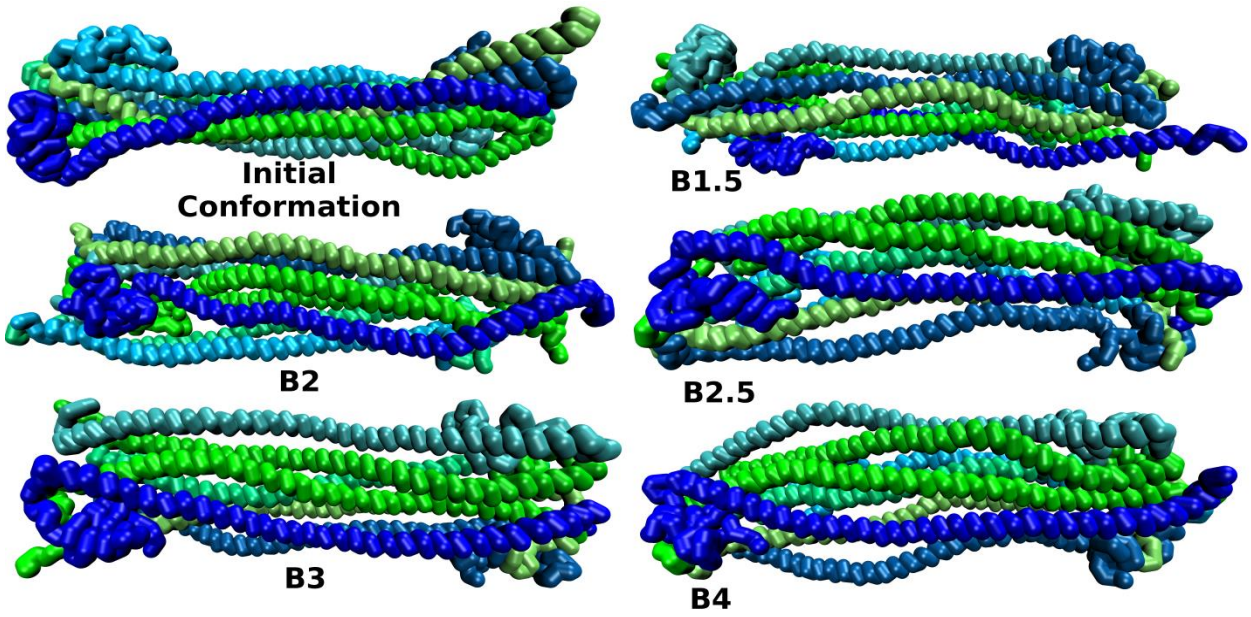

Figure 8: Initial (up at left) and final (510ns) conformations of the systems in the simulations without ethanol.

Figure 9: Picture of the formulations containing 10% ethanol and 4, 3, 2 and 1% of benzyl alcohol (from left to right). To notice the turbidity in the formulation BE4.

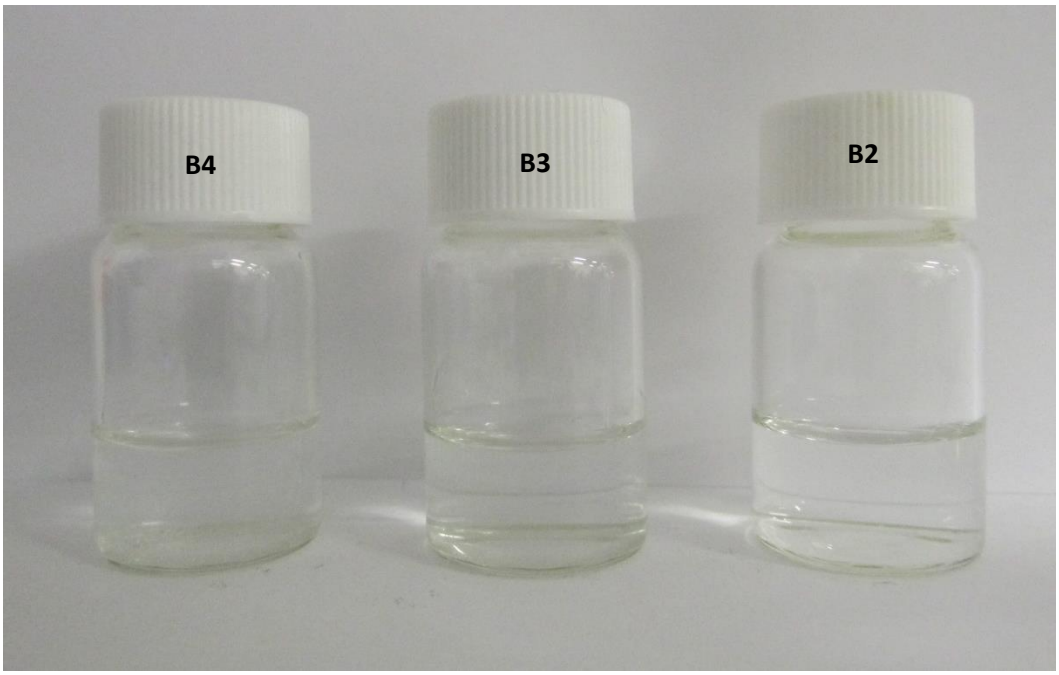

Figure 10: Picture of the formulations containing 4, 3 and 2% of benzyl alcohol (from left to right). To notice the turbidity in the formulation B4.

Notes: The simulation systems of BE4 and B4 (with 4 % (v/v) of benzyl alcohol and 10 % of ethanol in the BE4 formulation) were not included in the work presented in the main document. As it is visible in the Figure 3 and 4 the solutions with this benzyl alcohol

concentration present some turbidity, likely due to the fact that the 4 % concentration is in the limit of its solubility in water (3.5 g/100 mL at 20 ºC and 4.29 g/mL at 25 ºC). The turbidity had impact in the preliminary fluorescence tests that we made, and we conclude that these formulations do not allow the achievement of reliable results. Because we cannot compare the simulations results of the systems with BE4 and B4 formulations with experimental data, we exclude these simulations from the work, although in the simulations there are no problem with the solubility, showing that the use of molecular dynamics simulations it may be advantageous to test cosmetic compositions, comparing with the use of aqueous solutions in the laboratory.

United Atoms simulations

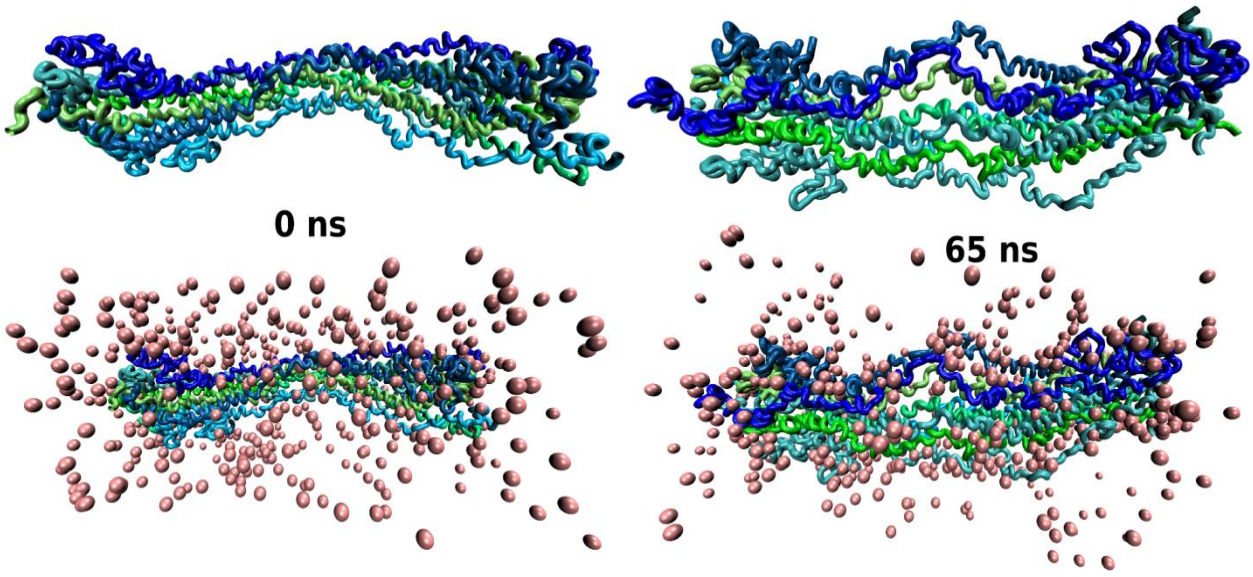

Figure 11: Graphic representations of united atom simulations. The system was composed of one protofibril (the keratins are represented as tubes, each one with different color) in the BE3 formulation. In the upper pictures it is represented the evolution of the protofibril structure over 65ns, and the bottom pictures represent the same time evolution of the protofibril and benzyl alcohol molecules (pink beads). The remaining solvent molecules were excluded from the pictures for clarity. In these simulations it is clear the lateral disassembling of the keratin chains, as well the tendency of benzyl alcohol molecules to be located near to the fiber, such as in the coarse grained simulations.

Radial Distribution function Graphics

BE0.5

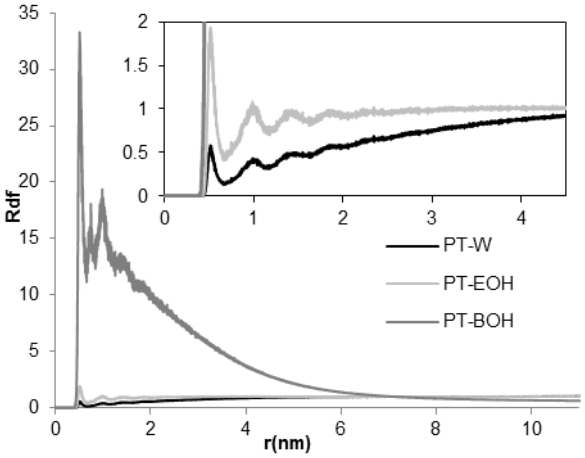

BE1

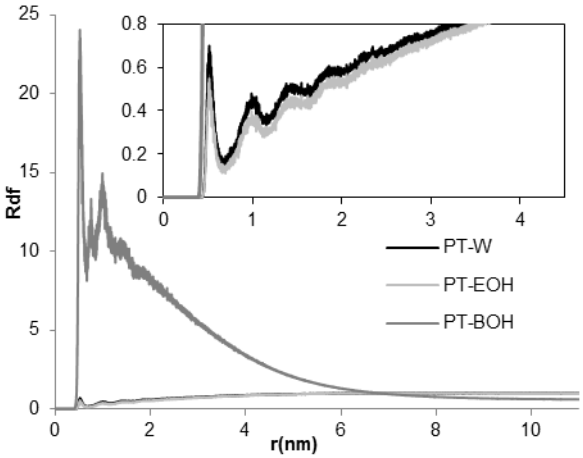

BE1.5

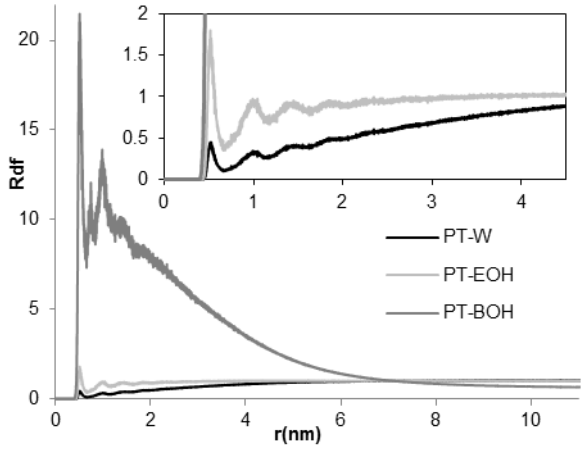

B1.5

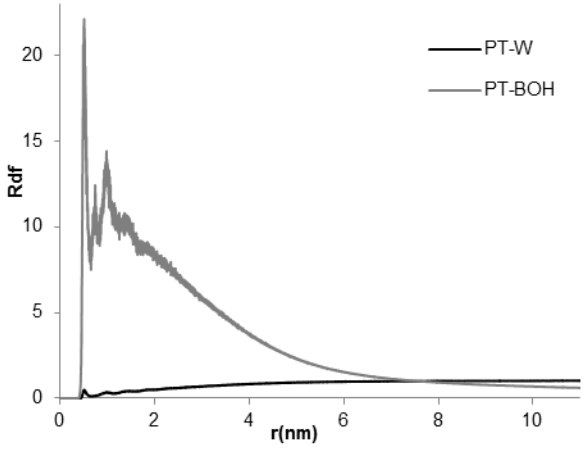

BE2

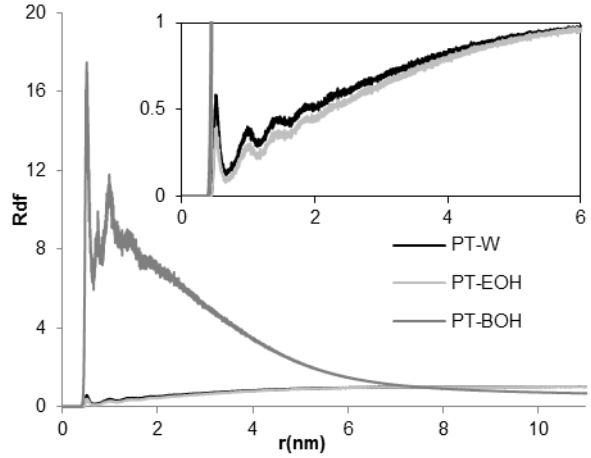

B2

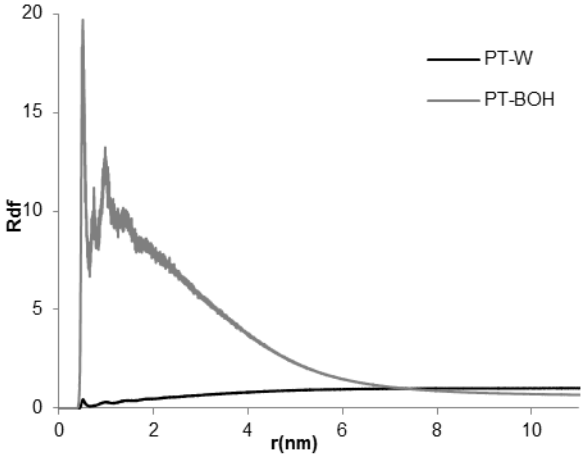

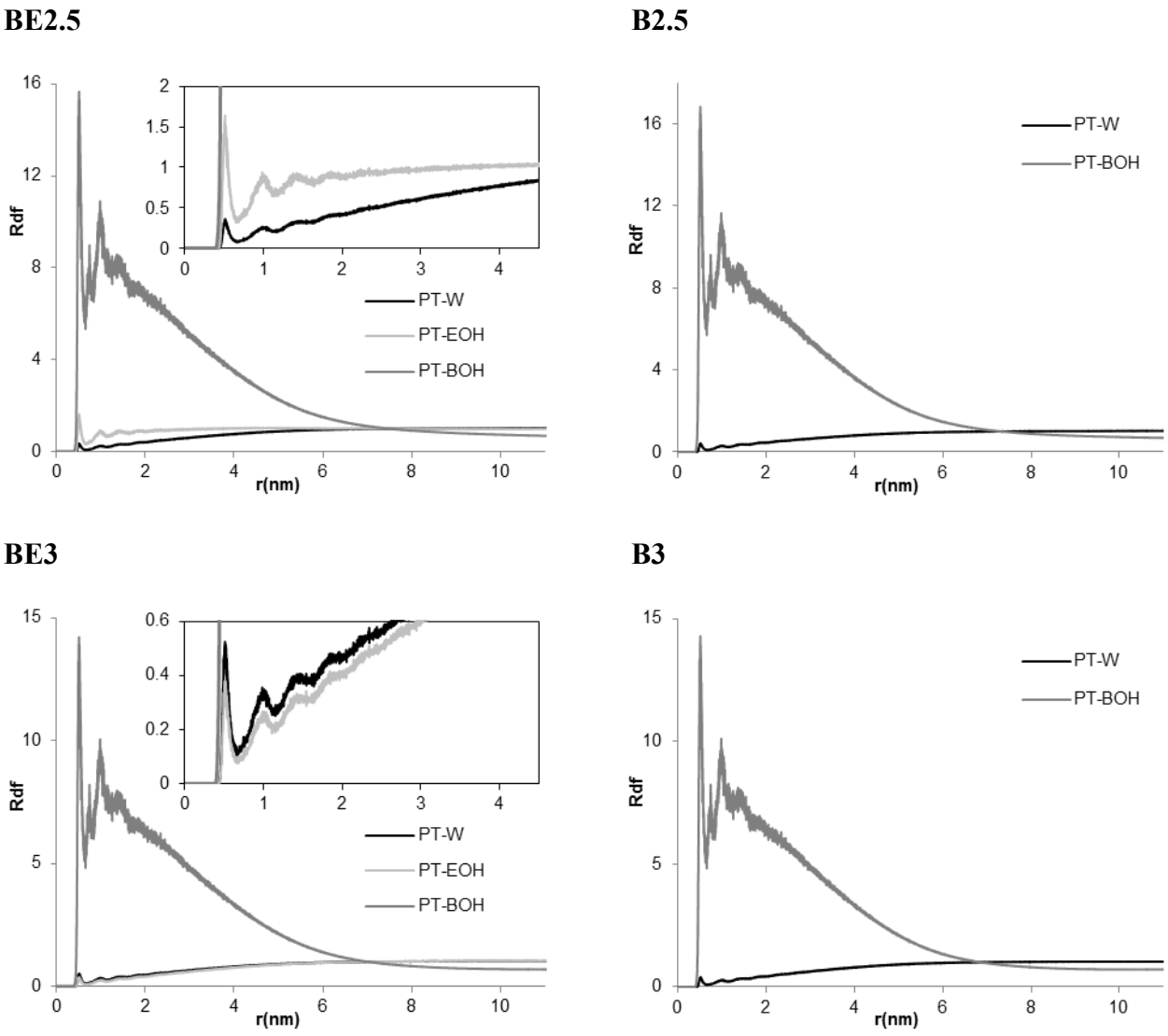

Figure 12: Radial distribution function of the systems simulated. It is clear the tendency of benzyl alcohol molecules to be located near to the protofibril chains.

Benzyl alcohol parametrization

Itp file:

[moleculetype]

; molname nrexcl

BNOH 1

[atoms]

; id	**type**	**resnr**	**resid**	**atom**	**cgnr**	**charge**	**mass**
1	SC5	1	BNOH	R1	1	0	26.0378
2	SC5	1	BNOH	R2	2	0	26.0378
3	SC5	1	BNOH	R3	3	0	25.0299
4	P1	1	BNOH	R4	4	0	31.0343

[constraints]

; i j	**funct**	**length**
1 2	1	0.27
2 3	1	0.27
1 3	1	0.27
3 4	1	0.27

[angles]

; i	**j**	**k**	**funct**	**angle**	**force.c.**
1	3	4	2	117	100
2	3	4	2	175	100

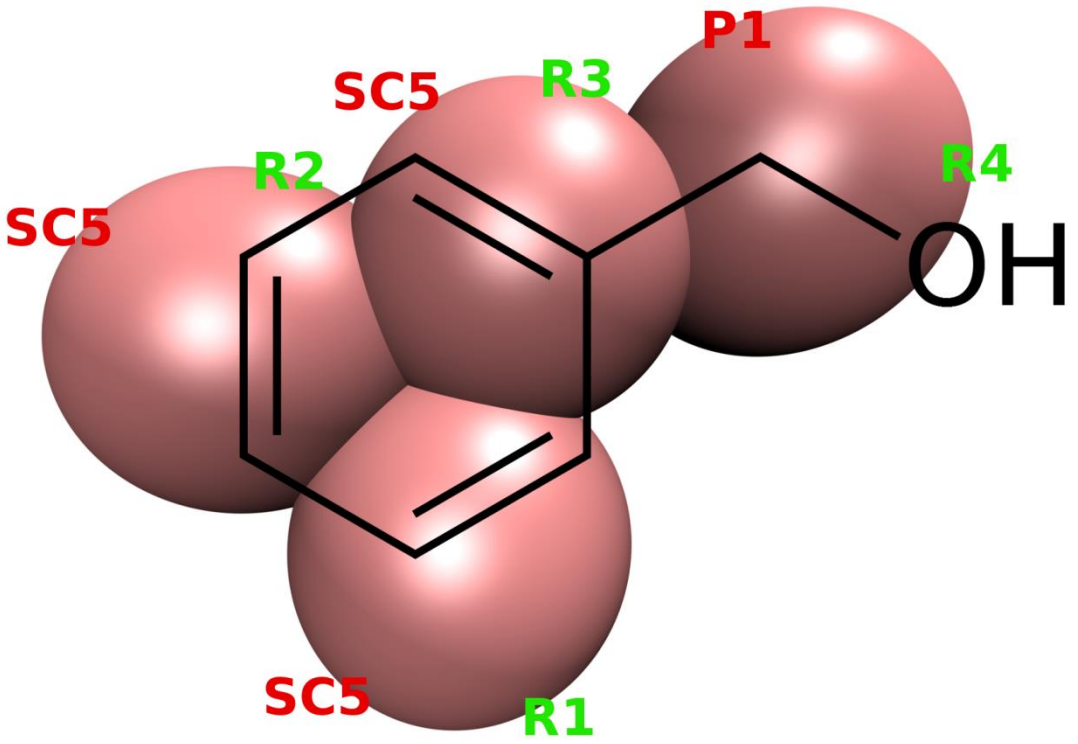

Figure 13: Schematic representation of the Benzyl alcohol molecule parametrization. Each bead represents two atoms. The green labels indicates the "atom number" according with the itp file, and the red labels the type of bead according the Martini force field developers.

Chapter II

Hair Keratin Molecular Dynamics Studies.

Insights on the mechanical behavior of keratin fibrils.

This chapter is based on the following publication:

Egipto Antunes, Célia F. Cruz, Nuno Azoia, Artur Cavaco-Paulo. Insights on the mechanical behavior of keratin fibrils. *Int. J. Biol. Macromol.*, 2016, 89, 477-483.

DOI: 10.1016/j.ijbiomac.2016.05.018

Chapter II abstract:

A computational molecular model of a truncated keratin protofibril (8 chains of hair keratin) was used, to run a series of steered molecular dynamics simulations obtaining strain-stress curves. These results were compared with experimental mechanical data on hair fibers. Our data demonstrate that the molecular dynamics simulations can model hair mechanical properties. Simulations done in vacuum showed a better agreement with experimental Young's Modulus (YM) values. The role of hydrogen bonds and the secondary structure of keratin on the mechanical properties was evaluated in detail. The incubation with a fragment of one surfactant protein, the SPD-2 peptide (QAAFSQ), showed the improvement of YM of the hair keratin either by simulations and experimental data. For the first, our research provides mechanistic insights on mechanical microscopic properties of keratin protofibrils through molecular dynamics simulations.

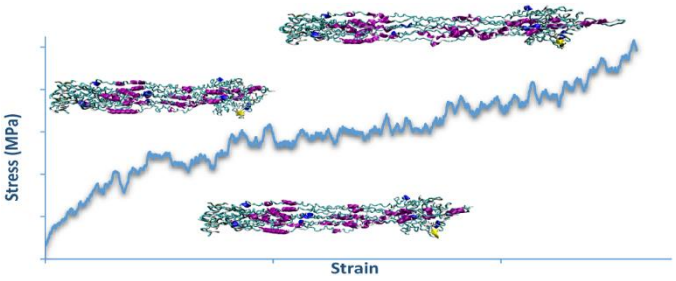

Figure II: Graphical abstract of Chapter II

Introduction

Human hair is mainly composed by proteins and lipids (about 90 % of proteins and 1-9 % of lipids by dry weight), and can be divided into three zones: the cuticle (outermost zone), the cortex (middle zone) and in coarser hairs the medulla (innermost zone). The cuticle corresponds to a 5μm protective surface composed of several layers of overlapping scales. The medulla is made of hollow cells with amorphous material and air spaces, it has 5-10 μm thickness and is not always present. The cortex, with 45-90 μm of thickness, is responsible for 90 % of hair mass. It is composed by long cylindrical assembled cortical cells and the cell membrane complex. These cells are constituted by macrofibrils and intermacrofibrilar material. The macrofibrils are further divided into intermediate filaments (IFS also known as microfibrils) and a matrix of associate proteins and remains of keratinocytes. The lateral assembling of coiled-coil α-keratin (α-KRT) proteins and keratin associate proteins (KAPs) results in KRT dimers, tetramers, protofibrils (two tetramers) and finally IFS (4 protofibrils).[1,2] The Figure 1(a) represents this hierarchical structure of hair.

The hair and other keratinaceous fibers such as wools, quills and spines are widely studied at macroscopic level, from the response to chemical treatments[3-5] to inherent mechanical properties.[6-9] However at molecular level there is much lesser information about these fibers and their ultrastructure. This is probably due to the limitations in the characterization of the entire IFS structure, since it has some highly disordered regions difficult to crystallize, challenging the use of traditional techniques such as X-ray crystallography and NMR. In a few works, computational methods have been applied with success in the study of these fibers structure at molecular level, overcoming these limitations. Computational molecular models of keratin structures (mainly dimers and some tetrameters of α-keratin) have been developed, gathering the available data from several sources such as the known amino acid sequence of keratin proteins, the crystallographic structure of some keratin fragments already unveiled and available information about other fibrous proteins like vimentin and lamin which share similar ultrastructure of the IFS with keratin.[10–13]

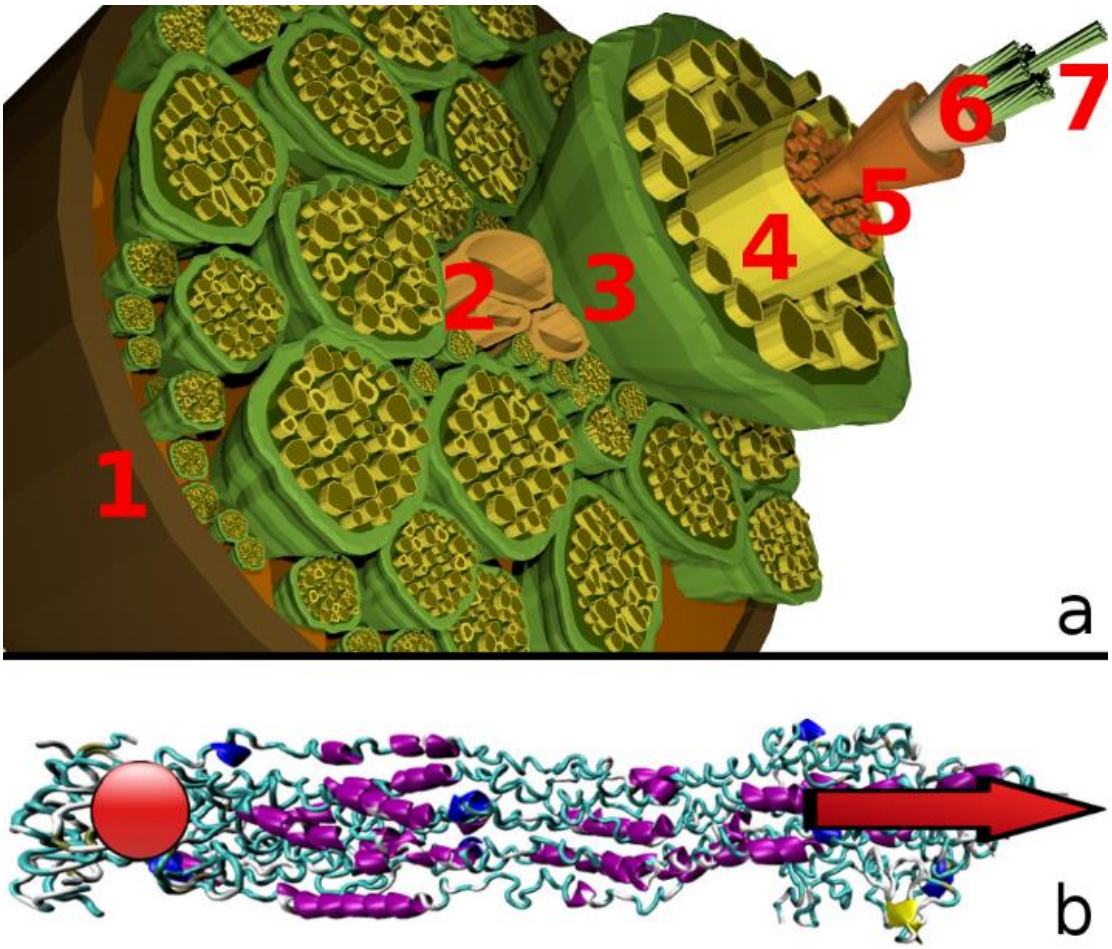

Figure 1: **(a)** Schematic 3D representation of one hair shaft cut. 1 - hair cuticle; 2 – hollow medulla cells; 3 - cell membrane complex; 4 - macrofibril; 5 - matrix; 6 - microfibrils or intermediate filaments; 7 - protofibril. **(b)** Schematic representation of steered simulations, the red ball indicates the fixed zone of the truncated protofibril and the arrow the zone where the pulling force is applied as well its direction.

Previously a coarse-grained computational model of a truncated keratin protofibril (from the linker 2 region to the tail) was developed in our group, and it was used in several molecular dynamics simulations to study the interaction of hair protein content with alcoholic formulations. The performed simulation and experimental tests showed that the increase of a peptide affinity towards hair fibers can be modulated by the solvent composition of formulations.[14] In this work we intend to apply the molecular dynamics simulations in the study of mechanical properties of the truncated protofibril model and unveil how these properties are affected by the interaction with a fragment of one pulmonary protein, the SPD-2 peptide. We performed steered simulations, applying a pulling force to stretch the fiber and

subsequently calculate the Young's modulus (YM) in different conditions (see Figure 1(b)). For the same purpose, mechanical experimental tests with bleached Caucasian hair shafts were performed in similar conditions to the ones simulated, including the interaction with the peptide.

Materials and methods

Molecular Dynamics Simulations

A coarse-grained model of a truncated protofibril, assembling 8 truncated α-keratins, was previously built by us. The truncated zone corresponds to 2B domain of the α-keratins (from the L2 link to the C tail). The model is composed by four keratin 34 – keratin 86 parallel dimers, and each dimer assembles with the adjacent dimers in anti-parallel way according the A_{22} model.[14]

Although in this previous work the suitability of the coarse-grained model developed for the type of studies performed was shown, the MARTINI force-field[15] applied there do not allow dynamic conformational flexibility of the protein secondary structure due to its coarse-grained nature. This limits the study of mechanical studies proposed in the present work and in consequence the coarse-grained model was converted into a united-atom model by the "Backward" tool from the MARTINI force-field web site (http://md.chem.rug.nl/cgmartini/).

All molecular dynamics simulations were performed with the Gromacs 4.0.7 package using the GROMOS96 43A1 united-atom force-field,[16–18] with periodic boundary conditions, applying the LINCS[19] and the SETTLE[20] algorithms to constrain the peptide and water bonds respectively. The simulations ran with a time step of integration of 2 fs and the single point charge (SPC) model[21] was used to represent the waters. When needed the temperature was maintained at 300 K with the V-rescale thermostat[22,23] whereas the Parrinello-Rahman barostat[24,25] (with semi-isotropic coupling) was used to maintain the pressure at 1atm. Van der Walls and electrostatic interactions were treated by a twin-range

method, with short and long range cutoffs (0.8 and 1.4 nm, respectively), with a reaction field correction for electrostatic using a dielectric constant of 54,[26] and the neighbor list was updated every 5 steps.

Preparation Simulations

Initially all systems were energy minimized for around 2000 steps with the steepest descent method. Afterwards the systems were initiated to a series of three short equilibration simulations (500ps each simulation), with positions restraints allowing the slow relaxation of the structures for the final production run (the atoms were restrained with an harmonic force of 10^3 kJ/mol.nm^2). In the aqueous systems the equilibration simulations consisted of three short runs. The first in the NVT ensemble (number of particles, volume and temperature constant) applying positions restraints to all heavy atoms. The second one simulation in the NPT ensemble (number of particles, pressure and temperature constant) with positions restraints to the same atoms. Finally the third simulation ran also in NPT ensemble but with positions restrains only in the alpha-carbons atoms of the proteins. The equilibration simulations of the vacuum systems followed the same protocol in terms of positions restrains, but in all the three simulations, the NVE ensemble (number of particles, volume and energy constant) was applied.

After the systems equilibration by the preparatory simulations, were performed 50 ns of NPT (aqueous systems) or NVE (vacuum systems) simulations, without any position restrains. This allowed the keratin chains to acquire a stable conformation in response to their surrounding (water or vacuum) as well to the interaction with the SPD-2 peptide when presented.

SPD-2 Peptide

The SPD-2 peptide (QAAFSQ) is a fragment of pulmonary associated surfactant protein D (SPD), that belongs to a group of proteins present in the lung which have been studied in our group as enhancer agents in the recovery of damaged hair.[14,27–29] The computational model of the peptide was built using the Pymol software.[30] The peptide model was subject to preparation simulations by the same protocol described previously. After the equilibration, the resulting systems were subject to 50 ns of simulations without

any position restraints to relax the peptide structure. The resulting structures were used to test the effect of this peptide on the keratin fiber, inserting 10 molecules in the simulation box and following the previous protocol for systems equilibration.

Steered Simulations

The final conformations of the previous runs were used to initiate the steered molecular dynamics simulations, where a spring elastic constant force was applied to one tip of the keratin fiber whilst the other tip was fixed, promoting the protofibril stretch and allowing the study of mechanical properties such as the YM. The centers of mass of the first amino acids, in the region 2B of each keratin fiber, were fixed with a strong harmonic restraint with a spring constant of 10^3 kJ/mol.nm^2, while the last amino acids at the opposite end of the same region were pulled by a spring with an elastic constant of 100000 kJ.mol^{-1}.nm^{-2} (see Figure 1(b)). The aqueous systems were simulated in an NPT ensemble while the vacuum system ran in an NVE ensemble. The pulling force (F) and the distance between the fixed and the pulled groups (L) were recorded during the simulation allowing the calculation of the engineered stress (σ) and strain (ε), which are described as:

$$\sigma = \frac{F}{A_0}$$

and

$$\varepsilon = \frac{\Delta L}{L_0}$$

where F, A_0, ΔL and L_0 are the pulling force, the cross-sectional area of the fiber, the displacement and the initial length, respectively. YM is a mechanical property that relates the engineered stress and strain providing a measure of the material stiffness. It can be calculated using the following expression:

$$YM = \frac{\sigma}{\varepsilon} = \frac{\frac{F}{A_0}}{\frac{\Delta L}{L_0}}$$

Hair treatments

Caucasian hair fiber samples were provided by International Hair Importers & Products (New York). Hair tresses were subjected to eight cycles of bleaching, which destroys the hair exterior lipid layer and damages hair cuticle, reducing its influence in the mechanical tests and contributing to a keratin fiber more similar to the one simulated. Each bleaching cycle consisted of the application of 10 % H_2O_2 (v/v) in Na_2CO_3/NaHCO pH 9.0 buffer at 50 ºC for 1 h. Between cycles, the hair was washed with running water.

Subsequently, the bleached hair was treated with 700 µM of the SPD-2 peptide in 0.05M PB, pH 7.5. The engineered peptide was synthesized by JPT Peptide Technologies GmbH (Berlin, Germany). Peptide treatments were performed for 2 h at 37 ºC with orbital agitation, 50 rpm. After treatment, the hair samples were washed with distilled water.

Mechanical Properties Evaluation

Hair samples mechanical properties were evaluated following the guidelines for tensile testing of fibers outlined in ASTM D1445-95. Measurements were performed in an Instron 4505 tensile tester, with a maximum load cell capacity of 2.5 N. A set of 15 single hair fibers was randomly taken from the hair tresses for each sample measurement. Each hair fiber was individually mounted in the tensile jig through a paper scaffold with a fixed gauge length of 20mm. Before the test started, the scaffold was cut across, so the hair fiber was fixed in a continuous length within the jig. All the samples were kept under the same conditions before measurements. The wet samples were soaked in distilled water for at least 5 minutes previous to the measurement. Measurements were performed at a constant rate of 1.5 mm/min until breakage, under 60±5 % relative humidity. For each hair, the applied load against extension was recorded, assuming an average mean diameter of 70 µm (measured in previous studies by light microscopy on transversal cut hair samples). All data were converted to stress (load/unit area) against strain (% extension).

Results and discussion

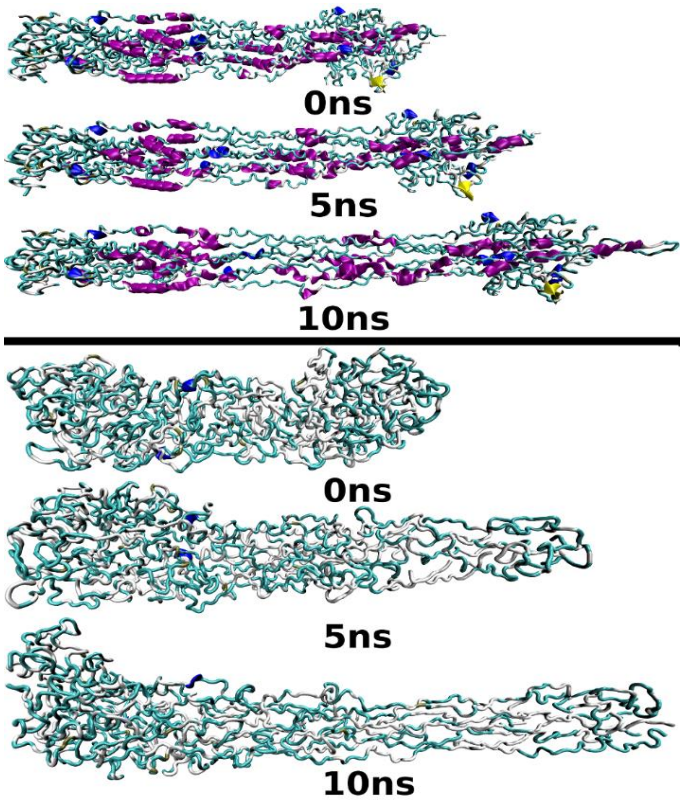

Figure 2: Snapshots of aqueous (up) and vacuum (down) steered simulations. The centers of mass of the first amino acids at left in the region 2B of each keratin fiber were fixed while the first right amino acids of the same region were pulled.

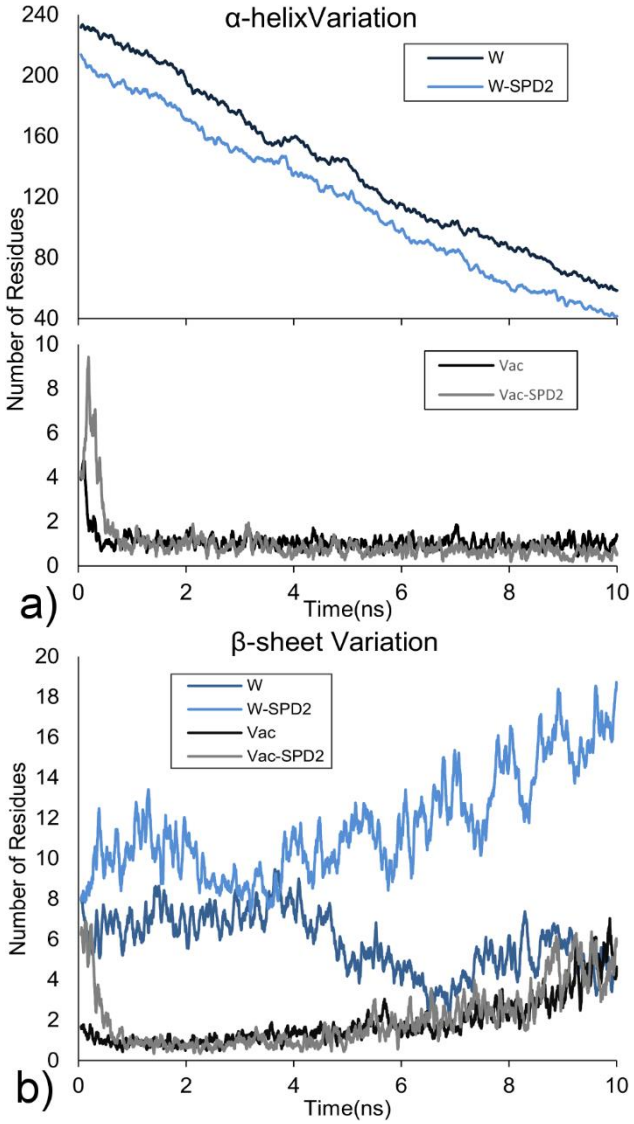

Figure 3: Graphical representation of the number of residues in α-helix (**a**) and β-sheet (**b**) conformation along the simulation time. The variation of α-helix residues from aqueous and vacuum simulations is separated due the difference in values range. W: truncated protofibril in water; Vac: truncated protofibril in vacuum simulations.

Figure 2 shows the time evolution of protofibril in water and in vacuum steered simulations. The stretching of the chains and the consequent structural deformation are clear. The first zones to deform in response to the applied force are the less coiled zones. With the time evolution the more coiled domains, like the α-helix (at violet in the Figure 2), also begin to stretch and unfold (this behavior can be better perceived in the video 1 of supplementary material at publisher website, see Chapter II attachments for more information). Although the initial conformation of the truncated protofibril in vacuum is more compact, the fibers are less structured, a fact that in conjugation with the absence of water, seems facilitate the fiber stretching.

The DSSP algorithm ("Define Secondary Structure of Proteins")[31] describes the amino acids secondary structure and provides a more reliable information about the protofibril conformation. The variation of the secondary motifs α-helix and β-sheets along the simulated time for all the systems is represented in Figure 3.

In the aqueous simulations there is a clear decrease in number of amino acids in the form of α-helix, which is expected in response to the fiber stretching. The vacuum systems almost do not present α-helix motifs and their number is almost constant during the simulations, showing a tiny initial increase that could be a result of the unfold of the fibers from an initial highly compact conformation. On the contrary, the β-sheets motifs slightly increase along the simulation except for the fiber in water system. There is an initial β-sheets decrease in the vacuum systems, again probably due to the initially high compaction of the structure, and also a decrease at 4 ns of simulation of the protofibril in water. The α-helix to β-sheet transition in response to the keratin fiber stretching is described in literature for more than 50 years,[32,33] and although very small, some α-helix to β-sheet transition is shown in the previous results and in the simulations pictures.

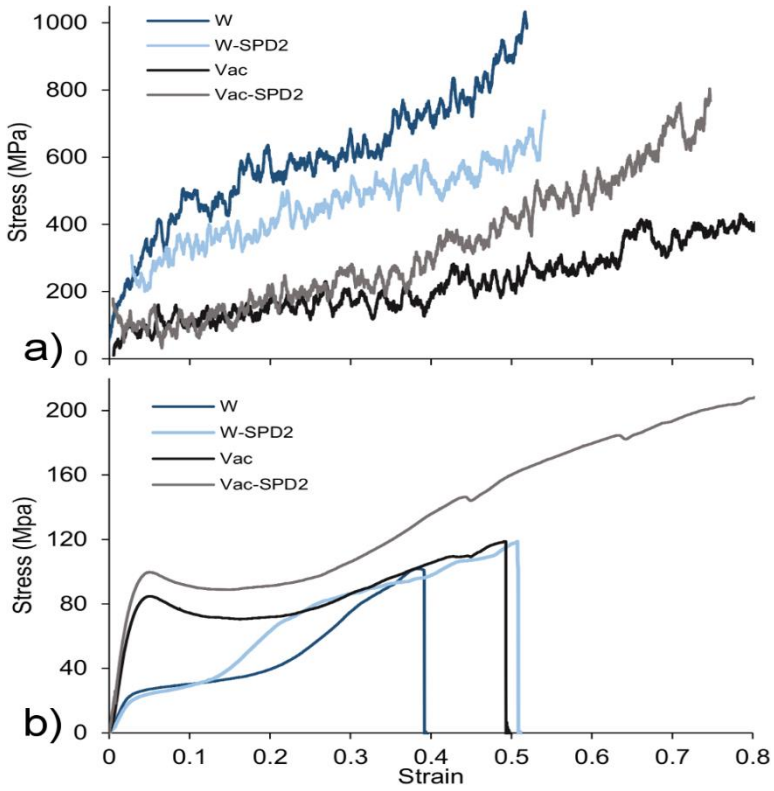

Figure 4: (**a**) Mechanical analysis of the truncated protofibril under steered simulations. (**b**) Mechanical analysis of hair shafts under tensile deformation. W: truncated protofibril in water simulations or humid hair shafts; Vac: truncated protofibril in vacuum simulations or dry hair shafts.

In Figure 4(a) the averaged strain-stress curves resulting from the pulling simulations are presented. Several works, either theoretical or experimental, with keratin filaments such as hair and wool, or even with other intermediate filaments like vimentin describe three regions in its strain-stress graphics,[34-37] namely:

I-"Linear elastic region" or "Hookean region" (0-2 % of strain): characterized by the linear increase of the stress with the strain until a plateau is reached;

II-"Yield region" (2-30 % of strain): the stress maintains almost constantly over a long period;

III- "Post yield region" (above 30 % of strain): the stress increases rapidly with the strain until the fiber failure.

The identification of these three zones in the strain-stress curves is not always easy, or even possible, due to big variations of the slope.[11,36]

As shown in Figure 4(a), the identification of the three zones in our simulations was only possible for the truncated protofibril in water (curve W). For these systems the Hookean region seems to end around 0.1 of strain (10 % of fiber elongation) and the Yield region around 0.35. Although the stress values are not constant between the strain values of 0.1 and 0.35 its increase is much lower than in the other regions of the curve. For the remaining systems the division of the graphs in three zones is not clear. The strain-stress graph for the protofibril in vacuum (curve Vac in Fig.4a) is clearly different of the aqueous system, showing an almost constant increase of the stress values along the simulation. The aqueous systems with the peptide (W-SPD2 in Fig.4a) seems to have only the regions I and II. Just as in the simulations of the fiber alone in water there is a quick increase of stress values until around 0.1 of fiber strain, but after this point the stress increases with almost constant rate until the end of the simulations. On the other hand the vacuum systems with SPD-2 (Vac-SPD2 in Fig.4a) presented a constant increase of the stress values until 0.35 of strain, where the slope of the curve increases, opposing to the behavior of the fiber in vacuum. In this case the slope change is an indication of the transition from the region II to III.

Figure 4(b) presents the same study for the real hair shafts. Taking into consideration the typical strain-stress curve for keratin and the global behavior of all 15 replicas per

condition (in Chapter II attachments all the curves are presented), only one replica is represented. On the contrary to the simulation results, the stress values of dry hair are higher to ones for wet hair. However, like in the theoretical tests, the maximum strain values for dry hair samples are higher. The addition of the peptide clearly affects the strain stress curves in both conditions, resulting in the increase of both the stress and strain values. This increase in stress promoted by the SPD-2 treatment begin much earlier in dry hair samples (1 % in dry hair elongation against 10 % for wet samples). In these strain-stress curves it is easy to define the elastic zone. It ends around 0.02 and 0.05 of strain for wet and dry samples, respectively. The transition from the yield to the post yield region is harder to define, mainly for the dry samples results. It seems to happen at 10 % of elongation for the wet hair samples, incubated with peptides and at around 20 % for the remaining samples.

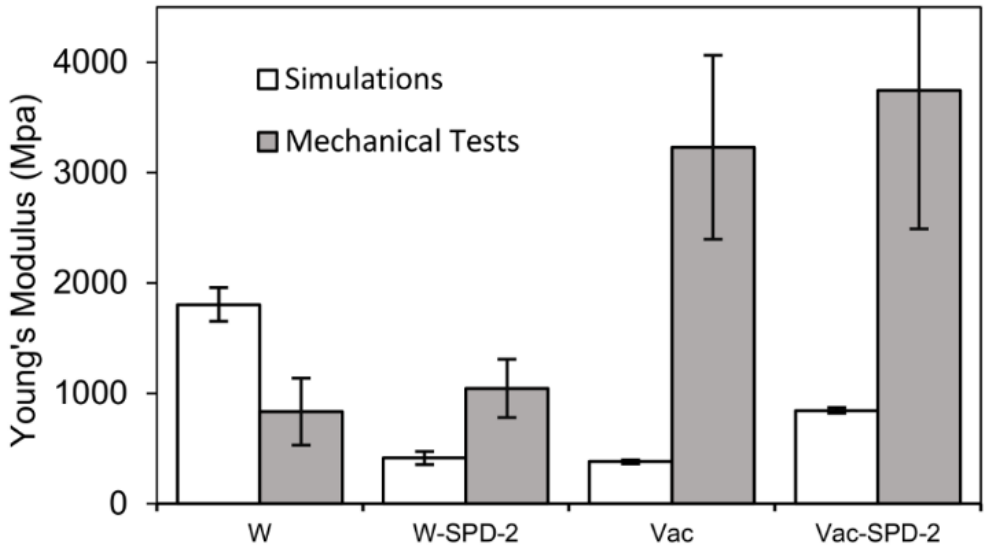

Figure 5: Young's Modulus values calculated from simulations (white columns) and mechanical tests (gray columns) W: truncated protofibril in water simulations or humid hair shafts; Vac: truncated protofibril in vacuum simulations or dry hair shafts.

Figure 5 shows the Young's Modulus (YM) for the different conditions. The variation in these values shows a good agreement between simulation and mechanical assays. Nevertheless the calculated YM value for the simulations of the protofibril in water is higher than it is supposed to be, being the highest value calculated for all simulations. This value was expected to be lower than the value calculated for the protofibril in vacuum. This

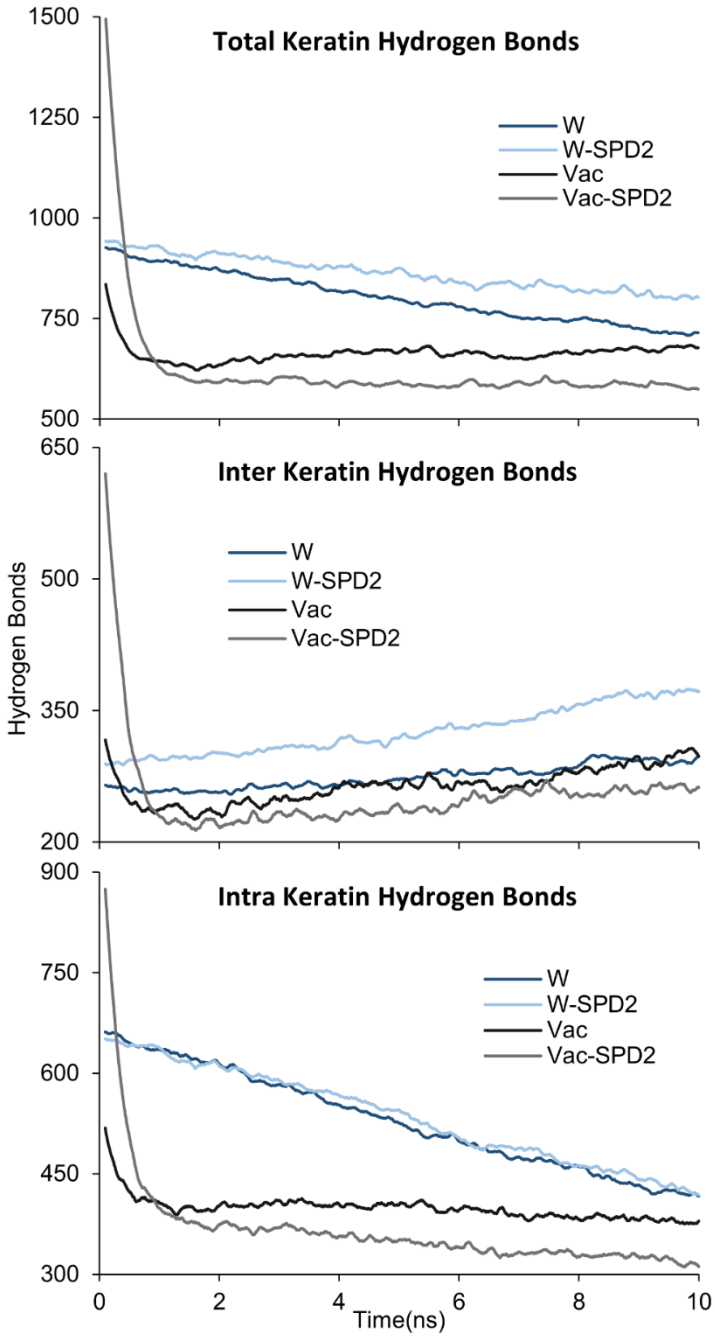

Figure 6: Hydrogen bonds between keratin residues along the simulation. **Up:** total hydrogen bonds variation (total HB); **Middle:** variation of hydrogen bonds between residues of the same keratin chain (intra-HB); **Down:** variation of hydrogen bonds between residues of the different keratin chains (inter-HB). W: truncated protofibril in water simulations; Vac: truncated protofibril in vacuum simulations.

variation also contradicts the literature since it is well known that water molecules are capable of interacting with hair fibers plasticizing their components, and resulting in a lower force requirement for extending the fibers and consequently lower the elastic modulus.[6,35] However, this water effect is observed for the simulations with SPD-2, where the YM values from the aqueous simulations are lower than the corresponding values for the vacuum simulations.

Hydrogen bonds (HB) variation was studied in an attempt to unveil the mechanisms behind the previous results. The HB between atoms from different (inter-HB) and from the same keratin chains (intra-HB) were evaluated. The averaged results are presented in Figure 6. The total HB number between protofibril atoms (inter and intra-HB) decreases along the simulation for all aqueous systems, being more pronounced when the protofibril is not accompanied by the peptide. This decrease is

expected due to the stretching of the keratin chains that leads to the break of the initial HB. However the vacuum systems only presented significant HB decrease at the beginning of the simulation, and in the protofibril in vacuum system (Vac in Fig.6) the total HB begin to increase after 2 ns of simulation. The separate study of inter and intra-HB (Figure 6) reveals additional interesting information.

The first noticeable feature is that the HB between keratin residues of the same chain (intra-HB) are in a higher number than the HB between residues from different chains (inter HB). There is a small increase of inter-HB during the simulation for all systems, opposing to the intra-HB, that are almost constant in the protofibril in vacuum systems and decrease in the remaining systems. The inter and intra-HB graphs also depicted that the difference between the final number of total protofibril HB in water systems is due to the inter-HB, since the peptide presence leads to a bigger increase of inter-HB in these systems, whereas the intra-HB are very similar in the two aqueous systems. The competition for HB donors and acceptors can explain this phenomena, namely the presence of the peptides that can limit the access of some keratin atoms to water molecules that otherwise would make HB with these waters. Once free, these keratin atoms can connect with other atoms from the surrounding chains, increasing the inter-HB. This also agrees with the fact that the peptide presence does not significantly affect the number of inter-HB in vacuum systems. Note that some of the inter-HB increase is simply due to the keratin chain stretching, since there is an increase of these HB in all the conditions.

The difference of final number, in vacuum systems, of total HB is mainly due to the intra-HB that decrease less when peptides are not presented. In this case the competition could be between acceptors and donors from the same chain versus from the chain and peptides; there is less available spots to make HB inside the same chain because some of them are making HB with the adjacent peptides.

The observed overall decrease of HB is expected, the fiber stretching leads to the breakage of the HB. The vacuum systems presented one faster decrease of protofibril HB, probably as a result of the initial highest compaction of the fibers due to the vacuum, which allows more HB connections. This compaction is not natural and the fiber quickly expands with the applied stress force, breaking many of these bonds.

All together the results showed that the molecular dynamics simulations can be a useful and valuable research tool in the study of mechanical properties of hair fibers, although precaution is needed in the simulation results analysis. The strain-stress curves of the mechanical tests showed a typical profile for keratinaceous materials, while in the simulations only the systems with protofibril in water presented more clearly the three discussed regions. In addition, the stress values of vacuum systems in the simulations results are lower than ones for the aqueous simulations, which goes against the literature and our mechanical results. Other theoretical studies with hair keratin structures, presented strain-stress curves with the three elastic, yield and post yield regions clearly identified, but in some cases the curves presented are also different from the typical.[11,36] Chou and Buehler performed pulling simulations in three hair keratin structures,[11] namely in one dimer, one truncated tetramer without cysteine bonds and one truncated tetramer with cysteine bonds (between the adjacent dimers). All the three conditions presented different strain-stress curves and only one from the dimer structure is similar to the typical. This shows that in these simpler keratinaceous systems, comparing to the more complex structures present in the hair, small changes can affect the strain-stress response. The strain-stress graphs of keratin dimers simulations with cysteine bonds between its two chains in Duchstein work[38] did not present significant differences for the same study in the Chou and Buehler work, which seems to indicate that the absence of cysteine bonds in our model is not the cause of these inconsistencies.

The YM results presented a good agreement between simulation and mechanical results, except for the simulations of the protofibril in water. Previous studies in our research group, depicted big affinity of the surfactant pulmonary peptides with hair keratin and its potential as helper agents in the recovering of damaged hair mechanical properties.[14,27,28] In consequence we expected an increase of YM values for the aqueous systems when the peptides are present. These previous works findings, the mechanical tests results and the bigger stress values for aqueous systems seem to point to an overestimation of stress and YM values for aqueous simulations that is larger when the peptide is absent. This overestimation can be result of an increase of protofibril rigidity due to the protofibril interaction with the bulk water in the aqueous simulations, which could be minimized by the peptide presence. The water molecules surrounding the keratin fiber seem to promote more stable keratin-

keratin HB, mainly the intra-HB. It should be remembered that the keratin fibers in the hair are surrounded by proteinaceous materials and although the water content in the hair interior varies with the environmental humidity, the keratinous fibers are not surrounded by bulk water. The YM results for the vacuum simulation and the dry hair shafts, on the contrary, presented similar variation, although the simulations values are around 5-8 times smaller. The presence of the peptide in the vacuum simulations increases the YM of the protofibril as expected from the previous works. These results show that the vacuum simulations can be used to qualitatively evaluate peptides effects on the mechanical properties of hair keratin structures.

The SPD-2 peptide leads to the increase of hair resistance to deformation, since its addition increases the stress values in the mechanical tests, as well as the YM in the mechanical tests and vacuum simulations. Thus, the potential of surfactant pulmonary peptides as helper agents in the recovery of damaged hair is confirmed.

Conclusions

In the last years many researchers have driven efforts to unveil the molecular structure properties of keratin fibers, trying to relate them with the macroscopic properties of hair tresses.

In this work we showed that molecular dynamics simulations can have an active role in the connection between the molecular and macroscopic study of hair. The application of steered molecular dynamics simulations, in a previously developed computational model of hair truncated protofibril, provided information about its mechanical properties compatible with laboratory tests performed with hair shafts. Vacuum simulations and laboratory mechanical tests showed an increase of YM after SPD-2 treatment, confirming its capacity to improve mechanical properties of hair, already observed in previous works. The agreement between these simulation results with the laboratory tests, as well as with previous findings about the surfactant pulmonary peptides effects on hair, demonstrates the potential of

molecular dynamics simulations and also of the used model, in the study of mechanical properties of hair keratin fibers and the way these properties are affected by peptides treatment.

Acknowledgments

We acknowledge the access of Minho University “SeARCH” ("Services and Advanced Research Computing with HTC/HPC clusters") cluster. We also thank the Portuguese Foundation for Science and Technology (FCT) for providing Célia F. Cruz the grant for PhD studies (scholarship SFRH/BD/100927/2014).

References

[1]. L.J. Wolfram, Human hair: a unique physicochemical composite, *J. Am. Acad. Dermatol.,* 2003, 48, S106–14.

[2]. C. Popescu, H. Höcker, Hair--the most sophisticated biological composite material, *Chem. Soc. Rev.*, 2007, 36, 1282–91.

[3]. R. Dawber, Hair: Its structure and response to cosmetic preparations, *Clin. Dermatol.,* 1996, 14 105–112.

[4]. C. Weathersby, A. McMichael, Brazilian keratin hair treatment: a review, *J. Cosmet. Dermatol.*, 2013, 12, 144–8.

[5]. A. Pielesz, A. Wlochowicz, W. Biniaś, Evaluation of structural changes in wool fibre keratin treated with azo dyes by Fourier Transform Infrared Spectroscopy, Spectrochim, *Acta - Part A Mol. Biomol. Spectrosc.,* 2000, 56, 1409–1420.

[6]. T. Gao, Evaluation of hair humidity resistance/moisturization from hair elasticity, *J. Cosmet. Sci.*, 2007, 58, 393–404.

[7]. H. Tohmyoh, M. Ishihara, M. a. Salam Akanda, S. Yamaki, T. Watanabe, T. Iwabuchi, Accurate determination of the structural elasticity of human hair by a small-scale bending test, *J. Biomech.*, 2011, 44, 2833–2837.

[8]. K. Jelen, M. Skřontová, L. Šimkova, J. Zeman, E. Tlapáková, O. Fanta, Changes in the mechanical parameters of hair in a group of women in reproductive age, *Neuro Endocrinol. Lett.*, 2014, 35, 481–9.

[9]. W. Yang, J. McKittrick, Separating the influence of the cortex and foam on the mechanical properties of porcupine quills, *Acta Biomater.*, 2013, 9, 9065–9074.

[10]. C.-H. Lee, M.-S. Kim, B.M. Chung, D.J. Leahy, P. a Coulombe, Structural basis for heteromeric assembly and perinuclear organization of keratin filaments, *Nat. Struct. Mol. Biol.*, 2012, 19, 707–15.

[11]. C.-C. Chou, M.J. Buehler, Structure and mechanical properties of human trichocyte keratin intermediate filament protein, *Biomacromolecules.*, 2012, 13, 3522–32.

[12]. C. Danciulescu, B. Nick, F.-J. Wortmann, Structural stability of wild type and mutated alpha-keratin fragments: molecular dynamics and free energy calculations, *Biomacromolecules*, 2004, 5, 2165–75.

[13]. Z. Qin, M.J. Buehler, Computational and theoretical modeling of intermediate filament networks: Structure, mechanics and disease, *Acta Mech. Sin.,* 2012, 28, 941–950.

[14]. E. Antunes, C.F. Cruz, N.G. Azoia, A. Cavaco-Paulo, The effects of solvent composition on the affinity of a peptide towards hair keratin: experimental and molecular dynamics data, *RSC Adv.*, 2015, 5, 12365–12371.

[15] S.J. Marrink, H.J. Risselada, S. Yefimov, D.P. Tieleman, A.H. de Vries, The MARTINI force field: coarse grained model for biomolecular simulations, *J. Phys. Chem. B.*, 2007, 111, 7812–24.

[16]. H.J.C. Berendsen, D. van der Spoel, R. van Drunen, GROMACS: A message-passing parallel molecular dynamics implementation, *Comput. Phys. Commun.*, 1995, 91, 43–56.

[17]. E. Lindahl, B. Hess, D. van der Spoel, GROMACS 3.0: A package for molecular simulation and trajectory analysis, *J. Mol. Model.*, 2001, 7, 306–317.

[18]. W.R.P. Scott, P.H. Hu, I.G. Tironi, A.E. Mark, S.R. Billeter, J. Fennen, et al., The GROMOS Biomolecular Simulation Program Package, *J. Phys. Chem. A*, 1999, 103, 3596–3607.

[19]. B. Hess, H. Bekker, H.J.C. Berendsen, J.G.E.M. Fraaije, LINCS: A linear constraint solver for molecular simulations, *J. Comput. Chem.*, 1997, 18, 1463–1472.

[20]. S. Miyamoto, P.A. Kollman, Settle: An analytical version of the SHAKE and RATTLE algorithm for rigid water models, *J. Comput. Chem.*, 1992, 13, 952–962.

[21]. J. Hermans, H.J.C. Berendsen, W.F. Van Gunsteren, J.P.M. Postma, A consistent empirical potential for water-protein interactions, *Biopolymers*, 1984, 23, 1513–1518.

[22]. H.J.C. Berendsen, J.P.M. Postma, W.F. van Gunsteren, A. DiNola, J.R. Haak, Molecular dynamics with coupling to an external bath, *J. Chem. Phys.*, 1984, 81, 3684.

[23]. G. Bussi, D. Donadio, M. Parrinello, Canonical sampling through velocity rescaling., *J. Chem. Phys.*, 2007, 126, 014101.

[24]. M. Parrinello, A. Rahman, Polymorphic transitions in single crystals: a new molecular dynamics method, *J. Appl. Phys.*, 1981, 52, 7182–7190.

[25]. S. Nosé, M.L. Klein, Constant pressure molecular dynamics for molecular systems, *Mol. Phys.*, 1983, 50 1055–1076.

[26]. P.E. Smith, W.F. van Gunsteren, Consistent dielectric properties of the simple point charge and extended simple point charge water models at 277 and 300 K, *J. Chem. Phys.*, 1994, 100, 3169.

[27]. N.G. Azoia, M.M. Fernandes, N.M. Micaêlo, C.M. Soares, A. Cavaco-Paulo, Molecular modeling of hair keratin/peptide complex: Using MM-PBSA calculations to describe experimental binding results, *Proteins Struct. Funct. Bioinforma*, 2012, 80, 1409–1417.

[28]. M. Fernandes, A. Cavaco-Paulo, Protein disulphide isomerase-mediated grafting of cysteine-containing peptides onto over-bleached hair, *Biocatal. Biotransformation.*, 2012, 30, 10–19.

[29]. M. Fernandes, A. Cavaco-Paulo, Protein disulphide isomerase-assisted functionalization of proteinaceous substrates, *Biocatal. Biotransformation.*, 2012, 30, 111-124.

[30]. Schrodinger LLC, The PyMOL Molecular Graphics System, Version 1.1, 2010.

[31]. W. Kabsch, C. Sander, Dictionary of protein secondary structure: Pattern recognition of hydrogen-bonded and geometrical features, *Biopolymers*, 1983, 22, 2577–2637.

[32]. W.T. Astbury, H.J. Woods, X-Ray Studies of the Structure of Hair, Wool, and Related Fibres. II.-The Molecular Structure and Elastic Properties of Hair Keratin, *Proc. R. Soc. B Biol. Sci.*, 1934, 114, 314–316.

[33]. E.G. Bendit, The α–β Transformation in Keratin, *Nature*, 1957, 179, 535–535.

[34]. B.M. Chapman, 15—A REVIEW OF THE MECHANICAL PROPERTIES OF KERATIN FIBRES, *J. Text. Inst.*, 1969, 60, 181–207.

[35]. J. McKittrick, P.Y. Chen, S.G. Bodde, W. Yang, E.E. Novitskaya, M. a. Meyers, The structure, functions, and mechanical properties of keratin, *JOM*, 2012, 64, 449–468.

[36]. C.-C. Chou, E. Lepore, P. Antonaci, N. Pugno, M.J. Buehler, Mechanics of trichocyte alpha-keratin fibers: Experiment, theory, and simulation, *J. Mater. Res.*, 2015, 30, 26–35.

[37]. Z. Qin, L. Kreplak, M.J. Buehler, Hierarchical structure controls nanomechanical properties of vimentin intermediate filaments, *PLoS One*, 2009, 4, e7294.

[38]. P. Duchstein, T. Clark, D. Zahn, Atomistic modeling of a KRT35/KRT85 keratin dimer: folding in aqueous solution and unfolding under tensile load, *Phys. Chem. Chem. Phys.*, 2015, 17, 21880–21884.

Chapter II Attachments

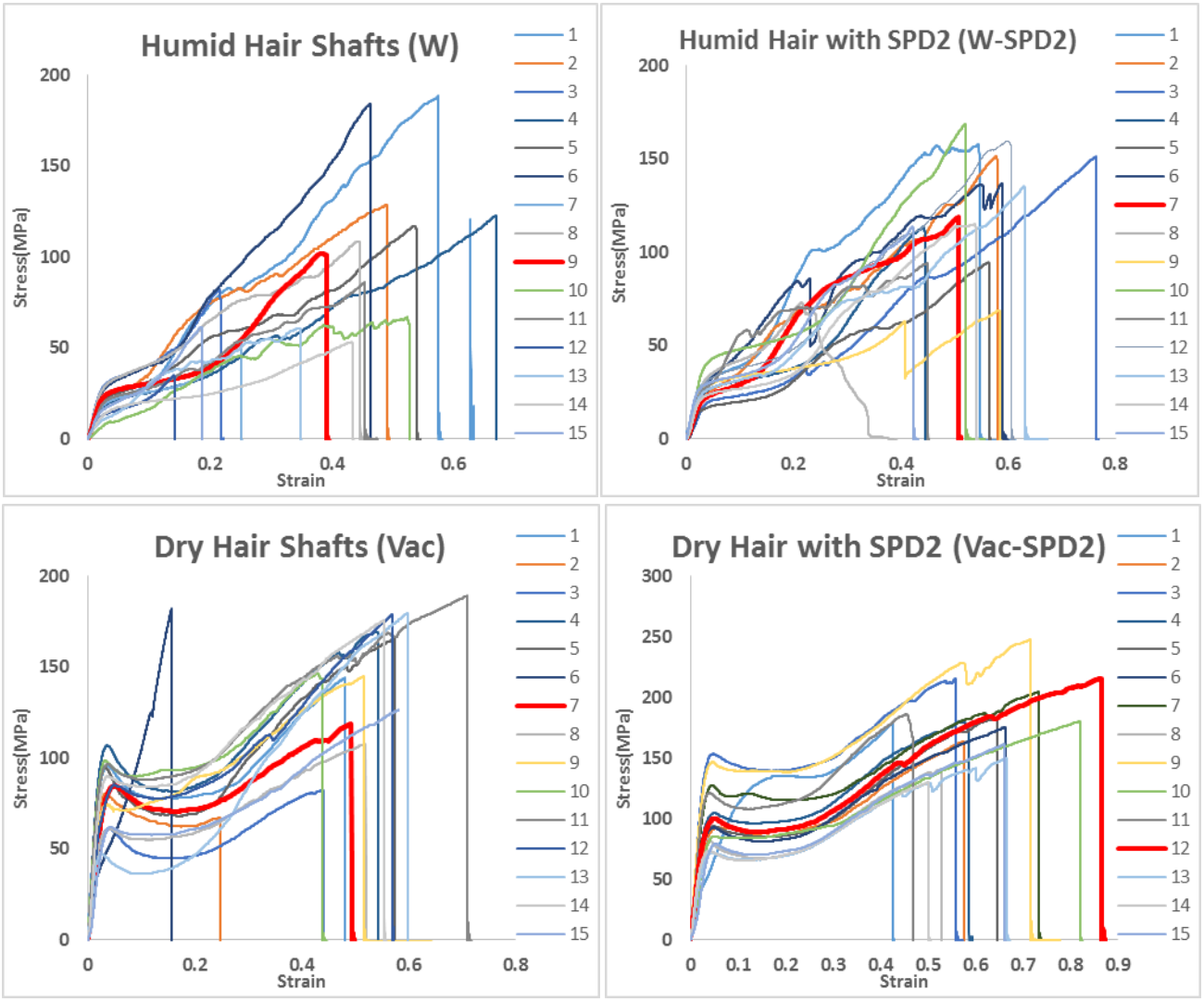

Figure 7: Graphical representation of the mechanical analysis of hair shafts under tensile deformation force. The thick red lines correspond to the replicas chosen to represent the hair shafts response to the deformation force under the different conditions (see Figure 4).

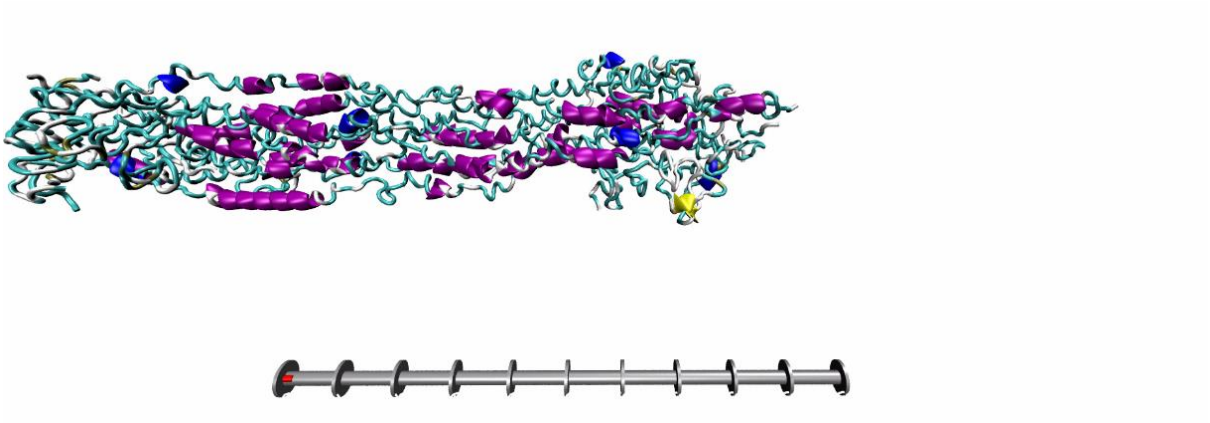

Figure 8: Snapshot of the produced video of the pulling simulation of keratin protofibril in water. The water molecules were omitted for clarity. The bar below indicates the 10 ns evolution of the simulation. See the video 1 at https://www.sciencedirect.com/science/article/pii/S0141813016304287

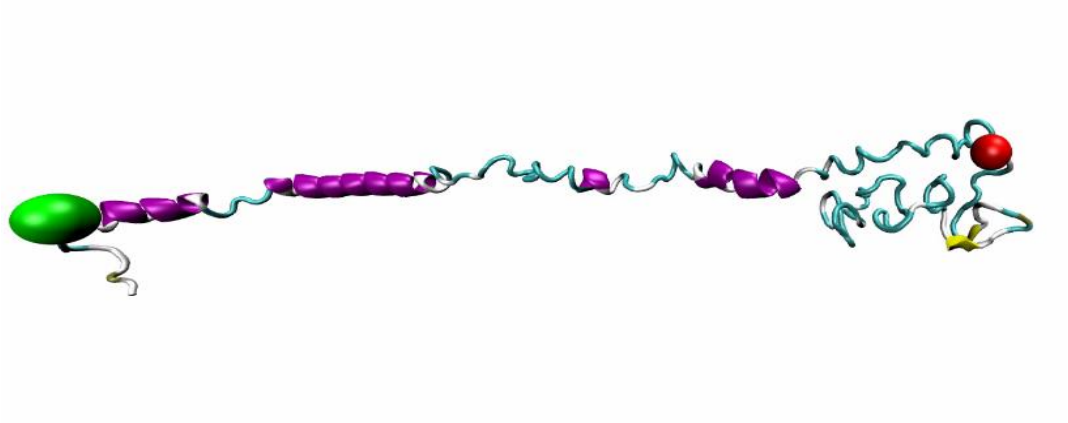

Figure 9: Snapshot of other produced video of the same simulation, but representing only one keratin chain. The green ball points the center of mass fixed during the pulling simulation. The red ball indicates the center of mass where the pulling force was applied. See the video 2 at https://www.sciencedirect.com/science/article/pii/S0141813016304287

Chapter III

Skin Barrier Molecular Dynamics Studies

Overview of molecular dynamics studies about skin lipid barrier function

This chapter is based on the following publication:

Egipto Antunes, Artur Cavaco-Paulo. Skin barrier molecular dynamics studies, *In submission process*, 2018.

Chapter III abstract:

The skin is an organ of the utmost importance, but many times overlooked. Its function of barrier and protection from the external environment is obvious, however it plays major roles in other functions, such as in homeostasis maintenance where it helps in the control of temperature, humidity and blood pressure, and in the external environment sensing.

The major barrier function of skin is usually attributed to its outermost layer, the stratum corneum, due to the presence of keratinized dead cells, the corneocytes, and the lipid matrix that surround these cells that acts as a cement. This arrangement it is often described as a "brick and mortar" model, where the bricks are the corneocytes and the mortar is the lipid matrix. Although the brick and mortar representation of stratum corneum, and the lipidic composition of lipid matrix are consistently describe in literature, the way as these lipids structurally arranged is an active target of debate.

Molecular dynamics simulations have a huge potential to improve this area of research due to its ability to study phenomena at molecular level in a dynamic way. The lack of consensus in the description of the lipid matrix at molecular level significantly limits the application of molecular dynamics in the study of lipid matrix barrier function. There are however a few computational studies were these type of simulations were applied to trying to model the skin, or some skin structures.

In this work we will discuss the known publications using molecular dynamics simulations to study skin. An extensive revision is made, with particular focus on the computational models used to mimic the skin lipid matrix structure, arrangement and dynamics. Finally, our recently developed model with unusual arrangement of lipids is also discussed.

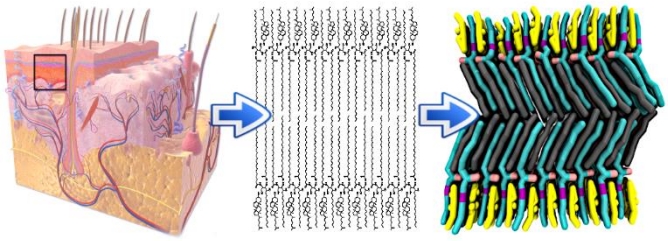

Figure III: Graphical abstract of Chapter III

Introduction

Skin is the outer tissue covering the vertebrates, the largest organ of humans with up to 16% of its body mass and covering an average surface area of 1,6 m^2.[1] The skin and its appendages such as the hair, nails and glands form the of integumentary system.

The mammals survival depends on the skin health, due to its role of interface between the body and the hostile environment, acting in three main scopes, namely: protection, body homeostasis maintaining and sensing of the world. The protection come from its barrier to external dangers as radiation, chemicals and microorganisms. In addition the skin plays a major role on the body homeostasis with the temperature and humidity maintenance, the control of blood pressure and the excretory ability. Finally the skin can sense the heat, the pressure, the radiation and the presence of allergens or microorganisms, which makes it a fundamental organ on sensing the external environment.

The skin is usually considered a multilayer structure, with three main layers (see Figure 1 left): the hypodermis, the dermis and the epidermis (from the deepest to the skin surface).

The hypodermis is a network of fat cells arranged in lobules (the adipocytes) and linked to the upper layer of dermis by collagen and elastin fibers. It acts as heat insulator, shock absorber and energy storage.

The dermis correspond to a hydrophilic layer irrigated by blood circulation. It have a densely network of collagen and elastin fibers (connected also to the bellow hypodermis) forming a gel, which provides mechanical strength to the skin.

The epidermis, the outer layer of the skin, is a keratinized stratified squamous epithelium with around 200µm thick. It have two cell types, the keratinocytes (95%) and the non-keratinocytes, the later constituted by melanocytes (pigmentation), Langerhans cells (immunological function) and Merkel cells (sensory function).[2] The epidermis can be further divided in 4~5 sub-layers or stratum (see Figure 1 right), based on the level of keratinization, namely the stratum basale (the inner layer of epidermis, in the frontier with the dermis also named basal layer), stratum spinosum (spinous layer), stratum granulosum

(granular layer), stratum lucidum (clear layer, only present on zones with thicker skin and without hair) and the stratum corneum (horny layer, the outer layer of the epidermis). In the keratinization process the living keratinocytes from stratum basale differentiate, dye and migrate upward into the stratum corneum (SC). During this process these cells increase its cytoplasm and form filaments and granules. The nucleus, mitochondria and ribosomes disintegrate and the keratinocytes become filed with keratin filaments and bundles. Finally these died, elongated and rich in protein keratinocytes reach the outer zone of the epidermis, and together with the exterior lipid matrix form the SC.[2,3]

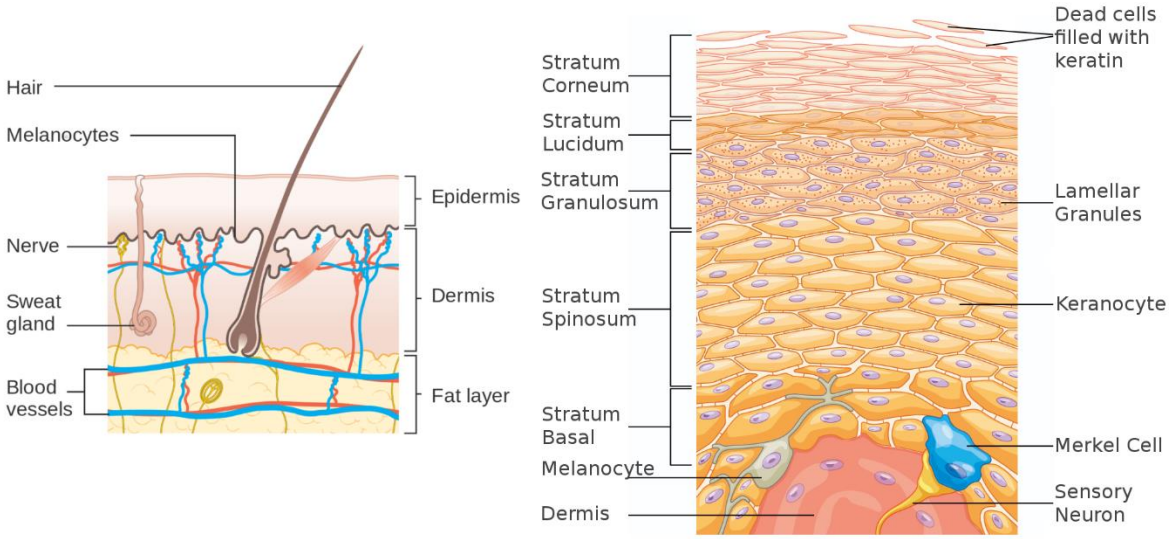

Figure 1: Schematic representation of skin (at left) and stratum corneum (at right) structural organization. Pictures adapted from Cancer Research UK and OpenStax College works under creative commons license.

The SC layer have around 10~40 µm thickness, and is recognized as the major player on the barrier role of the skin.[4,5] The keratinized dead cells off the SC, named corneocytes, are constantly being shed, have a flattened shape with about 30µm in diameter and 0.5~0.8µm in thickness,[6] which allows an organized packing of these cells on SC, without interstices, an arrangement that contributes to its barrier function.[7] Surrounding the corneocytes cells there is a lipid matrix (LM, also called lipid lamellae or intercellular lipids), which is the result of the lamellar granules present on below layers. These lipids are usually described as tightly packed into lamellar sheets, in a number of sheets that may vary within

the same tissue, being responsible by a great part of the SC impermeability and barrier function.[8,9] The SC arrangement of the corneocytes and the exterior lipids is usually referred as the "brick and mortar" model,[10] in which the keratinized cells are considered as bricks and the LM the cement that surround them and helps to fix all the SC structure.

On contrary to most biological membranes, the LM doesn't have phospholipids, being composed mainly by ceramides (CERs), cholesterols (CHOLs) and free fatty-acids (FFAs).[11,12] The recent studies have been reporting the matrix lipid proportion of 1:1:1 M (CER:CHOL:FFA)[13], although different proportions where described in the past[12] what can be the result of the difficulty to remove contamination from the SC to correctly measure the lipid content of the matrix. Skin ceramides differ from others by having great length variation on fatty-acid chains and these chains are generally longer than the sphingosine counterparts.[14] To date, 14 different CER types where identified in human skin that differ in headgroups and acyl chains structures.[15] Among them, the most common CER on skin are the CER NS (also named CER 2, is a combination of Nonhydroxy fatty acid and Sphingosine) and the CER NP (also named CER 3, is a combination of Nonhydroxy fatty acid and Phytosphingosine, see Figure 2).[16,17] Relatively to the FFA fraction in SC LM is essentially composed of saturated and long fatty-acids, being the most common the lignoceric FFA (24 carbons) with 39% molar (see Figure 2).[14]

Although it is consensual that the LM have a lamellar conformation, how that conformation is formed and how is structured at molecular level are still open issues. Landmann postulates that during the keratinocytes differentiation process the lamellar granules extrude its lipid content to intracellular space (in the border of stratum granulosum and SC) in form of disks, resulting in uninterrupted lipid sheets in a bilayer configuration called lamellar body-disks. These disks will fuse each other in the extracellular space and originate the LM of SC.[18] This model was generally accepted by the community, however more recent studies found that lipids extruded by granular cells are also found in other conformations, such as in a cubic phase.[19] In addition the process of lipids lamellar disks diffusion and fusion, as advocated by Landmann, is more energy consuming than just extrude all the lipid content at once. These considerations resulting in the postulation of other LM formation model, the membrane-folding model by Lars Norlén,[20] which states that the

lamellar body is not constituted by discrete vesicles or disks but by a single and coherent tuboreticular membrane network that unfolds its invaginations into the extracellular space forming the LM of SC.

The detailed molecular structure of the LM is also still debated. Most of the works just represent the LM as stacked lamellar sheets, each sheet in a bilayer conformation, as if were stacked cell-membranes.[21–23] This representation is likely resulting from analogies with the most advanced knowledge about cell-membrane lipid organization and phospholipids membranes. However the lipid content in LM and cell-membranes is very different, and the LM picture of stacked bilayers is changing with each new discovered fact. Some works focusing on cryo-electron microscopy pictures of SC provide some clues about this theme.[24,25] It seems to exist an electron pattern with alternation of major and minor bands between corneocytes, leading to the proposal of some models of lipid packing to explain that observation.[19,26,27] Bouwstra et al. suggested the lipids arrangement in a trilayer conformation with the inner one (more rich in CHOL and FFAs) in a fluid phase and the outermost layers in the crystalline state.[28] This model was named “the sandwich model”.

Norlén in 2001 proposed one single phase model of LM, and also address the fact that the CERs in the LM can be in an unusual conformation, namely in splayed chain conformation (with the two alkyl chains pointing in opposite directions).[19] More recently Iwai, Norlén and co-workers proposed a new model of LM molecular organization based on the computational reconstruction of cryo-electron microscopy images.[27] In these models is proposed by the first time that the CERs in the LM are fully splayed and the CHOLs are locate near to the CER sphingoid chains, while the FFAs are in the opposite site near to the fatty-acid moiety of CER (see Figure 2).

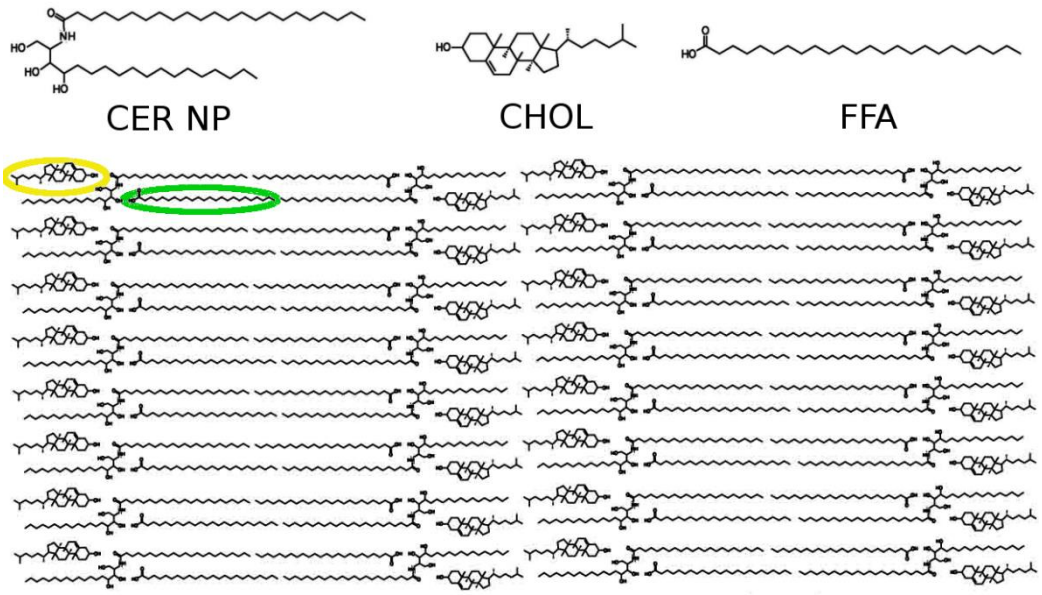

Figure 2: **Top:** Molecular representation of ceramide NP (CER NP), cholesterol (CHOL) and lignoceric free fatty-acid (FFA). **Bottom:** Schematic representation of Iwai suggested model of lipid matrix arrangement. Pictures adapted from Iwai work, one CHOL molecule was highlighted with yellow ellipse and one FFA with green ellipse.[27]

After the discussion of the importance of the skin, from beauty aspects to its barrier function, and all that is still unclear in this field, it is easy to perceive the need of maximize our knowledge about skin structure, composition and organization. Following this urge, several experimental models have been developed, from simple lipid membranes to skin excisions.[1,29,30] One approach that have been gain popularity to study this thematic is the molecular dynamics (MD) modeling. This is likely due to the popularity of this technique in the study of biological cell-membranes, and due to the type of precious data provided, that is hard or even impossible to obtain by other techniques.

In this work it will be discussed the current state of MD studies about the skin, or more precisely about LM barrier. We will present some of the most representatives and valuable MD works with skin lipids, as well the possibilities and limitations of MD approach on the study of the skin barrier function. Finally it will be presented our new and unique MD model of LM, based on the Iwai and Norlén work,[27] with fully splayed CERs. We expect that this new MD model provide a good base for the study of drugs interaction into the skin lipids, contributing to the improvement of the transdermal drug delivery research.

Stratum corneum lipid matrix modeling

Molecular simulations are already common in cell-membranes studies, usually using computational systems of bilayers with a few different cell-membrane lipids (phospholipids, cholesterol, etc.) solvated in water.[31–33] With this approach researchers were able to obtain information and data about cell-membranes, such as structure and mechanical properties, permeation resistance, phase transitions, dynamic properties etc., that proven to agree with laboratory assays.[34] Posteriorly, some researchers begun to take all the knowledge acquire with cell-membrane simulations, from methodology to analysis tools, to apply on the skin LM study. Some even extrapolate results of simulations with membrane models more similar to cell-membranes (composed for phospholipids instead of CERs) to evaluate computationally the transdermal permeability.[35] In this work we focus only in simulation with skin lipids because there are already a significant number of these MD studies, and this kind of system provide a more realistic modeling of skin lipid content.

There is some heterogeneity in the MD studies about the skin and is at several levels such as the type, species and number of lipids; how the lipids are assembled; the hydration level of the systems; the simulation methodologies; and the simulation resolution (fine or coarse-grained). In this work we opted to divide the discussion based in the number of different SC lipids types on the system, namely one lipid systems, two lipid systems and more than two lipid systems.

One Lipid Systems

The simplest computational molecular model representative of skin LM is one CER layer. It was already stated the heterogeneity of lipids in LM, however is generally accepted that the CERs are the principal responsible of the singular SC lipids barrier properties.[36] From our knowledge, the first MD study about SC LM with CERs was reported in 2007. Notman and co-workers used bilayers of CER NS trying to model computationally the mechanisms of interaction between dimethylsulfoxide (DMSO) and skin LM (see Figure

3a).[37] The CER membranes were in a gel-phase at 283 and 323K, and in liquid-crystalline phase at 363K what is consistent with experimental observations of 360K as the temperature of transition between these phases.[38] The authors show that high concentrations of DMSO induce the transition from gel-phase to liquid-crystalline. It was also perceive that at lower temperatures the CER gel-phase presented a orthorhombic arrangement and above 363K the liquid-crystalline phase pack its CERs in hexagonal conformation, agreeing with experimental data.[39] The calculated area per lipid of 0.374nm² at 323K, was also consistent with literature values of 0.378nm².[40] The observed narrow interfacial width together with the high number of hydrogen bonds that the CERs formed with each other, in the simulations of Notman work, provide explanations to the relatively low water permeability of SC. One year later Notman published another work about the DMSO interaction with CER layers.[41] There it was shown that the increase of DMSO concentration decrease the free-energy required to form a pore in the CER layers, what can explain the experimental evidence of DMSO to enhance permeability of SC. Thind et al. performed a similar study, but instead of DMSO they test the effect of ethanol on CER NS layers (see Figure 3b).[42] They simulated CER bilayers in ethanol-water mixtures from pure water to pure ethanol and showed that this alcohol can form water-permeable defects in the CER layers which promotes the extraction of some lipids from the bilayers, a phenomena already described experimentally.[43]

Imai and colleagues compared, by MD simulations, the CER and sphingomyelin bilayers with different acyl chains lengths (from 12 to 18 carbons) at 310K to evaluate the water residence on these membranes.[44] They found that the sphingomyelin membranes retain longer the water molecules at its surface and that the residence time of the water decreases for CERs with bigger mismatch between its two chains. Interestingly, their simulations showed that the chain length increase from 12 to 14 carbons lead to the ordering of lipids on the bilayers. However from 16 to 20 carbons emerges a disordered zone at the bilayer center, which is the result of chains mismatch. This inner zone in a phase more liquid-crystalline than gel was also described in the previous discussed work of Notman, and is consistent with the "sandwich model" of LM arrangement proposed by Bouwstra. CER NS bilayers were also compared with dioleoylphosphatidylcholine (DOPC) bilayers in a 2014 MD work of Paloncýová.[45] The objective of this work was study the effect of the membrane fluidity state (the CER bilayer was at gel-phase and the DOPC was fluid) on the penetration

of drugs. As expected the gel-phase exhibit higher penetration barrier (almost 3 times higher) due to the high ordering of the CER lipid chains.

Akinshina and co-workers tested by MD simulations the effect of monoglycerides and fatty acids on CER NS bilayers.[46] They choose six oils all having 18 carbons in the alcyl chain, but different saturation degrees. When the lipids were placed on the water phase they end up to spontaneously insert into the CER membrane. When these lipids were placed on the membrane from the beginning they were well accommodate by the CERs if its acyl chains is “straight”, otherwise when the acyl chain is unsaturated and present a “kink” the CER bilayers were destabilized and disorganize.

One of the most important condition for the correctly modeling of the component or phenomena to study in simulations is the force-field choice. The force-field include a set of potential functions as well some parameters for each type of particles or group of particles that allows the computationally description of the molecular interactions in the simulation. Accurate development of a new force-field or just the parameterization of a new compound for a given force-field is a demanding task, what lead the researchers to transfer the already described parameters for one compound to another based on the structure similarity. Nowadays all the most used force-fields such as the GROMOS, CHARMM, BERGER, OPLS and the MARTINI, as well the main software's packages of MD, are applied in all imaginable types of simulation systems. However some caution is needed since the force-fields are developed with specific systems or conditions in mind, at least initially, and the transferability of the force-field parameters is not straightforward. This important theme was studied by Papadimitriou et al. in one work where simulations were performed with five different force-fields.[47] The tested force-fields were OPLS, GROMOS, BERGER, CHARMM and GAFF, whereas the simulated systems corresponded to fully hydrated 128 CER NS in a bilayer conformation. Several properties such as bilayer thickness, area per lipid and hydrogen bonds were calculated and although some force-fields presented a slight better performance in predicting certain properties no one have a significant better performance in general. Every force-field gave results agreeing with the experimental data available, and the differences between the calculated numerical properties in different force-fields was less than 4%, what indicates that any off them is able to a satisfactory modeling of the tested systems.

Another important aspect of the MD studies is the molecular resolution used. All the previous discussed works have fine-grained (FG) resolution, meaning that each particle (each bead) of the systems represent one heavy atom (the non-polar hydrogens are not explicit, instead they can be associated to the particle representing the heavy atom in which the hydrogen is bonded). Although all the potential of FG simulations, perceived on the already discussed works, they have the limitation of high computational requirements. In the coarse-grained (CG) resolution each system particle represents more than one heavy atom (usually 4 atoms), what significantly decreases the computational power require to the simulations. Also, the parameterization process is simplified, since there is a small number of bonded and non-bonded terms for each CG molecule. This allows the simulation of bigger or more complex systems and also the increase of the simulated time. However the CG representation of the systems also lead to the loose or weaker representation of some properties dependent of fine interactions. There should exist one compromise between the coarse representation and the level of molecular detail needed to access the properties or phenomena of interest. The MARTINI[48] is a CG force-field widely used in CG simulations, with main incidence on lipid studies.[49] Sovová et al. studied huge CER NS layers with this force-field (the smaller systems had more than 500 CERs, see Figure 3c and 3d).[50] This group also built FG systems of CERs NS, and both resolution systems presented similar values for properties such as the area per lipid and bilayer thickness, although the phase transition temperature between the gel and the liquid-crystalline was around 20K bellow to the experimental value. The liquid-crystalline phase was widely studied on the Sovová work, with the simulations pointing to the stability of this more fluid phase only at high hydration, which later can originate bicontinuous phases mixed with water droplets or tubes depending on hydration level. Finally the CG parameterization of CER NS was able to reproduce both the compact hairpin conformation and also the extended or splayed conformation.

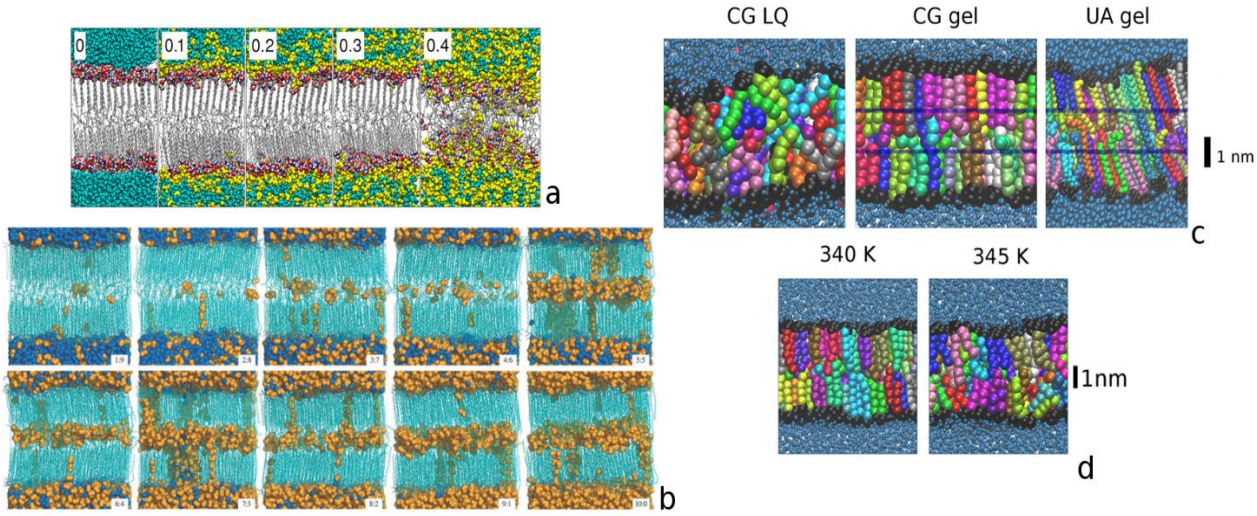

Figure 3: Pictures of CER layers simulations. **a:** Snapshots of CER bilayers with different mol fractions of DMSO (relatively to solvent). It are visible the defects promoted by this solvent. Waters molecules are in cyan, DMSO in yellow, CER tails at gray, CER nitrogens at blue, CER oxygens at red and ceramide hydrogens at withe. Picture adapted from the work of Notman.[37] **b:** Snapshots of CER bilayers in ethanol-water mixture (the ratio ethanol:water is depicted in the pictures), after at least 100ns. The CER molecules are at cyan, the water at blue and the ethanol at orange. Picture adapted from the work of Thind.[42] **c:** Snapshots of CER bilayer simulations at CG (left and middle) and united-atom (UA) resolutions. The CG systems were simulated at 360K (left) showing a liquid phase (LQ) and 300K (middle), showing a gel-phase. The UA was also simulated at 300K (right), showing a gel-phase. **d:** Snapshots of CG CER bilayers just below (left) and above (right) the phase transition. **c and d:** The smaller blue beads correspond to water molecules and the remaining larger beads to CER. Pictures adapted from the work of Sovová.[50]

The CERs are a key element for the unique LM properties, however it cannot be forget that FFAs and CHOLs are also in high quantity in SC. Therefore some authors tried to model the LM in simulations with only FFA lipids. Hadley and McCabe published in 2009 one MD work were they built CG amorphous and crystalline FFA layers to model skin LM.[51] They focus on the CG force-field development to describe FFA, optimizing the FFA CG parameters to accurate describe radial distributions of FG simulations, using the method of Reith, Pütz, and Müller-Plathe.[52]

MacDermaid and co-workers also model SC properties using only FFA lipids, in this case in a multilamellar membranes arrangement.[53] These authors simulated 18 different FG systems of lauric (12 carbons) and behenic (22 carbons) FFAs, varying its relative proportion , the level of protonation of the FFAs and the level of hydration. The number of lipid molecules in each of these simulations was almost 5200, and the waters in the bigger systems

reached the 62000, turning them in the largest systems on FG resolution for the MD study of SC lipid content. The authors chose the FFAs because their carboxyl groups are the only charged headgroups in LM composition and the authors want to study the interaction strength between the FFAs in a multilamellar stack and the water molecules located between the lamellae, and how the protonation state of the FFAs and the ions added to neutralize the systems influence that interaction strength. It was found that the stable multi-layers have both FFA in an ordered phase with its tails tightly packed, and when the separation between the layers is below 1nm multiple regions of contact are formed, with cations chelated by carboxyl groups of adjacent layers. That reorganization of the layers packing was attributed to the minimization of the interfacial tension entropy, which also leads to the formation of water droplets. They propose that the dehydration in SC occurs by intermediate steps where the multiple layers begin to adhere each other locally, in a reversible process.

Until this point the discussed MD works focused on systems with only one type of skin lipids. From our knowledge these were the main MD simulation studies about skin with this type of systems. There are more MD works with only one lipid type systems, but in a context of comparison with mixed skin lipid layers, so these studies will be discussed later.

Two Lipid systems

Surprisingly, the first MD study, from our knowledge, trying to model SC using lipid layers do not used CERs lipids. In 2001 Höltje and co-authors published a FG work with layers composed of FFAs (stearic and palmitic acids, with 18 and 16 carbons respectively) and CHOLs in a 1:1 proportion.[54] The lipid composition choice can seem strange take into consideration the discussed importance of CERs on the LM barrier properties, however the authors just used what was available at the time, namely the FFA and CHOL parameters from MD works about cell-membranes. The objective of the study was unveil the effect of CHOL on FFA bilayers and the simulations showed very ordered layers when only FFAs were presented, at skin temperature. That order was smoothed by CHOL molecules, these lipids seems to introduce large number of *gauche* conformers (conformation with less linear acyl chains) of FFA chains, leading to less ordered bilayers.

Ten years later Hadley and Cabe also studied FFAs and CHOLs lipid systems, but they used CG resolution due to their objective to study the self-assembly of these lipids.[55]

The time scale of SC lipid self-assembly is typically beyond the usual FG simulation times and the ordered phases observed on the skin lipid simulations result in low lipid mobility, requiring longer simulation times to study some properties or phenomena. The authors used its previous developed CG parameters for FFA (discussed in the previous section),[51] and for CHOL[56], however it was hard to obtain lipid layers free of defects through lipid self-assembly. They point the hydrophobic interactions as the main driver of the lipid aggregation while the hydrophilic interactions should direct the remaining self-assembly into structures such as the bilayers. It was also shown that the beginning dispersion of the lipids in water have impact on the final conformation of the lipids aggregates. Finally their simulations of pre-assembled layers were not stable with 12 and 24 carbons FFAs, although the last is the most common FFA on LM. The difficulty to obtain free of defects layers by self-assembly, and the instability of layers with 24 carbons fatty-acids could be caused by the lack of CERs in the simulated systems.

The last work rise an important issue in the LM simulations, namely the initial conformation of the lipids in the simulated systems. Most MD studies of SC lipids use pre-assembled bilayers configurations which may cause bias in the studies due to its possible influence on the subsequent states. Moore et al. also used CG self-assembly simulations trying to avoid this bias, but in this work the simulated systems were composed of CER NS and FFAs.[57] The authors used CG parameterization from their previous work,[58] where they applied the multistate iterative Boltzmann inversion (MS IBI[59]) to optimize the lipid radial distribution. Although they already performed some self-assembly simulations in the old work, the systems used for these simulations were composed only by CERs. In the more recent work were built disordered lipid systems that evolved to bilayer and multilayer conformations with the simulated time. The resulting structures shown properties consistent with FG studies and experimental data, and suggested that the CERs are presented in SC layers in both extended and hairpin conformations.

There are more MD works with two skin lipid type systems, however these systems were built in studies with mixed lipid composition systems to compare layers properties, therefore they will be discussed in the next section.

More than two Lipid systems

The simulation of simple lipid systems, with one or two types of skin lipids, in a tentative to correctly model skin SC lipid properties, provided valuable information, as discussed in previous sections. A realistic computational representation of the complex LM molecular composition is beyond current computational capabilities, however the lack of one of the three main LM lipids may result on systems that cannot correctly reproduce properties or phenomena of SC. Systems with three or more different lipids, in a multilayer conformation are feasibly to simulate in acceptable times with the current computational power. Anyway the firsts attempts to model SC with three lipid system were made by Das et al. in 2009.[5,60]

Das and co-workers perform initially several simulations of fully hydrated layers with different proportion of CER NS, CHOL and FFA (24 carbons). The molecular proportion in the systems vary from 0 to 7 for CER lipids, from 0 to 2 for CHOL and from 0 to 1 for FFA.[5] They studied systems with only one type of lipid, with two types and with the three main types of LM lipids in a tentative to be able to discriminate the individual effect of each lipids in the mixed layers. Was observed an interdigitation of CER longer chains at bilayer mid-plane, as described previously in the works about CERs layers,[37,42,44] as well the increase of in-plane density promoted by the CHOL that promotes lateral stress, which is relieved when the FFA lipids are presented. They also found that the hydrocarbon densities in these bilayers were quite larger compared to phospholipids bilayers, what explain the smaller water permeability of the SC LM.

In a contemporaneous work Das et al. calculated the water permeability in pure CER bilayers and in bilayers of CER NS, CHOL and FFA (24 carbons) with 1:1:1 or 2:2:1 molar ratios.[60] They found a nearly twice higher chemical potential barrier for SC bilayers comparing with phospholipids bilayers simulated with similar force-fields, at the same temperature. The estimated permeability was almost five orders of magnitude smaller than the permeability stated for DPPC bilayers simulations. The calculated free-energy profile correlated well with lipid density in the simulations, pointing that the higher free-energy barrier is due to the dense packing of CERs acyl chains, which can be due to the non-existence of charged head groups in CERs like in phospholipids in which some local repulsion is

promoted. Also interesting, was the observation that once a water molecule is inside hydrocarbon region of bilayers it moves more easily, without large extra free-energy costs along the orientation of the lipid chains. However the same is not true to perpendicular direction where the diffusivity is decreased by two orders of magnitude. This is another consequence of the high degree of hydrocarbon chains packing and order.

Chinmay Das continued to study the SC LM using MD simulations increasing into complexity, being an author of reference on this field. In 2013 Das and colleagues performed large scale FG simulations with approximately 6000 lipid molecules and 50000 waters, and reaching microseconds time scales.[61] The molar proportions of lipids (CER:CHOL:FFA) used were the usual 1:1:1 or 2:2:1, however they used three types of CERs, namely the CER NS, the CER NP and the CER EOS (also named CER 1, that has an additional linoleic acid conjugated to the fatty-acid tail) and also vary the number of carbons on the CER fatty-acid tails of each CER type, as well the number of carbons of the FFA portion. The simulations of these different lipid systems in water shown a tendency to form inverted micelles. In the same work the authors used an artificial CER layer to model the corneocyte bound lipid envelope. The corneocytes in mammalians are surrounded by a layer of ceramides with its fatty acid termination covalently bonded to the protein network of these cells. The authors wanted to study if this CER layer surrounding the corneocytes have impact on the assembling of LM, and they observed that SC lipids are induced to form layers by the wall that mimics the corneocyte lipid envelope. It was suggested that these findings explain the addition of sugar group of CERs when they are on stratum granulosum, otherwise the lipids would form inverted micelles and avoid their release to SC. Once the sugar is removed in SC, the lipids can form inverted micelles when in water rich regions, or form layers in dry regions, something that is also promoted by the corneocyte lipid envelope.

Later, Das studied the flip-flop of CHOL in double bilayers systems (with molar proportion of 2:2:1 of CER:CHOL:FFA see Figure 4a).[62] They found that the transfer of CHOL lipids between leaflets is orders of magnitude faster than in fluid phospholipids, which may lead to a reduced of curvature elastic cost of lipid multi-layers bending that can enhance the flexibility and energy absorbing effects of SC, explaining some skin properties.

More recent, the same author published a very complete work merging all the accumulated knowledge about the theme, trying to study questions such as the role of the different lengths of CERs tails, the role of CERs headgroup heterogeneity, the effect of CERs polydispersity in their fatty-acid chains and finally the role of long tailed CER EOS on SC lipid multi-layers.[63] The simulations shown that the asymmetry and tail polydispersity enhance the tail interdigitation in the mid plane of the multi-layers and the hydrogen bonds of CERs headgroups have little or no impact in the size of hydrogen bonded lipid clusters present in the layers. In addition the CER EOS reduce the tail ordering and remains in a single bilayer, contrary to other works,[64] however this may be consequence of the methodology used, as well the initial configurations used.

Most of the MD studies about SC rely on systems with lipids ratios similar to the ones described experimentally for normal skin. There is, however, some heterogeneity in the lipid composition of skin SC dependent of several conditions of the subject, such as its age, its state of hydration or its health. Huzil and counterparts addressed this question and studied four different ratios of CER NS, CHOL and FFA (lignoceric and stearic acids, with 24 and 18 carbons respectively) which represent different skin states, namely aged skin, young dry and young normal skin, and equimolar proportion.[65] The CERs and FFAs are the lipids with most significant variation on its proportion for the different skin states. In this work simulations, the FFAs were crucial to the formation of densely packed layers suggesting that the differences of FFAs composition may influence significantly the permeability of SC on the different skin states. The lateral diffusion of the lipids was inversely proportional to the hydrogen bonds between CERs and CHOLs, which decreases with the FFAs concentration increase, like happen on aged skin model.

Skin diseases such as atopic dermatitis, psoriasis and ichthyosis seem to be related with the increase of CERs with short fatty-acid chains (with 16 carbons) and the decrease of the typical skin CERs with longer chains (24 carbons),[21,66,67] that leads to the increase of water loss and the decrease of protection to external elements like allergens or xenobiotics. Paloncýová and co-workers addressed these questions in 2015 on a very complete MD work.[68] The authors built several bilayers with different compositions, they varied the CER NS fatty-acid chain length from 0 (corresponding to a sphingosine, see Figure 4b) to 24

carbons in FG and CG resolution (they used the MARTINI parameters from the previous discussed Sovová work[50]). Although they focused on the effect of CERs fatty-acid lengths on the skin lipid membranes they also simulated bilayers of FFA (lignoceric acid, with 24 carbons), bilayers of FFA and CHOL, and bilayers of CER, FFA and CHOL in a proportion of 1:1:1. Regarding the CER membranes they found that its thickness depends off the chain length, the bilayers off CERs with 6 or 8 carbons chains presented the lower thickness, and the lowest level of ordering, while its areas per lipid were high. However the effect of short CER chains is less significant on mixed systems (the ones with FFAs and CHOLs). In any case the bilayers with short-chain CERs presented higher permeability, which was explained by the tendency, observed on the simulations, of these shorter chains to stay more at membrane headgroup region, instead of the inner zones of the membrane, as happen with the longer chains. These results are consistent with the previous stated relation between skin diseases and the higher content of short-chain CERs in the skin patients.

Recently, Moore et al. also studied the effect of CER tail length on bilayer representatives of SC.[69] The simulations shown that the lipid conformation, at water-lipid interface, changed with lipid composition variation but do not changed with CER fatty-acid chain length. The hydrogen bonds between water-lipid and lipid-lipid were similar, with together to the previous observations suggested that possible variations of permeability in the model membranes are caused by changes in hydrophobic core of the layers structure.

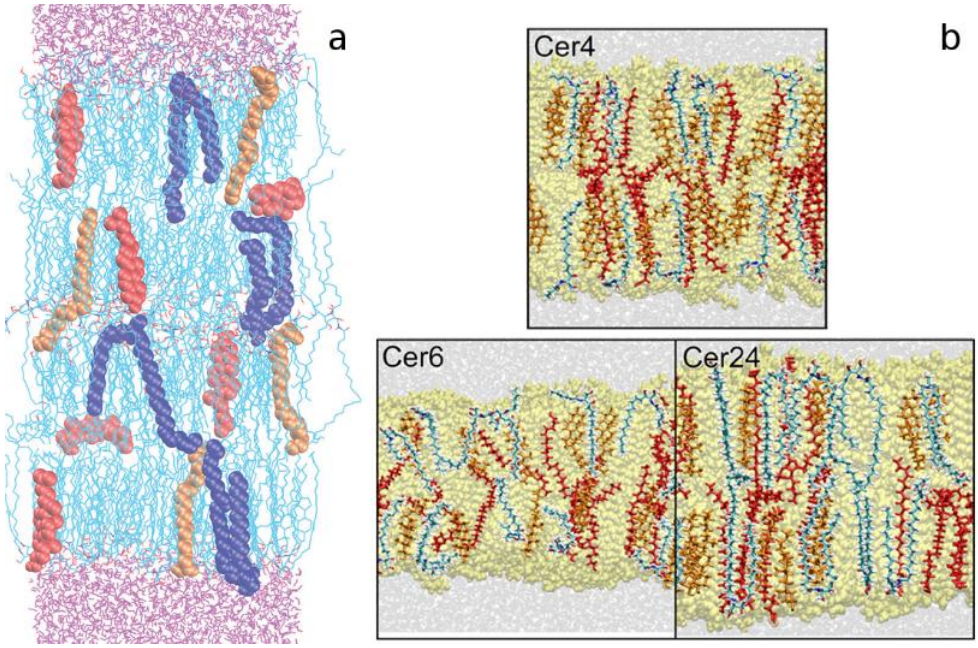

Figure 4: Snapshots of simulations of lipid layers with the three main lipids composing the skin LM, namely the CERs, CHOLs and FFAs. **a:** double bilayer (cyan sticks and colored beads) in water (magenta sticks). Some lipids are highlighted, the CERs at blue, the CHOLs at red and the FFAs at orange. Picture adapted from the work of Chinmay Das.[62] **b:** Snapshots of CER, CHOL and FFA bilayers simulations. The number of carbon atoms on the CER acyl chains was vary and is indicate at the pictures (Cer4, Cer6 and Cer24). The water molecules are represented as light gray beads, the lipid content as light yellow. Some lipids are highlighted in licorice representation, being the CERs cyan, the CHOLs orange and the FFAs red. Pictures adapted from Paloncýová work.[68]

Gupta and colleagues published one complete study about the molar ratio variation effect at wide temperature range (300-400 K).[70] Several systems were built, from only CER NS, CHOL and FFA (24 carbons) layers to mixed systems with ratios of 1:1:1, 1:0:1, 1:1:0 and 2:2:1 of CER:CHOL:FFA. The authors found that CER layers were at hexagonal gel phase at physiological temperature, which gets converted to liquid-crystalline phase at around 365K, and the CER tails interdigitate forming a more fluid environment at layer mid-plane. These observations are consistent with previous discussed works.[37,44] It was also found that the FFAs induce more interdigitation and more CER tails order. The CHOL molecules were located in the interior region of the lipid layers, and stabilized the layers at higher temperatures. In addition the CHOLs seemed to decrease tails order on mixed systems bellow phase transition temperatures, while increase that property in mixed systems at

temperatures above phase transition. The CHOLs also increased the area compressibility of bilayers contrary to FFA lipid effect.

The FFA fraction in SC is mainly composed by saturated fatty-acids, however unsaturated FFAs also exist, but at low concentration. The effect in SC of oleic acid, one unsaturated fatty-acid with 18 carbons, was studied by Hoopes and co-workers using bilayers with equimolar portions of CER NS, lignoceric FFA and CHOL.[71] The addition of unsaturated fatty-acid do not promoted significant impact on bilayer thickness neither on hydrogen bonding, however the carbon density at bilayer mid-plane decreased. Interestingly, the addition of oleic acid promoted the CHOL diffusion which in turn also increased CER and FFA diffusion on simulations.

The transdermal drug-delivery is likely the utmost goal of most of the researchers that study skin and its components, either in laboratory or *in-Silico*. The majority of the discussed studies in this work focus on the evaluation of the lipid layers simulated to check if they correctly model skin LM properties and to obtain some insights about it. With the increasing of robustness of the models the researchers are now more focused on the study of drugs, or other compounds, permeation into the SC models. There are now several examples of MD studies focusing on SC permeability. Azoia, for example, built a SC model composed by CER 2, CHOL, lignoceric FFA and CHOL sulfate with ratio portions based on young normal skin, in a configuration of double bilayers, which was used on three permeation studies. One about the permeation of nanoformulations,[72] other about ascorbyl tetraisopalmitate permeation, [73] and another about retinyl acetate permeation.[74] These three studies have laboratory and *in-Silico* parts, and the simulations shown consistent results with experimental assays. Gupta in turn studied the permeability of gold nanoparticles on skin, showing that the neutral nanoparticles penetrate into lipid bilayer (CER NS, lignoceric FFA and CHOL at equimolar ratios) interior, while the charged versions adsorbed on the surface in the simulated systems.[75]

There are some compounds, such as DMSO, which are able to enhance the skin permeability. Furthermore, menthol is described as having this property.[76] The menthol ability of skin permeability enhancement was studied by CG simulations of mixed lipid bilayer systems as SC model.[77] Wan et al. used CG bilayers of CER NS, lignoceric FFA and

CHOL as LM model systems (2:2:1 molar ratio), and added menthol molecules at mass concentration from 0 to 60%. The menthol molecules shown great affinity with lipid tails, and some affinity with the headgroups, led to a more fluid state of the layers and strongly destabilized the membrane at concentrations superior of 30%. The enhancement of skin permeability promoted by menthol is suggested, in this work, to be caused by the complete mixing of menthol molecules with SC lipids, which can fluidize and destabilize the skin barrier, contrary to other enhancers such as DMSO that seem to promote water pore formation (as discussed previously).

The discussed studies about skin permeability of several compounds are valuable, but were made only qualitative evaluations of the permeability, there are however some interesting studies were the authors applied steered MD simulations to be able to calculate the diffusivity and permeation of molecules. In these simulations it is applied one pulling force into the molecule to oblige it to cross the lipid layer, which allows the calculation of the potential of mean force for the molecule and consequently its diffusivity and permeation. Del Regno and co-workers applied this methodology to discover the water diffusivity and permeation on bilayers representatives of SC LM (CER NS:CHOL:FFA (24 carbons) at 1:1:1 and 2:2:1 ratios), at two different levels of hydration.[78] The authors used lipid systems at natural SC hydration level (two bilayers initially separated by a small region of water) and at water excess (one bilayer with big water regions at the top and the bottom). The simulations of the lipid layers showed the formation of heterogeneous mixture, with CHOL rich regions, for fully hydrated systems, while the lower hydrated systems presented an uneven distribution of water molecules, with the water concentrated in some ellipsoidal spots allowing direct contact between lipids of adjacent bilayers in the dry zones. The steered simulations shown that the water molecule permeation trough the layers is dependent of the lipid composition in the region that the molecule is crossing, and is facilitated in CHOL rich regions. The lateral diffusion of water molecules in the interior of the lipid membranes was high, and was similar in both fully and lower hydrated systems. Finally, the authors proposed a model of water permeation into LM that explain the transepidermal water loss, and the high barrier to water permeation found on SC MD studies (see Figure 5c). It was suggested that the water molecules could reach the interior of one lamellae in CHOL rich zones, and can

diffuse laterally until find another CHOL rich region. If that region is facing another CHOL rich spot in adjacent layer, it may allow the crossing of the water molecule between the layers.

Steered MD simulations were also used in another work of Gupta and collaborators for the permeability coefficients calculation of water, oxygen, ethanol, acetic acid, urea, butanol, benzene, DMSO, toluene, phenol, styrene and ethylbenzene on bilayers of CER:CHOL:FFA at equimolar portions (see Figure 5a).[79] The main penetration barrier for hydrophilic molecules was the interior of bilayer, whereas the hydrophobic molecules have more difficulty to cross the lipid-water interface. The calculated values were generally 1~2 orders of magnitude higher than the experimental values for hydrophilic molecules, while for the hydrophobic counterparts the calculated permeability was very much higher than experimental values.

The potential of mean force calculation after the steered MD simulations is a computational demanding task, since requires the execution of several small simulations for each compound of interest. Paolo Rocco and colleagues used alternative procedure to be able to calculate the skin permeability of 80 different molecules through MD.[80] In this work the potential of mean force calculation was substituted by physicochemical and structural descriptors such as polar surface area, surface and partition coefficient, which allowed the calculation of diffusivity and permeability. Interestingly, although this work used usual lipid composition of the systems models of LM, namely CER (CER EOS and CER NS at 25:75 molar percentage), CHOL and FFA (lignoceric acid) at equimolar ratio, the arrangement of lipids was different from all other discussed works. The lipids were initially arranged basing in the Iwai work (discussed in Introduction, see Figure 2) with CERs in the extended conformation. Although the unusual choice of structural arrangement of lipid layers to model skin LM, the authors do not discussed this choice on their work, it is even imperceptible if the lipids maintained the conformation that Iwai suggests. Relatively to the work focus, the researchers found that its methodology is more useful in clarifying the interactions between the molecules and the lipids, instead to reliably predict the molecule permeability, despite they had correlated the permeability coefficient with averaged physicochemical properties improving semi-empirical methods available.

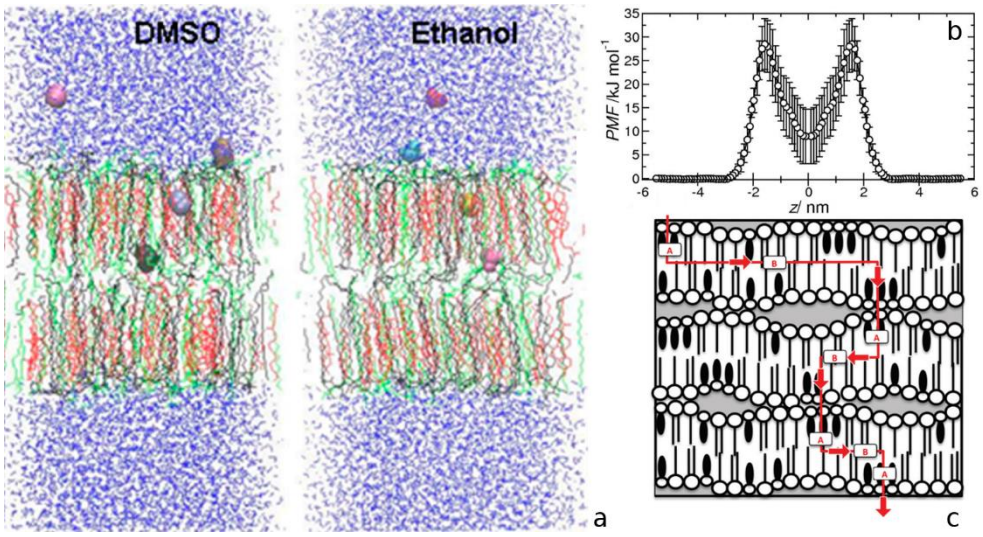

Figure 5. **a:** Snapshots of steered MD simulations with several positions of the permeating molecule represented in the same view. The waters are represented as purple sticks, the lipids as sticks (CERs at gray, CHOLs at red and FFAs at green) and the permeating molecules as big beads. Pictures adapted from the work of Gupta.[79] **b:** Typical potential of mean force profile for steered simulations of one water molecule crossing a LM bilayer. The two peaks presented are for the interface water lipid region. **c:** Proposed pathway for the permeation of small polar molecules through SC lipid layers. The CERs and FFAs are represented by circles with two (CERs) and one (FFA) lipid tails. The CHOLs are represented as smaller circles with black ellipses. The A correspond to the permeation between different layers in CHOL rich regions, and the B to the lateral diffusion along the bilayers inner zones. **c and d:** Pictures adapted from the work of Del Regno.[78]

Gajula and collaborators also used steered MD simulations and the potential of mean force in the calculation procedure of skin permeability of compounds, but in a multiscale methodology.[81] In this work the diffusion was obtained through the MD simulations and the calculated values were used posteriorly in macroscopic models to predict the drug release profiles through SC. For the MD simulations the authors used CER NS, CHOL and FFA (24 carbons) bilayers at equimolar ratios to model the LM, and the molecules that were forced to cross the bilayers were naphthol, caffeine and fentanyl. The diffusion calculated was consistent with experiments, as well as the final drug release profiles obtained.

Recently developed models, with splayed Ceramides

The correct arrangement of lipids into the LM structure is not yet fully understood. This lack in skin structural knowledge led the researchers, which want to model the SC lipid content through MD simulations, to use the traditional bilayer format that coming from cell-membranes MD studies, or to use arrangements resulting from self-assembling simulations.

Recently, in our group we developed a lipid model with a unique conformation of its lipids, which tries to mimic the Iwai suggested model of lipid packing in LM (see Figure 6).[82] The previous discussed work of Rocco already used lipid layers based on the Iwai model, however the arrangement of lipids presented on the work seemed differ significantly from the Iwai model and the authors do not discussed this thematic. In our model the lipid composition is also based on the Iwai work, with CER NP, CHOL and lignoceric FFA at 1:1:1 molar ratio. The system is in CG resolution to allow the sampling of longer times and bigger systems. The differentiation factor of this new model is the fact that the CERs are in fully extended conformation, with CHOL molecules near its shorter chains, the sphingoid chains, and the FFAs stay near the longer acyl chains of CERs (see Figure 6).

The simulations with MARTINI force-field at physiological temperatures shown that the unusual conformation of the lipids is very stable but dependent of the initial arrangement. The arrangement proposed by Iwai is maintained in the several simulations performed, even when another molecules such as Nile Red, poly lactic acid and poloxamer are included in the simulated systems, or during steered MD simulations.

The self-assembling simulations with the same molecular composition, however, resulted in disorganized systems, showing that it is necessary an initial imposition for the lipids arrange into that unique form. It should be noted that the formation of the LM continue to be a debatable issue, as was discussed on Introduction section with two presented models of LM creation, and in addition the Chinmay Das simulations with CERs mimicking the corneocyte lipid envelope shown that this structure may induce the formation of layers in LM. These facts suggest that the necessary initial imposition of the lipid structure to present that unusual conformation can also occur in the nature explaining the Iwai work results and why in all MD studies the lipids do not self-assemble into this configuration.

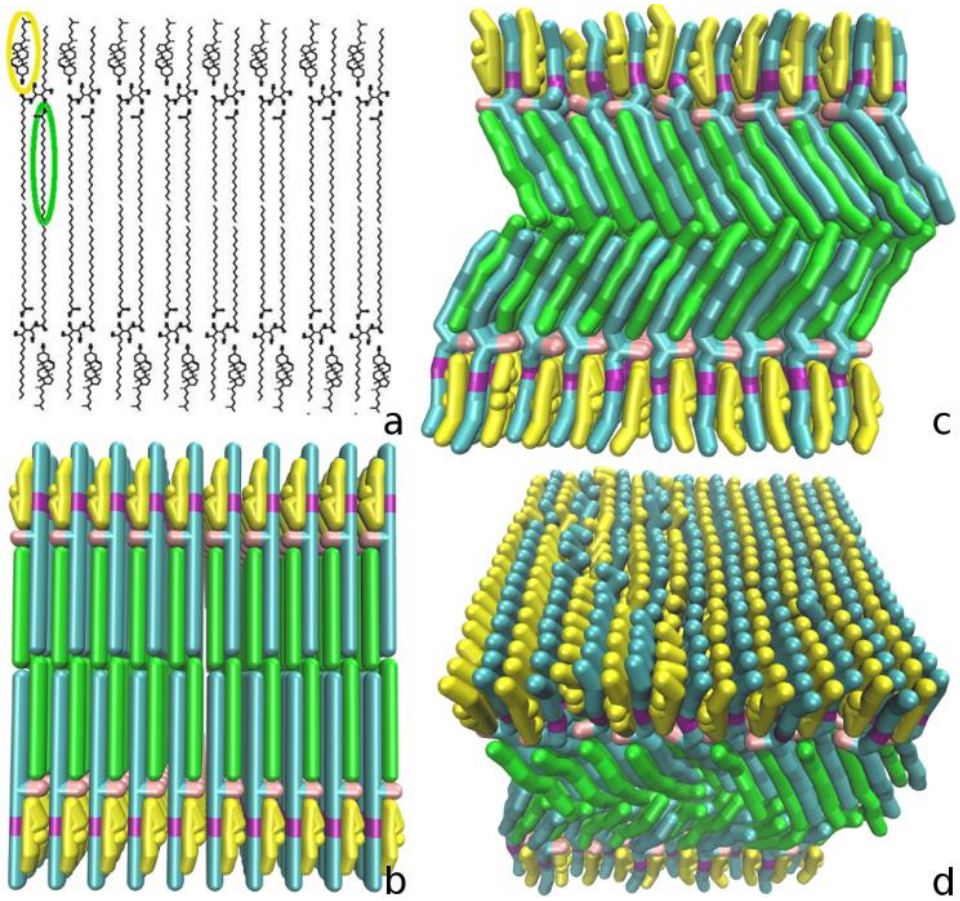

Figure 6: **a:** Iwai suggested model of bilayer lipid arrangement in the SC LM. One CHOL molecule was highlighted with yellow ellipse and one FFA with green ellipse. Picture adapted from Iwai work.[27] **b:** Initial structure of our recently developed model based on Iwai suggestion, the CERs are colored in cyan, the CHOLs in yellow and the FFAs in green. The same model after 600ns of simulation is show at front view (**c**) and inclined view (**d**).

The simulations with the new model shown that this type of packing results in a very compact and ordered structure with very low diffusion of the lipids, which provide a high and effective lipid barrier that even lipophilic compounds have difficulty to penetrate (see Figure 6c and 6d). Steered MD simulations presented energetic profiles consistent with these observations, with high potential energy barriers to the penetration and to the crossing of some regions of the model layers. The higher barriers are in the interface water-lipid, and in the crossing of the region were CERs headgroups are located.

Lundborg, Wennberg, Narangifard, Lindahl and Norlén published recently four articles about skin LM with MD simulations.[83-86] In two of them they focused on the

development of a LM model and in the prediction of the skin permeability of drugs.[83,84] The model applied in these two works was also based in the Iwai suggested lipid packing with splayed ceramides. However it have atomic resolution and they changed the composition, added CER EOS and also changed the lipid packing to better mimic cryo-electron microscopy images of skin SC samples. According their results the best model to fit with the microscopy images is the one composed of CER, CHOL and FFA at 1:1:1 (molar ratio) with 5% of the CER content being CER EOS, and 75% of CHOLs near to the sphingosine chains of CERs.[83] The model was able to predict permeability properties for compounds such as benzene, dimethyl sulfoxide, ethanol, codein or nicotine, that are compounds know by their potential to increase TD, providing also clues about how the mechanisms of action of these compounds in LM that improve TD.[84]

The other two works focused more in the process of LM formation, and point to that this barrier formation occurs via a cubic to lamellar lipid phase transitions.[85,86]

The results of our work and from the last four works discussed, suggests that the completely splayed CERs configuration, as well the preferential division of CHOLs and FFAs by the two CER chains should represent a more accurate description of the molecular arrangement of the LM, and in consequence will allow a better modeling of this lipidic barrier properties.

Discussion and Future Perspectives

The overview of the available studies about skin lipid barrier properties using MD simulations is demonstrative of the type of valuable and unique data that this technique can offer, showing its potential in the increase of LM fundamental knowledge as well in the development of systems for transdermal drug-delivery. There are however some open questions in LM knowledge, and the topics that seem more important to focus, at the moment, to further increase the potential of the LM study through MD simulations are summarized next:

Lipid Composition

The lipid composition of LM is not a theme with much debate in the literature, however in the simulations the modeled systems have low heterogeneity, which may neglect a correct modeling of some LM properties. As always in MD studies, should exist a balance between the modeled system complexity and the interest properties to study, and although the lipid composition of three or more lipid type seem logical more studies are needed to unveil important questions such as how the composition affects the lipid assembling or the permeability of the layers.

Molecular scale lipid assembling

The way as the LM content assemble at molecular level is not yet well understood. Several models, either in experimental and *in-Silico* works, were already suggested, from bilayers configurations to disordered lipid mixtures, with CERs in hairpin or splayed forms, with or without water at stacks interfaces, with more ordered or more disordered chains, etc. MD studies have lot of potential to solve some questions about the molecular assembling of the lipids, and although many of the discussed works also addressed these questions more work is needed to achieve a more realistic model which can be used more generally in MD studies. Our work,[82] together with the more recent MD works about the LM,[83-86] favor the description of LM layers with splayed CERs, with CHOL predominantly located near the sphingosine chain of CERs.

Higher scale lipid assembling

This point is related with the previous, since the molecular level arrangement will influence the higher level assembling, however was poorly studied through simulations. Most of MD studies about SC used systems with only one bilayer stack of LM lipids, however it is known that the LM is composed by multiple stacks. The presence of several layers in the simulated systems impact negatively in the computational costs of the simulations, however some properties may need bigger systems to be correctly sampled in the simulations, such as the formation of lipid domains, the correct phase transition temperatures, the possibility of the CERs to conform into splayed configuration etc.

MD simulations methodologies and Force-Fields parameters

The development of force-field parameters for skin lipids have been addressed in many of the discussed studies, mainly for CERs, and although the authors considered the parameterization valid it may be improved. The parameterization have impact on the previous points, and can help to solve questions such as the conformation of CERs in the LM layers. In turn the impact of MD simulation protocol is not an active theme of study. Aspects like the impact in the simulation results of the chosen electrostatic representation scheme, the type of pressure bath and pressure chosen, among others should be target of study. In addition more benchmark studies about force-fields and MD protocol parameters are needed to improve the correctly modeling of LM.

Like in any other technique there are some limitations of MD simulations. Apart the limitations in size and simulated time, which are common to all MD works, the more noticeable limitation of the discussed computational studies is the initial structure uncertain. The MD simulation is an ideal tool to study the interactions at molecular level of the LM molecules, however the correct assemble of the lipids may be hard to obtain. We discussed some studies with self-assembling simulations of the LM content, however the obtained configurations may not correctly represent the structural arrangement of the lipids in real SC. This happen because could exist high energetic barriers during the process, that the simulations are not able to sample. In addition could exist an initial structural imposition as discussed previously.

Relatively to the future of this field it is expected the solving or improvement of the previous described points, resulting in better models, better force-field parameters and better MD methods. The modeling of the LM barrier function should continue to increase in reliability, and with this another questions should appear. There are already some studies with MD simulations that try to obtain insights on transdermal of some compounds without the traditional use of lipid layers systems. Instead the authors used skin keratins filaments as representation of the proteinaceous environment of corneocytes interior.[87-89] Machado and co-works also raised an interesting point when used a layer with cell-membrane lipid composition to model the transdermal permeation of one molecule through the skin hair

follicle infundibulum region.[73] The infundibulum is an epithelial region on hair follicle bulb, that is many times stated as be more permeable to transdermal drug-delivery due to its lower keratination level.[90] This work, the work of Chinmay where is addressed the question of corneocyte lipid envelope, and the works with keratin proteins shows that the future of the study of skin barrier function by MD simulations should pass by an integrative and multi scale approach where several points are in equation. Although the principal focus can be maintain into LM, aspects as the potential of some drug to interact with corneocyte, or its proteinaceous material, the region and type of skin were the drug is added, the influence of corneocytes lipid envelope, between other, are needed to be taken into consideration, to a full comprehension of the drug potential to permeate the skin.

Conclusions

This document present an extensive overview about the MD studies of skin LM and its impermeable barrier function. The discussed work results are self-explanatory of the huge potential of this computational technique to study the LM at molecular level, even take into consideration its inherent limitations and the lack of consensus on the molecular lipid arrangement in the SC.

The number of MD studies in this field is much lower than in the study of cell-membranes, showing that the use of this technique in the skin area is yet in its infancy phase. This situation will likely change with the time, and the researchers will take more advantage of the MD potential.

We expect that our recently developed LM model be a step on that direction, improving the skin barrier research.

Acknowledgments

We want to thank the access of Minho University “SeARCH” ("Services and Advanced Research Computing with HTC/HPC clusters") cluster. We also thank the Portuguese Foundation for Science and Technology (FCT) for providing the grant for part of Egipto Antunes PhD studies (scholarship SFRH/BD/122952/2016), and to Tarsila Castro for its advices and text revision.

References

[1]. Limbert, G. Mathematical and Computational Modelling of Skin Biophysics: A Review, *Proc. R. Soc. A Math. Phys. Eng. Sci.,* 2017, 473, 20170257.

[2]. Monteiro-Riviere, N. A. *Toxicology of the Skin*; CRC Press, 2010.

[3]. Freinkel, R. K.; Woodley, D. T. *The Biology of the Skin*, CRC Press: London, 2001.

[4]. Wertz, P. W.; van den Bergh, B. The Physical, Chemical and Functional Properties of Lipids in the Skin and Other Biological Barriers, *Chem. Phys. Lipids,* 1998, 91, 85–96.

[5]. Das, C.; Noro, M. G.; Olmsted, P. D. Simulation Studies of Stratum Corneum Lipid Mixtures, *Biophys. J.,* 2009, 97, 1941–1951.

[6]. Holbrook, K. A.; Odland, G. F. Regional Differences in the Thickness (Cell Layers) of the Human Stratum Corneum: An Ultrastructural Analysis, *J. Invest. Dermatol.,* 1974, 62, 415–422.

[7]. Menton, D. N. A Minimum-Surface Mechanism to Account for the Organization of Cells into Columns in the Mammalian Epidermis, *Am. J. Anat.,* 1976, 145, 1–22.

[8]. Scheuplein, R. J.; Blank, I. H. Permeability of the Skin, *Physiol. Rev.*, 1971, 51, 702–747.

[9]. Elias, P. M. Lipids and the Epidermal Permeability Barrier, *Arch. Dermatol. Res.,* 1981, 270, 95–117.

[10]. Michaels, A. S.; Chandrasekaran, S. K.; Shaw, J. E. Drug Permeation through Human Skin: Theory and Invitro Experimental Measurement, *AIChE J.,* 1975, 21, 985–996.

[11]. Norlén, L.; Nicander, I.; Lundh Rozell, B.; Ollmar, S.; Forslind, B. Inter- and Intra-Individual Differences in Human Stratum Corneum Lipid Content Related to Physical Parameters of Skin Barrier Function in Vivo, *J. Invest. Dermatol.,* 1999, 112, 72–77.

[12]. Weerheim, A.; Ponec, M. Determination of Stratum Corneum Lipid Profile by Tape Stripping in Combination with High-Performance Thin-Layer Chromatography, *Arch. Dermatol. Res.,* 2001, 293, 191–199.

[13]. Philip, W.; Lars, N. *Skin, Hair, and Nails: Structure and Function*, CRC Press: New York, 2003.

[14]. Norlén, L.; Nicander, I.; Lundsjö, A.; Cronholm, T.; Forslind, B. A New HPLC-Based Method for the Quantitative Analysis of Inner Stratum Corneum Lipids with Special Reference to the Free Fatty Acid Fraction, *Arch. Dermatol. Res.,* 1998, 290, 508–516.

[15]. Rabionet, M.; Gorgas, K.; Sandhoff, R. Ceramide Synthesis in the Epidermis, *Biochim. Biophys. Acta*, 2014, 1841, 422–434.

[16]. Farwanah, H.; Raith, K.; Neubert, R. H. H.; Wohlrab, J. Ceramide Profiles of the Uninvolved Skin in Atopic Dermatitis and Psoriasis Are Comparable to Those of Healthy Skin, *Arch. Dermatol. Res.,* 2005, 296, 514–521.

[17]. Ponec, M.; Weerheim, A.; Lankhorst, P.; Wertz, P. New Acylceramide in Native and Reconstructed Epidermis, *J. Invest. Dermatol.,* 2003, 120, 581–588.

[18]. Landmann, L. Epidermal Permeability Barrier: Transformation of Lamellar Granule-Disks into Intercellular Sheets by a Membrane-Fusion Process, a Freeze-Fracture Study, *J. Invest. Dermatol.,* 1986, 87, 202–209.

[19]. Norlén, L. Skin Barrier Structure and Function: The Single Gel Phase Model, *J. Invest. Dermatol.,* 2001, 117, 830–836.

[20]. Norlén, L. Skin Barrier Formation: The Membrane Folding Model, *J. Invest. Dermatol.,* 2001, 117, 823–829.

[21]. Janssens, M.; van Smeden, J.; Gooris, G. S.; Bras, W.; Portale, G.; Caspers, P. J.; Vreeken, R. J.; Hankemeier, T.; Kezic, S.; Wolterbeek, R.; *et al.* Increase in Short-Chain Ceramides Correlates with an Altered Lipid Organization and Decreased Barrier Function in Atopic Eczema Patients, *J. Lipid Res.,* 2012, 53, 2755–2766.

[22]. Bouwstra, J. A.; Gooris, G. S. The Lipid Organisation in Human Stratum Corneum and Model Systems, *Open Dermatol. J.,* 2010, 4, 10–13.

[23]. CHA, H. J.; HE, C.; ZHAO, H.; DONG, Y.; AN, I.-S.; AN, S. Intercellular and Intracellular Functions of Ceramides and Their Metabolites in Skin [Review), *Int. J. Mol. Med.,* 2016, 38, 16–22.

[24]. Madison, K. C.; Swartzendruber, D. C.; Wertz, P. W.; Downing, D. T. Presence of Intact Intercellular Lipid Lamellae in the Upper Layers of the Stratum Corneum, *J. Invest. Dermatol,* 1987, 88, 714–718.

[25]. Al-Amoudi, A.; Dubochet, J.; Norlén, L. Nanostructure of the Epidermal Extracellular Space as Observed by Cryo-Electron Microscopy of Vitreous Sections of Human Skin, *J. Invest. Dermatol.,* 2005, 124, 764–777.

[26]. Mojumdar, E. H.; Groen, D.; Gooris, G. S.; Barlow, D. J.; Lawrence, M. J.; Deme, B.; Bouwstra, J. A. Localization of Cholesterol and Fatty Acid in a Model Lipid Membrane: A Neutron Diffraction Approach, *Biophys. J.,* 2013, 105, 911–918.

[27]. Iwai, I.; Han, H.; Hollander, L. Den; Svensson, S.; Öfverstedt, L.-G.; Anwar, J.; Brewer, J.; Bloksgaard, M.; Laloeuf, A.; Nosek, D.; *et al.* The Human Skin Barrier Is Organized as Stacked Bilayers of Fully Extended Ceramides with Cholesterol Molecules Associated with the Ceramide Sphingoid Moiety, *J. Invest. Dermatol.,* 2012, 132, 2215–2225.

[28]. Bouwstra, J. A.; Dubbelaar, F. E.; Gooris, G. S.; Ponec, M. The Lipid Organisation in the Skin Barrier, *Acta Derm. Venereol. Suppl. (Stockh),* 2000, 208, 23–30.

[29]. Čuříková, B. A.; Procházková, K.; Filková, B.; Diblíková, P.; Svoboda, J.; Kováčik, A.; Vávrová, K.; Zbytovská, J. Simplified Stratum Corneum Model Membranes for Studying the Effects of Permeation Enhancers. *Int. J. Pharm.,* 2017, 534, 287–296.

[30]. Berkers, T.; Visscher, D.; Gooris, G. S.; Bouwstra, J. A. Topically Applied Ceramides Interact with the Stratum Corneum Lipid Matrix in Compromised Ex Vivo Skin, *Pharm. Res.,* 2018, 35, 48.

[31]. Li, Z.; Ding, H.; Ma, Y. Interaction of Peptides with Cell Membranes: Insights from Molecular Modeling, *J. Phys. Condens. Matter,* 2016, 28, 83001.

[32]. Antunes, E.; Azoia, N. G.; Matamá, T.; Gomes, A. C.; Cavaco-Paulo, A. The Activity of LE10 Peptide on Biological Membranes Using Molecular Dynamics, in Vitro and in Vivo Studies, *Colloids Surfaces B Biointerfaces,* 2013, 106, 240–247.

[33]. Loverde, S. M. Molecular Simulation of the Transport of Drugs across Model Membranes, *J. Phys. Chem. Lett.,* 2014, 5, 1659–1665.

[34]. Lyubartsev, A. P.; Rabinovich, A. L. Recent Development in Computer Simulations of Lipid Bilayers, *Soft Matter,* 2011, 7, 25–39.

[35]. Rim, J. E.; Pinsky, P. M.; van Osdol, W. W. Multiscale Modeling Framework of Transdermal Drug Delivery, *Ann. Biomed. Eng.,* 2009, 37, 1217–1229.

[36]. Notman, R.; Anwar, J. Breaching the Skin Barrier - Insights from Molecular Simulation of Model Membranes, *Adv. Drug Deliv. Rev.,* 2013, 65, 237–250.

[37]. Notman, R.; den Otter, W. K.; Noro, M. G.; Briels, W. J.; Anwar, J. The Permeability Enhancing Mechanism of DMSO in Ceramide Bilayers Simulated by Molecular Dynamics, *Biophys. J.,* 2007, 93, 2056–2068.

[38]. Shah, J.; Atienza, J. M.; Rawlings, A. V; Shipley, G. G. Physical Properties of Ceramides: Effect of Fatty Acid Hydroxylation, *J. Lipid Res.,* 1995, 36, 1945–1955.

[39]. Moore, D. J.; Rerek, M. E.; Mendelsohn, R. FTIR Spectroscopy Studies of the Conformational Order and Phase Behavior of Ceramides, *J. Phys. Chem. B,* 1997, 101, 8933–8940.

[40]. Brockman, H. L.; Momsen, M. M.; Brown, R. E.; He, L.; Chun, J.; Byun, H.-S.; Bittman, R. The 4,5-Double Bond of Ceramide Regulates Its Dipole Potential, Elastic Properties, and Packing Behavior, *Biophys. J.,* 2004, 87, 1722–1731.

[41]. Notman, R.; Anwar, J.; Briels, W. J.; Noro, M. G.; den Otter, W. K. Simulations of Skin Barrier Function: Free Energies of Hydrophobic and Hydrophilic Transmembrane Pores in Ceramide Bilayers, *Biophys. J.,* 2008, 95, 4763–4771.

[42]. Thind, R.; O'Neill, D. W.; Del Regno, A.; Notman, R. Ethanol Induces the Formation of Water-Permeable Defects in Model Bilayers of Skin Lipids, *Chem. Commun.,* 2015, 51, 5406–5409.

[43]. Kai, T.; Mak, V. H. W.; Potts, R. O.; Guy, R. H. Mechanism of Percutaneous Penetration Enhancement: Effect of N-Alkanols on the Permeability Barrier of Hairless Mouse Skin, *J. Control. Release,* 1990, 12, 103–112.

[44]. Imai, Y.; Liu, X.; Yamagishi, J.; Mori, K.; Neya, S.; Hoshino, T. Computational Analysis of Water Residence on Ceramide and Sphingomyelin Bilayer Membranes, *J. Mol. Graph. Model,* 2010, 29, 461–469.

[45]. Paloncýová, M.; DeVane, R. H.; Murch, B. P.; Berka, K.; Otyepka, M. Rationalization of Reduced Penetration of Drugs through Ceramide Gel Phase Membrane, *Langmuir,* 2014, 30, 13942–13948.

[46]. Akinshina, A.; Das, C.; Noro, M. G. Effect of Monoglycerides and Fatty Acids on a Ceramide Bilayer, *Phys. Chem. Chem. Phys.,* 2016, 18, 17446–17460.

[47]. Papadimitriou, N. I.; Kainourgiakis, M. E.; Karozis, S. N.; Charalambopoulou, G. C. Studying the Structure of Single-Component Ceramide Bilayers with Molecular Dynamics Simulations Using Different Force Fields, *Mol. Simul.,* 2014, 7022, 1–15.

[48]. Marrink, S. J.; Risselada, H. J.; Yefimov, S.; Tieleman, D. P.; de Vries, A. H. The MARTINI Force Field: Coarse Grained Model for Biomolecular Simulations, *J. Phys. Chem. B,* 2007, 111, 7812–7824.

[49]. Marrink, S. J.; Tieleman, D. P. Perspective on the Martini Model, *Chem. Soc. Rev.,* 2013, 42, 6801–6822.

[50]. Sovová, Ž.; Berka, K.; Otyepka, M.; Jurečka, P. Coarse-Grain Simulations of Skin Ceramide NS with Newly Derived Parameters Clarify Structure of Melted Phase, *J. Phys. Chem. B,* 2015, 119, 3988–3998.

[51]. Hadley, K. R.; McCabe, C. A Coarse-Grained Model for Amorphous and Crystalline Fatty Acids, *J. Chem. Phys.* 2010, 132, 134505.

[52]. Reith, D.; Pütz, M.; Müller-Plathe, F. Deriving Effective Mesoscale Potentials from Atomistic Simulations, *J. Comput. Chem,* 2003, 24, 1624–1636.

[53]. MacDermaid, C. M.; DeVane, R. H.; Klein, M. L.; Fiorin, G. Dehydration of Multilamellar Fatty Acid Membranes: Towards a Computational Model of the Stratum Corneum, *J. Chem. Phys.,* 2014, 141, 22D526.

[54]. Höltje, M.; Förster, T.; Brandt, B.; Engels, T.; Von Rybinski, W.; Höltje, H. D. Molecular Dynamics Simulations of Stratum Corneum Lipid Models: Fatty Acids and Cholesterol, *Biochim. Biophys. Acta - Biomembr.,* 2001, 1511, 156–167.

[55]. Hadley, K. R.; McCabe, C. A Simulation Study of the Self-Assembly of Coarse-Grained Skin Lipids, *Soft Matter,* 2012, 8, 4802–4814.

[56]. Hadley, K. R.; McCabe, C. A Structurally Relevant Coarse-Grained Model for Cholesterol, *Biophys. J.,* 2010, 99, 2896–2905.

[57]. Moore, T. C.; Iacovella, C. R.; Leonhard, A. C.; Bunge, A. L.; McCabe, C. Molecular Dynamics Simulations of Stratum Corneum Lipid Mixtures: A Multiscale Perspective, *Biochem. Biophys. Res. Commun.,* 2017, 1–6.

[58]. Moore, T. C.; Iacovella, C. R.; Hartkamp, R.; Bunge, A. L.; McCabe, C. A Coarse-Grained Model of Stratum Corneum Lipids: Free Fatty Acids and Ceramide NS, *J. Phys. Chem. B,* 2016, 120, 9944–9958.

[59]. Moore, T. C.; Iacovella, C. R.; McCabe, C. Derivation of Coarse-Grained Potentials via Multistate Iterative Boltzmann Inversion, *J. Chem. Phys.,* 2014, 140, 224104.

[60]. Das, C.; Olmsted, P. D.; Noro, M. G. Water Permeation through Stratum Corneum Lipid Bilayers from Atomistic Simulations, *Soft Matter,* 2009, 5, 4549.

[61]. Das, C.; Noro, M. G.; Olmsted, P. D. Lamellar and Inverse Micellar Structures of Skin Lipids: Effect of Templating, *Phys. Rev. Lett.,* 2013, 111, 1–5.

[62]. Das, C.; Noro, M. G.; Olmsted, P. D. Fast Cholesterol Flip-Flop and Lack of Swelling in Skin Lipid Multilayers, *Soft Matter,* 2014, 7346–7352.

[63]. Das, C.; Olmsted, P. D. The Physics of Stratum Corneum Lipid Membranes, *Philos. Trans. R. Soc. A Math. Phys. Eng. Sci.,* 2016, 374, 20150126.

[64]. Engelbrecht, T.; Hauß, T.; Süβ, K.; Vogel, A.; Roark, M.; Feller, S. E.; Neubert, R. H. H.; Dobner, B. Characterisation of a New Ceramide EOS Species: Synthesis and Investigation of the Thermotropic Phase Behaviour and Influence on the Bilayer Architecture of Stratum Corneum Lipid Model Membranes, *Soft Matter,* 2011, 7, 8998.

[65]. Huzil, J. T.; Sivaloganathan, S.; Kohandel, M.; Foldvari, M.; Kotsireas, I.; Melnik, R.; West, B. Modeling the Effects of Lipid Composition on Stratum Corneum Bilayers Using Molecular Dynamics Simulations, In: *AIP Conference Proceedings,* 2011, 175, 175–178.

[66]. Holleran, W. M.; Takagi, Y.; Uchida, Y. Epidermal Sphingolipids: Metabolism, Function, and Roles in Skin Disorders, *FEBS Lett.,* 2006, 580, 5456–5466.

[67]. Tawada, C.; Kanoh, H.; Nakamura, M.; Mizutani, Y.; Fujisawa, T.; Banno, Y.; Seishima, M. Interferon-γ Decreases Ceramides with Long-Chain Fatty Acids: Possible Involvement in Atopic Dermatitis and Psoriasis, *J. Invest. Dermatol.,* 2014, 134, 712–718.

[68]. Paloncýová, M.; Vávrová, K.; Sovová, Ž.; DeVane, R.; Otyepka, M.; Berka, K. Structural Changes in Ceramide Bilayers Rationalize Increased Permeation through Stratum Corneum Models with Shorter Acyl Tails, *J. Phys. Chem. B,* 2015, 119, 9811–9819.

[69]. Moore, T. C.; Hartkamp, R.; Iacovella, C. R.; Bunge, A. L.; McCabe, C. Effect of Ceramide Tail Length on the Structure of Model Stratum Corneum Lipid Bilayers, *Biophys. J.,* 2018, 114, 113–125.

[70]. Gupta, R.; Rai, B. Molecular Dynamics Simulation Study of Skin Lipids: Effects of the Molar Ratio of Individual Components over a Wide Temperature Range, *J. Phys. Chem. B*, 2015, 119, 11643–11655.

[71]. Hoopes, M. I.; Noro, M. G.; Longo, M. L.; Faller, R. Bilayer Structure and Lipid Dynamics in a Model Stratum Corneum with Oleic Acid, *J. Phys. Chem. B*, 2011, 115, 3164–3171.

[72]. Martins, M.; Azoia, N. G.; Ribeiro, A.; Shimanovich, U.; Silva, C.; Cavaco-Paulo, A. In Vitro and Computational Studies of Transdermal Perfusion of Nanoformulations Containing a Large Molecular Weight Protein, *Colloids Surfaces B Biointerfaces,* 2013, 108, 271–278.

[73]. Machado, N. C. F.; dos Santos, L.; Carvalho, B. G.; Singh, P.; Téllez Soto, C. A.; Azoia, N. G.; Cavaco-Paulo, A.; Martin, A. A.; Favero, P. P. Assessment of Penetration of Ascorbyl Tetraisopalmitate into Biological Membranes by Molecular Dynamics *Comput. Biol. Med.,* 2016, 75, 151–159.

[74]. dos Santos, L.; Téllez S, C. A.; Sousa, M. P. J.; Azoia, N. G.; Cavaco-Paulo, A. M.; Martin, A. A.; Favero, P. P. In Vivo Confocal Raman Spectroscopy and Molecular Dynamics Analysis of Penetration of Retinyl Acetate into Stratum Corneum, *Spectrochim. Acta - Part A Mol. Biomol. Spectrosc.,* 2017, 174, 279–285.

[75]. Gupta, R.; Rai, B. Effect of Size and Surface Charge of Gold Nanoparticles on Their Skin Permeability: A Molecular Dynamics Study, *Sci. Rep.,* 2017, 7, 1–13.

[76]. Olivella, M. S.; Lhez, L.; Pappano, N. B.; Debattista, N. B. Effects of Dimethylformamide and L-Menthol Permeation Enhancers on Transdermal Delivery of Quercetin, *Pharm. Dev. Technol.,* 2007, 12, 481–484.

[77]. Wan, G.; Dai, X.; Yin, Q.; Shi, X.; Qiao, Y. Interaction of Menthol with Mixed-Lipid Bilayer of Stratum Corneum: A Coarse-Grained Simulation Study, *J. Mol. Graph. Model.,* 2015, 60, 98–107.

[78]. Del Regno, A.; Notman, R. Permeation Pathways through Lateral Domains in Model Membranes of Skin Lipids, *Phys. Chem. Chem. Phys.,* 2017, 20, 2162–2174.

[79]. Gupta, R.; Sridhar, D. B.; Rai, B. Molecular Dynamics Simulation Study of Permeation of Molecules through Skin Lipid Bilayer, *J. Phys. Chem. B,* 2016, 120, 8987–8996.

[80]. Rocco, P.; Cilurzo, F.; Minghetti, P.; Vistoli, G.; Pedretti, A. Molecular Dynamics as a Tool for in Silico Screening of Skin Permeability, *Eur. J. Pharm. Sci.,* 2017, 106, 328–335.

[81]. Gajula, K.; Gupta, R.; Sridhar, D. B.; Rai, B. In-Silico Skin Model: A Multiscale Simulation Study of Drug Transport, *J. Chem. Inf. Model.,* 2017, 57, 2027–2034.

[82]. Antunes, E.; Cavaco-Paulo, A. Stratum Corneum Lipid Matrix with Unusual Packing: A Molecular Dynamics Study, *In submission process,* 2018.

[83]. Lundborg M, Narangifard A, Wennberg CL, Lindahl E, Daneholt B, Norlén L. Human skin barrier structure and function analyzed by cryo-EM and molecular dynamics simulation, *J Struct Biol.*, 2018, 203, 149–161.

[84]. Lundborg M, Wennberg CL, Narangifard A, Lindahl E, Norlén L. Predicting drug permeability through skin using molecular dynamics simulation, *J Control Release,* 2018, 283, 269–279.

[85]. Wennberg CL, Narangifard A, Lundborg M, Norlén L, Lindahl E. Structural Transitions in Ceramide Cubic Phases during Formation of the Human Skin Barrier, *Biophys J.*, 2018, 114, 1116–1127.

[86]. Narangifard A, den Hollander L, Wennberg CL, Lundborg M, Lindahl E, Iwai I, et al. Human skin barrier formation takes place via a cubic to lamellar lipid phase transition as analyzed by cryo-electron microscopy and EM-simulation, *Exp Cell Res.*, 2018, 366, 139–151.

[87]. Marzinek, J. K.; Lian, G.; Marzinek, J. K.; Mantalaris, A.; Pistikopoulos, E. N.; Zhao, Y.; Han, L.; Chen, L.; Bond, P. J.; Noro, M. G. Molecular and Thermodynamic Basis for EGCG-Keratin Interaction-Part I: Molecular Dynamics Simulations, *AIChE J.,* 2013, 59, 4816–4823.

[88]. Kumar, S.; Zakrewsky, M.; Chen, M.; Menegatti, S.; Muraski, J. A.; Mitragotri, S. Peptides as Skin Penetration Enhancers: Mechanisms of Action, *J. Control. Release,* 2014, 199, 168–178.

[89]. Gennari, C. G. M.; Franzè, S.; Pellegrino, S.; Corsini, E.; Vistoli, G.; Montanari, L.; Minghetti, P.; Cilurzo, F. Skin Penetrating Peptide as a Tool to Enhance the Permeation of Heparin through Human Epidermis, *Biomacromolecules,* 2015, 17, 46–55.

[90]. Schneider, M. R.; Paus, R. Deciphering the Functions of the Hair Follicle Infundibulum in Skin Physiology and Disease, *Cell Tissue Res.,* 2014, 358, 697–704

Chapter IV

Skin Barrier Molecular Dynamics Studies

Development and study of a stratum corneum lipid matrix molecular dynamics model with unusual lipid packing and coarse-grained resolution.

This chapter is based on the following publication:

Egipto Antunes, Artur Cavaco-Paulo. Stratum Corneum Lipid Matrix with Unusual Packing: A Molecular Dynamics Study, *In submission process*, 2018.

Chapter IV abstract:

The skin is an effective barrier against the external elements being the stratum corneum, with its lipid matrix surrounding the corneocytes, considered the major player responsible by its low permeability. The delivery of drugs through the skin is intensively studied nowadays due its unique advantages such as the patient compliance, although overcome the skin barrier is a challenging work.

The use of computational models to study the transdermal delivery of compounds have a huge potential to improve this research area, but requires reliable models of the skin components. In this work, we developed molecular dynamics models with coarse-grained resolution, of the stratum corneum lipid matrix and the sebum. The lipid matrix model was developed with unusual lipid packing configuration as some recent works support. The simulation results indicate that this configuration can be stable and can explain the low permeability of stratum corneum. The sebum simulations shown that this oily skin product can have significant impact on the transdermal potential of drugs.

We hope that the developed lipid models can be an effective tool in the study of drug transdermal delivery, helping to understand molecular mechanisms behind this process and to develop improved drugs or strategies for this route of drug administration.

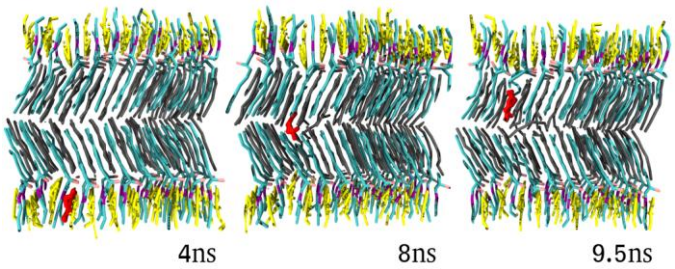

Figure IV: Graphical abstract of Chapter IV

Introduction

The transdermal delivery (TD) of drugs is nowadays an intense field of research. The increase of the patient compliance due to the noninvasiveness and to the self-administration possibility of this technique is likely its main advantage over other drug delivery routes such as oral or injection. Other advantages of TD are the avoidance of gastrointestinal and liver metabolism, the possibility of continuous and controlled administration and the reduction of side effects. The skin is however an efficient barrier to external compounds, turning the TD a very challenging process for most of drugs.

The soft tissue covering the vertebrates, called skin, is fundamental to the survival on land due to its interface role between the environment and the body interior. Protection, homeostasis maintaining and external world sensing are the three areas were skin plays major roles. The skin acts as a barrier between the external hostile environment and the vertebrate's interior. It protects against mechanical injuries, chemicals, pathogens, radiations and most importantly, against the water and electrolytes lost.[1]

The skin has a multilayer structure, with three main layers, namely the epidermis, dermis and hypodermis (from the skin surface to the interior). The epidermis can be divided in sub-layers or stratum according the level of keratinization of its cells, namely the stratum corneum (SC, outmost sub-layer), stratum lucidum (only on thicker skin zones), stratum granulosum, stratum spinosum and stratum basale (inner sub-layer). The living keratinocytes of stratum basale suffer a keratinization during the migration along the epidermis, in which these cells dye, elongate and become filed with granules, keratin filaments and the reminiscent of the cells organelles. The resulting differentiated and dead cells in the SC are named corneocytes and are surrounded by a lipid matrix (LM).[2] The SC is considered the layer responsible by the barrier properties of the skin, which results of its corneocytes organization (tight and without interstices) and keratinization, as well due to the presence of LM surrounding these cells.[3,4]

Contrary to most biological membranes the LM doesn't have phospholipids, instead is mainly composed by ceramides (CER), cholesterol (CHOL) and free fatty-acids (FFA), in an equimolar lipid proportion.[5-7] The CER are a complex group of sphingolipids containing sphingosine bases in amide linkage with fatty-acids, existing a great variability of the fatty-acid length on skin CER. The most common CER in LM are the CER NS (nonhydroxy fatty acid sphingosine CER), also named CER 2, and the CER NP (nonhydroxy fatty acid phytosphingosine CER), also named CER 3.[8,9] Most of FFA in the SC are saturated and long, being the lignoceric FFA (with 24 carbons length) the most common.[10]

The LM is most of the time represented as stacked lamellar sheets of lipids, with each sheet in a bilayer conformation similar to the cell-membranes. There is however some debate in the literature about how the CER, CHOL and FFA lipids are packed in the LM. Bouwstra and collaborators suggested that the LM lipids arrange into a trilayer organization, with the inner zone with higher content of CHOL and FFA turning it more fluid.[11] Later Norlén proposed that the LM is a single gel phase and that the CER can be presented in unusual splayed chain conformation, with its two alkyl chains pointing into opposite directions.[12] Recent works applying techniques such as cryo-electron microscopy and neutron diffraction have been providing new clues in this field.[13-15] Iwai, Norlén and colleagues proposed in 2012 a new model of the lipid packing in the LM, based on computational reconstruction of the band patterns presented between corneocytes in cryo-electron microscopy pictures of SC.[15] Contrary to the common representation of LM as stacked sheets of lipid bilayers, the proposed model suggests a lipid assembling with all CER in the splayed conformation, being the CHOL molecules locate near the CER sphingoid chains and the FFA near to the fatty-acid moieties of the CER (see Figure 1 (a)). This model can explain the barrier properties of the LM since the packing of the lipids is much more thigh and ordered than the packing in the most biological lipid layers.

The skin SC and LM, as the main players in skin barrier, are extensively studied for the development of new and more effective strategies for TD of drugs. However, the researchers also have been driving their attention for the drug delivery through hair follicles, because recent works shown that the potential of this rout in TD can be much

higher than previously thought.[16-18] Hair follicles occupy only about 0.1 % of skin surface, fact that led to the overlooking of their importance to TD. Nevertheless, these structures greatly increase the skin surface area since they correspond to invaginations of epidermis. The hair follicle ducts are filled with sebum that can influence the transfollicular delivery (TF) of drugs, turning important the better understand of its composition, formation and properties, in order to increase the TD potential of some drugs.

The sebum is the oily product of the sebaceous glands, which are found in almost all mammals. The mainly function of human sebum, as well the metabolic pathways regulating its secretion and composition are not fully understood. There are, however, some suggested functions. The sebum may serve as a delivery system for antioxidants (vitamin E), antimicrobial lipids and pheromones, providing a protective and hydrophobic coating to skin surface and hairs.[19,20] The lipids that compose this oily product are the squalene (SQ), FFA, triglycerides (TG), wax esters (WE), CHOL and cholesterol-oleate (CHOLO), with median molar percentage values for human samples of 10.6 %, 28.3 %, 32.5 %, 25 %, 4 % and 2 %, respectively.[21] The sebum also present vestiges of vitamin E and its composition is characteristic of each specie, with the SQ and WE lipids not found elsewhere in mammal's bodies.

Nowadays, most of research for determining the skin permeability of drugs and to develop better TD strategies, is mainly performed through *in vitro* or *ex vivo* assays. These experiments are expensive, time consuming and the society as well the governments are disapproving or even banning the use of animal skin for testing. Molecular dynamics (MD) simulations may serve as an excellent tool to investigate the molecular mechanisms of drug permeation through the skin, overcoming some of these problems. There are some works applying MD with the objective to unveil the potential of some chemicals to cross the skin barrier. Recently we did an extensive literature review of MD studies about LM [22], showing that there are a plenitude of different LM models, varying in terms of composition, lipid packing and complexity. However, like in any computational simulation, the ability to correlate the simulation results with the real world depends of the strong and reliability of the computational model. Models too simple, or with structural fails, may lack important features which can lead to artifacts, but models too complex may turn the simulation to

computationally consuming or even impracticable. In this work we developed coarse-grained MD models of skin SC LM and of sebum to unveil insights on the molecular mechanisms of TD as well to obtain robust MD models to use in future assays. The LM model is based on the alternative way of LM packing suggested by Iwai, with all CERs in the splayed form. From our knowledge, is the first time that one coarse-grained model of LM with this packing is built, and the first time that sebum is studied using MD.

Materials and methods

Molecular Dynamics Simulations

All the simulations were ran with the GROMACS 4.0.7 software package,[23] using the MARTINI force-field.[24] The MARTINI force-field have lower molecular resolution since one MARTINI bead usually represent 4 heavy atoms, which decreases largely the computational costs, allowing the simulation of larger systems or the sampling of longer times. The lower resolution has the drawback of some atomic properties lacking, which can result in less reliable simulation results depending of the study targets and objectives. However, this force-field was developed from the beginning for lipid systems, basing its parametrization in the correct modeling of partition free energies of a large number of compounds, and it is been applied in several MD studies with success.[24-26] The simulations boxes were triclinic, the time step varied between 20 to 30 fs and the LINCS algorithm was used as bond constraint.[27]

The simulation protocol was similar to all systems, it begins with the energy minimization of the systems for 5000 steps using the steepest descent method, followed by one short run (1.5 ns) in the isothermal-isobaric ensemble (NPT, constant number of molecules, pressure and temperature) applying positions restraints to all non-solvent beads (with an harmonic force of 10^3 kJ/mol.nm^2). This preparatory run allows the structures relax and generate velocities according to a Maxwell-Boltzmann distribution for the temperature of 306 K. Many MD works about LM use the human body temperature of 310

K as reference, but the temperature of skin epidermis is slightly lower, being in the interval of 301~306 K (28~33 ºC).[28] After the minimization and initialization steps, production runs were performed with a simulation time of at least 500 ns in an NPT ensemble. Berendsen couplings were used to maintain the temperature of the systems at 306 K with 0.3 ps as relaxation time, and to maintain the pressure at 1 atm with 1 ps as time constant. The pressure coupling was semi-isotropic with compressibility of $3x10^{-5}$ bar in both directions.[29] The electrostatics and van der Waals interactions were treated with shift potentials, as suggested in the MARTINI website (www.cgmartini.nl), being the electrostatics interactions in the range of 0-1.2 nm shifted to 0, while the Lenard-Jones interactions are shifted to 0 in the 0.9-1.2 nm range. The simulations were always performed in triplicate.

Steered Simulations

Steered simulations were performed to obtain insights about the permeation potential of the lipid structures (LM models and sebum). The simulation protocol was the same, with the exception that in the production run one target molecule is forced to cross the lipid structures through the application of an harmonic force of 1000 $kJ.mol^{-1}.nm^{-2}$ to its center of mass during approximately 15 ns. Nile-Red (NRD) and water were the molecules chosen. The resulting trajectories allowed the generation of different configurations along the *z* coordinate to perform umbrella sampling simulations[30] and later calculate the potential of mean force (PMF) of the crossing process using free weighted histogram analysis (g_wham tool of GROMACS).[30,31]

Molecules Parametrization

Different compounds were used in this work, most of them were lipids. Due to its acyl chains and to the coarser nature of MARTINI, the parametrization of lipids is very similar between them. All the topologies parameters, except for the CHOL, CHOLO, SQ, polylactic acid (PLA) and NRD were built according topologies for similar compounds available in the MARTINI website (see the "martini_v2.0_lipids.itp" and "martini_v2.0_surfactants.itp" files, available at http://www.cgmartini.nl/index.php/60-downloads/forcefield-parameters/specific-topologies), which generally result of the force-field developers works and follow the force-field guidelines.[32,33]

The CHOL, CHOLO and triolein (glyceril trioleate, TO) topology parameters were obtained from MARTINI website and are based on Ingólfsson work for CHOL,[33] and on Vuorela work for CHOLO and TO.[34]

Because the topologies for SQ, NRD and PLA, or similar molecules, were not in MARTINI database we parameterized them applying the protocol described in the force-field webpage for new molecules parameterization using atomistic simulation (http://www.cgmartini.nl/index.php/tutorials-general-introduction/parametrzining-new-molecule). We used the Automatic Topology Builder server (atb.uq.edu.au) to obtain atomistic topologies parameters for these molecules (for GROMOS 54A7 force-field).[35,36] Then the generated atomistic data of in water simulations was used as reference to coarse-grained parametrization. Note that the PLA was parameterized with 100 monomers of lactic acid.

Finally, the poloxamer (PLX) molecule parametrization follow a different approach. This molecule is a triblock polymer with central hydrophobic monomers of polypropylene oxide (PPO) flanked by hydrophilic monomers of polyethylene oxide (PEO). To model these monomers we add two new particle types to the standard 18 particles in MARTINI, following a the methodology described in one Hwankyu Lee work, in which the PEO monomer topology parameters are studied.[37] The parameters calculated in this work, as well in one posterior work of the same author,[38] were used for the new particle representing the PEO monomer. For the PPO particle, the parameters were taken from the work of Hezaveh and colleagues.[39]

It should be noted that the coarse nature of MARTINI, in which one particle generally models 4 heavy atoms, limits the resolution. Two FFA, for example, can differ in just one heavy atom (one carbon) being impossible to represent such difference in the MARTINI resolution. So, exemplifying, when we talk about the palmitic (16 carbons) FFA coarse-grained model we should remember that this model can be a coarser representation of FFAs with 14 to 18 carbons (16±2 carbons).

Lipid Matrix Model Building

As stated previously the coarse-grained models of LM built in this work were based on the model suggested by Iwai and collaborators (see Figure 1a). Also, the lipid composition was the same, with CER NP, CHOL and FFA (lignoceric acid) at 1:1:1 molecular proportion. These lipids and proportion reflect the composition of SC LM, according the literature, and allows the comparison between the works. To obtain such configuration we initially built 3D conformation files of the three lipids with more straight structures, mainly for the CER and FFA acyl chains, respecting the MARTINI force-field parameters for bond distances. After, we put one CHOL and one FFA molecules models very near to the CER sphingoid and fatty-acid moieties, respectively, with their polar groups aligned with the CER headgroup, as suggested in Iwai work. The resulting three lipids conformation was posteriorly replicated in the *x*, *y*, and *z* directions using the GROMACS tool genconf, obtaining very ordered layers with the wanted configuration (see Figure 7(a) in Chapter IV attachments). Finally, we follow the simulation protocol described previously, to check the stability of the model.

The first simulations performed resulted in MD models very similar to the Iwai model, however some molecules of CHOL and FFA diffuse from its initial position to the opposite CER moiety or presented some disorganization (see Figure 7(b) and 7(c) in Chapter IV attachments). This should be consequence of the initial low density of the system due to the way how the LM structure was built. The pressure coupling was not fast enough to compact the lipid structure for the system reach the proper density without allow the escape of some lipids from its initial zone.

Running the simulations at lower temperatures was a good strategy to overcome the initial lipid diffusing issue. We observed that simulations at low temperature resulted in a very ordered lipid packing, similar to Iwai suggested LM model, without diffusing of CHOL or FFA from their initial zones (see Figure 7(d) in Chapter IV attachments). To obtain the final LM models we applied one heating protocol, the simulations begun at 50 K by 600 ns, then three smaller steps of 300 ns were ran, increasing the temperature to 100, 200 and 306 K respectively. The resulting MD models of LM shown packing stability and were used in the following work.

In addition, the spontaneous packing of these lipids was evaluated, building systems, in vacuum and in water, with the same lipidic composition but randomly dispersed in the simulation box. The systems were simulated as usual at 306 K by 600 ns (Figure 8 in Chapter IV attachments).

Previously, in our group, one coarse-grained model of LM was already developed by Nuno Azoia.[40] That model consist of CER NS, CHOL, lignoceric FFA and cholesterol-sulfate (CHOLS) with ratio portions based on young normal skin, in a configuration of double bilayers. In the present work we ran simulations with the Azoia model for comparison its performance with our models.

Sebum Model Building

The composition of our sebum model is present in the Table 1. There are already several works were the composition of sebum was studied,[41-43] however, there is some variation on the data that probably results from the difficulty of removing the sebum compounds from the rest of skin compounds such as SC lipids or cells debris.

Some authors have been developing formulations of artificial sebum, to test drugs transport properties. In 2006, Stefaniak and Harvey summarized the reported composition of skin surface film liquids (sweat and sebum) as well of artificial sebum formulations, published until that time.[21] More recently, Lu in 2009 and Stefaniak in 2010 developed new artificial sebum formulations based on the 2006 review but with compositions more complex and similar to real human sebum.[44,45] Our model composition is based on these works and in one work of Nordstrom and colleagues, in which the lipid composition of follicular casts were studied.[46] We used the most common saturated and unsaturated lipids for WE, TG and FFA, in concentrations according these works to have a reliable description of human sebum.

Table 1: Sebum model mass fraction composition.

Lipid Types	Lipids	(w/w %)
	Squalene (SQ)	10
Free fatty-acids (FFA)		**26**
	Palmitic acid (PA)	12
	Palmitoleic acid (PO)	14
Wax Esters (WE)		**26**
	Palmityl Palmitate (PP)	14
	Oleyl Oleate (OO)	12
Triglycerides (TG)		**32**
	Tripalmitin (TP)	20
	Triolein (TO)	12
Sterols		**6**
	Cholesterol (CHOL)	2
	Cholesterol Oleate (CHOLO)	4

To build the sebum model we insert randomly the computational models of the lipids, according the mass percentages depicted in table1, in a simulation box that was filled with water molecules. Then the simulations ran by 600 ns at 306 K according the protocol described before. In this way the sebum lipids aggregated forming a big lipid ball. In order to have a sebum layer, instead of a ball, we ran also for 600 ns one triclinic simulation box completely filled only with the sebum lipids. The resulting sebum layer shown also be stable in water systems.

Results and discussion

Lipid Matrix and Sebum Models Development

The Figure 1 shows the schematic representation of Iwai suggested LM packing and our MD models. Two main models were used in this work, the double layer model (DOUB, two layers of splayed CER, see Figure 1b and the bi-double layer model (BIDOUB, four layers of splayed CER, see Figure 1c. These models reflect the repetitive nature of the LM stacks layers, having the BIDOUB all possible interfaces between the three lipids, according to this type of packing.

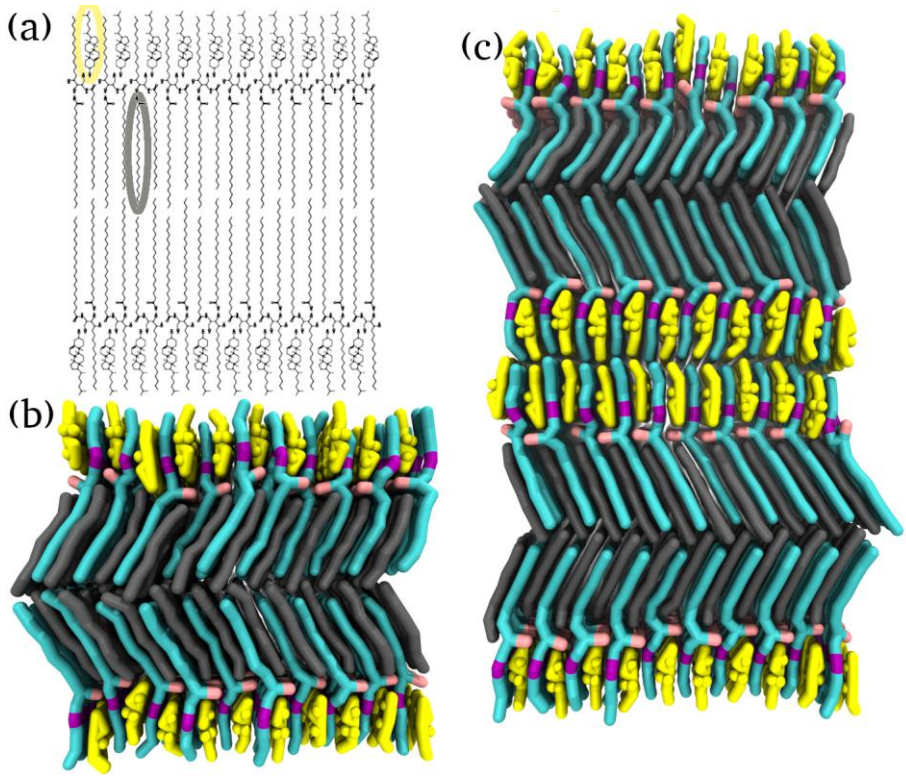

***Figure 1*: (a)** Iwai LM model, with one CHOL and one FFA highlighted at yellow and grey, respectively. Developed LM models, with two (**(b)** - DOUB model) and four layers (**(c)** - BIDOUB model). The lipids in the computational models are represented by wide sticks, with the CER at cyan (with polar groups in pink colors), the CHOL at yellow and the FFA at grey.

It seems that the initial configuration of the lipids is very important to obtain ordered models. The imperfections observed in the first developed systems emerge at the very beginning of the simulations and later the resulting lipid packing remains very stable. The application of the low temperature overcome the problem of lipid diffusion and disorganization of the first tests, and the following increase of temperatures did not promote lipid destabilization. The difference between the models with or without the application of the heating protocol can be found in the Figure 7 in Chapter IV attachments. Both DOUB and BIDOUB models present very ordered structures, with the CER fully splayed and showing some tilt in the FFA chains together with the adjacent fatty-acid moieties of CER. The tilt appears in all the systems but with some small differences and, interestingly, is different even inside the same model as show in the Figure 1c. The simulations did not present significant differences between the DOUB and BIDOUB models, either alone or interacting with other compounds.

Self-assembling simulations of the LM molecules were also performed. The CER, CHOL and FFA were inserted randomly and disperse in vacuum or aqueous simulations boxes, with the same number of lipids of previous simulations. The resulting structures were disorganized or mainly in bilayer conformation (in aqueous systems), similar to cell-membranes, with the CER in the hairpin configuration and the three lipids equally distributed by the two layers (see Figure 8 in Chapter IV attachments). This shows that the ordered structure of our models only can be achieved in the simulations with some initial imposition of the lipid arrangement. The energy barrier to the lipids assemble as Iwai suggested should be high, turning it inaccessible to be sampled in regular simulations, even at coarse-grained resolutions. The formation and the assembling of lipids in SC LM are process still not fully understood. Some undescribed mechanisms may facilitate the conformation suggested in Iwai work and in our computational models. One example of these mechanisms was presented in one MD work by Chinmay Das, which shows that the corneocyte lipid envelop layer surrounding the mammals corneocytes can induce the formation of layers in the adjacent LM.[47]

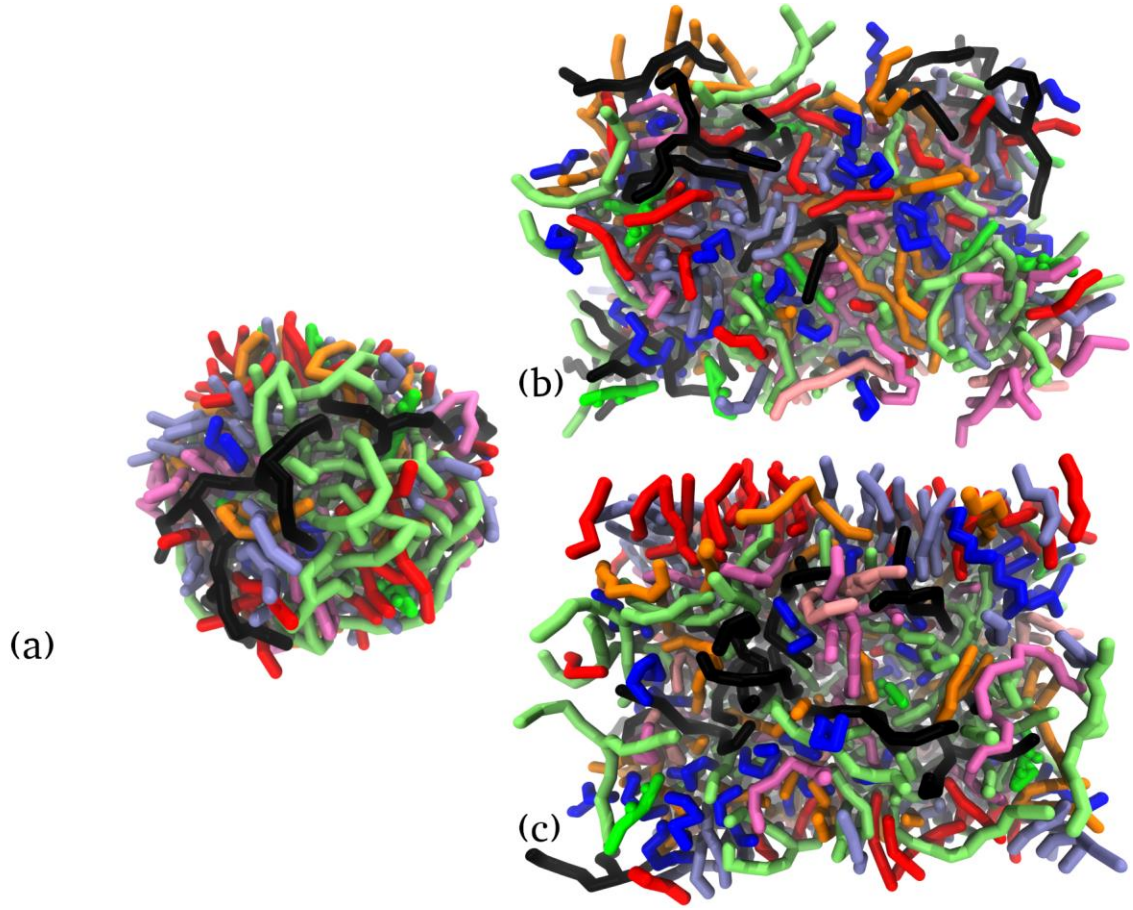

Figure 2: Configurations after 600 ns of sebum lipids self-assembling simulations. **(a)** Sebum lipids in water, assembled into spherical structure. **(b)** Sebum lipids assembled in vacuum. **(c)** The previous system after the addition of water. The lipids are depicted as wide sticks, with the following color code: SQ: blue; PA: red; PO: ice-blue; PP: orange; OO: mauve; TP: lime; TO: black; CHOL: green; CHOLO: pink. The water molecules were omitted for clarity.

In Figure 2 it is presented the sebum in the sphere and layer forms, after self-assembly simulations of Table 1 lipids. The resulting structures shown much more fluidity than the LM models. When the water is present in the simulated systems, the FFA lipids of the sebum are located more in its surface, with their acids moieties facing the water molecules and their acyl tails more buried in the sebum lipids interior. The remaining lipids are randomly distributed but more in the lipidic interior. The simulations also showed that although the sebum lipid clusters formed are fluid they are stable and there are not lipids diffusing away from the cluster even briefly pointing to some viscosity in the model.

Interaction Simulations

Nile-Red

After the achievement of stable LM and sebum models we perform simulations to study the interaction of these models with some different compounds and between them. One chosen molecule was NRD. This is a probe widely used in laboratory assays, because it is lipophilic and fluorescent in water allowing to sense changes in its environment lipophilicity.[48,49] Due to the lipophilic nature of NRD we expected the insertion of these molecules in the LM interior, however the NRD was not able to fully insert in the LM model, only some adsorption at LM-water interface was visible.

In the first systems, built with 10 NRD molecules, was observed some aggregation of NRD molecules in the water-LM interface, so we increased the number of NRD molecules in the simulated systems for 20, 100 and 200, testing possible concentration effects. The simulations were also elongated reaching times of 1800 ns. Even at higher concentrations and larger simulated times the NRD molecules do not were able to insert in the LM, neither destabilize its lipids, however the adsorption at water-lipid interface was more evident, with some NRD forming small grooves on LM surface. In addition, in some replicas with high concentration of NRD molecules, emerged zones with the NRD aligned with each other. These observations are depicted in the Figure 3.

The interaction simulations of NRD with sebum showed the expected behavior, namely the full insertion of these lipophilic molecules in the sebum interior as shown in the Figure 3c (whether in spherical and layer sebum forms). In this case the NRD easily inserts in the sebum interior, being located more near to the sebum lipids with oleic acyl chains (excepting the PO) and to SQ (see the radial distribution function in Graph 3 at Chapter IV attachments). This location could result of stronger interactions with these lipids or because they are located more in the sebum clusters interior.

Relatively to our group old LM model, from Azoia,[40] the simulation results of its interaction with NRD is similar to the sebum, with the full insertion of the NRD molecules in the LM interior, mainly at the middle of the bilayer. In these simulated systems the

interaction of NRD is stronger with the CER and FFA molecules of LM (see the radial distribution function in Graph 4 at Chapter IV attachments).

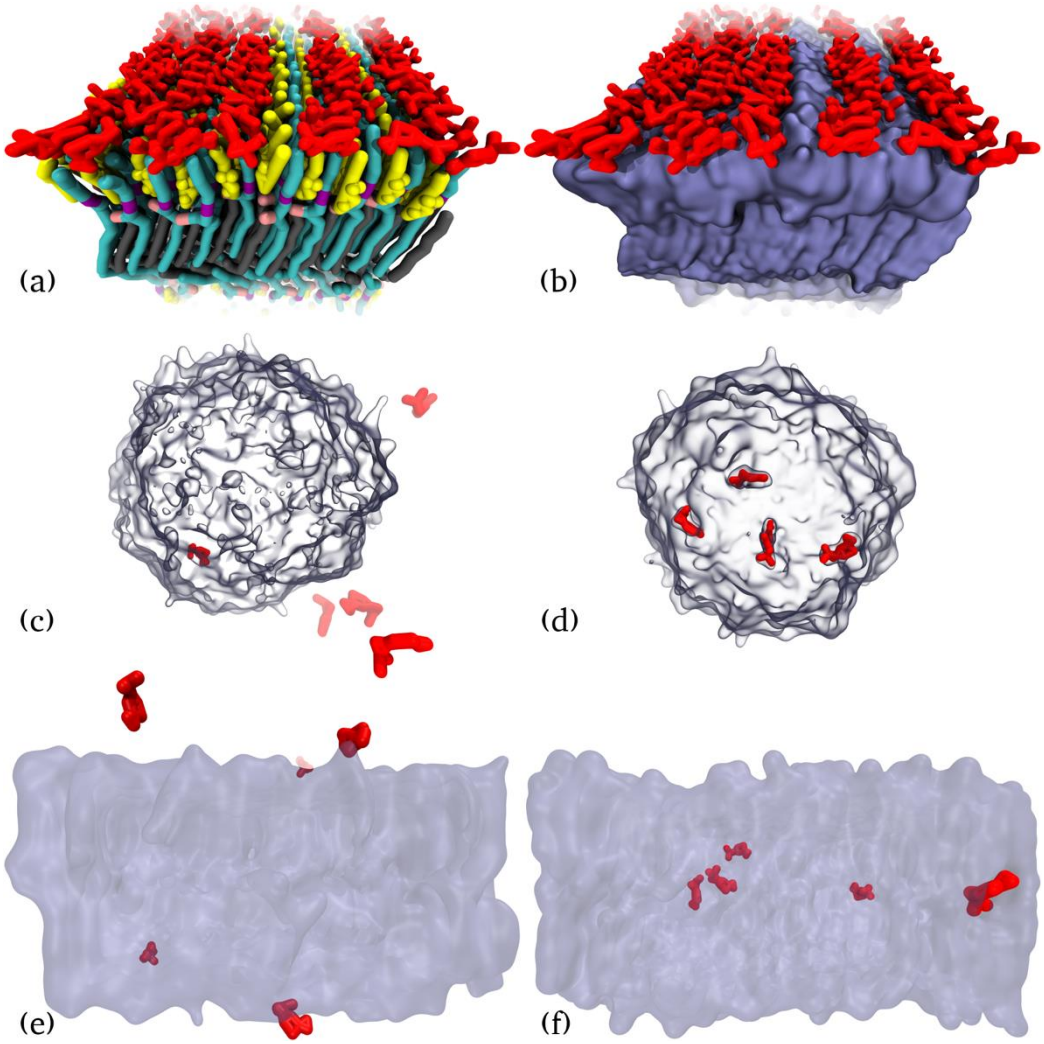

Figure 3: Snapshots of NRD interaction with the different lipidic structures. **Top:** developed LM final configuration after 1200 ns simulation with 200 NRD molecules, in wide colored sticks **(a)** and ice blue surface **(b)** representation. **Middle:** initial **(c)** and after 600 ns **(d)** snapshots of 5 NRD (at red) interacting with the sebum sphere (at translucid surface) simulation. **Bottom:** initial **(e)** and after 600 ns **(f)** snapshots of 5 NRD (at red) interacting with old LM model (at translucid surface). The water molecules in all systems were excluded for clarity. Note that all the NRD molecules in **(c)** and **(e)** snapshots are outside the lipidic structures.

The simulation results of the systems with sebum and old LM interacting with the NRD point to that the alignment of lipids in the developed new LM may be too tight, acting

as a barrier even to lipophilic molecules such as the NRD. This barrier is entirely physical since the NRD molecules had no problem to insert in the other lipidic structures, which in the case of the old LM model have similar lipidic composition.

Polylactic acid and Poloxamer polymers

PLA nanoparticles produced through precipitation, using PLX as surfactant, were developed in our group as drug delivery systems for skin.[50] These particles presented good stability, efficiency of drug entrapment and drug release profile, without toxicity for skin cells. Due to the promising results of this work we performed some simulations of PLA and PLX polymers interaction with the LM, sebum, NRD and between each other.

In all the simulated systems with PLA no interaction was verified between this molecule and the other molecules, these polymers just aggregate together, and stay located in the solvent. This effect is stronger in simulations with acetone as solvent (see Figure 9 in Chapter IV attachments).

The PLX presented a different behavior. This polymer is amphipathic, with 74 central hydrophobic monomers (PPO monomer) and 26 hydrophilic monomers, 13 in each polymer terminal, (PEO monomers). Although its central part is hydrophobic, the aggregation of the PLX in water simulations was weaker than the PLA aggregation at same conditions. The simulations of NRD interacting with the PLX exhibit the accumulation of NRD molecules in hydrophobic cores formed by some aggregation of the PLX central parts.

The simulations of PLX interaction with sebum and old LM models shown interesting features. When interacting with the old LM model the PLX was able to insert its hydrophobic PPO monomers into the lipidic layer, promoting some destabilization of the LM model. The PLX, however, was not able to insert the same monomers at sebum model interior, whether the sebum was spherical or layered. In this case, the PLX just adsorbs at sebum surface, and do not promote changes in the localization of the lipids inside the sebum structure.

Finally, the interaction simulations of this polymer with the new LM model presented results similar to the interaction of this LM model with the NRD molecules. The

PLX adsorbs at LM surface, with its PPO monomers in more close contact with the lipids and the PEO monomers drifting to the water. Such as in the NRD interaction simulations, the PLX seems to promote a very slight destabilization at the lipids surface, however is so small that the PLX cannot insert into the LM interior (see Figure 4).

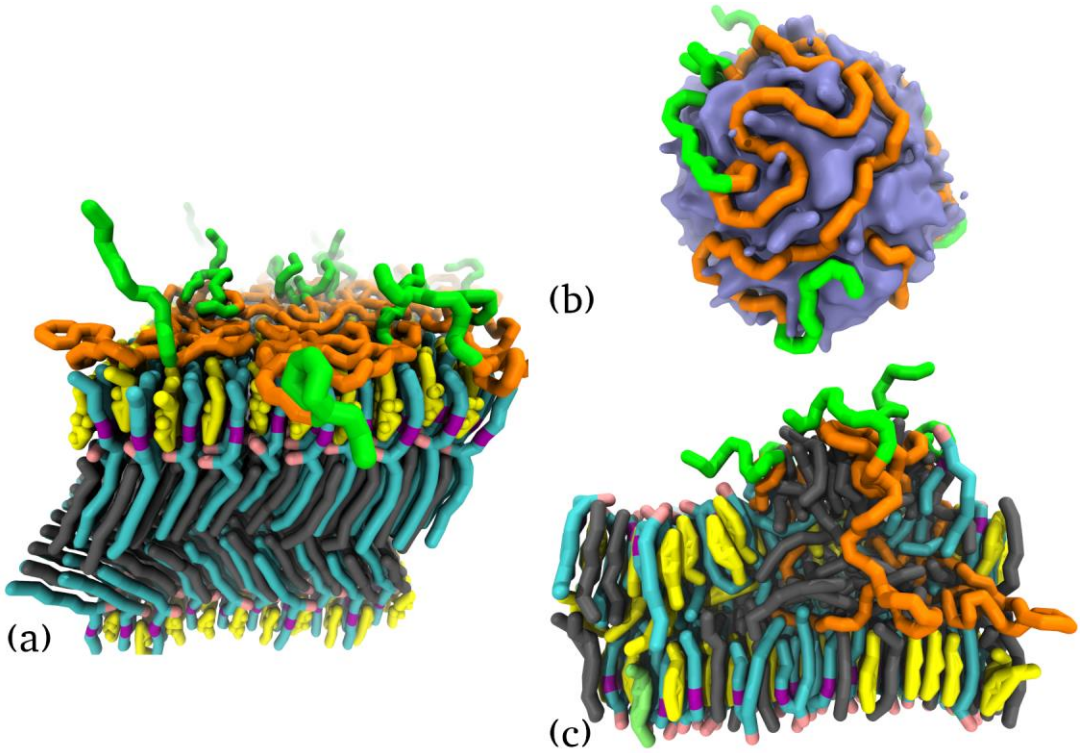

Figure 4: Lipidic systems snapshots after 600 ns of interaction simulations with PLX polymers in water. **(a)** Developed LM model. **(b)** Sebum model. **(c)** Old LM model. The developed and old LM models were represented by wide sticks, with CER at cyan (with polar groups at pink), CHOL at yellow, CHOLS at lime (only in the old model) and FFA at gray. The sebum sphere is represented as ice blue surface. The PEO monomers of PLX (hydrophilic) are depicted as green sticks while the PPO (hydrophobic) are orange. The water was omitted for clarity.

Lipid Matrix and Sebum Interaction

As already stated, the sebum may have significant effect on the TD of compounds, mainly if the compounds are designed to accumulate into follicular ducts. The interaction simulations between one sphere of sebum and the new LM model showed a quick adsorption of the sebum lipids at LM surface, forming a layer (see Figure 5). This process just takes around 40 ns of simulation time. Taking into account the previous results, where

no compound was able to significantly interacts with this LM model, was surprisingly to see that the sebum adsorption at LM surface lead to the diffusion of few CHOL molecules from the LM to the sebum layer (see Figure 5). This diffusion was quick and do not promoted significant structural changes in the LM model. Although we elongate the simulations until 1200 ns, the LM maintained stable and no more CHOL drifted from their initial zones at LM structure.

In the case of the older LM model, the simulation of its interaction with sebum sphere was completely different. When the sebum sphere found the old LM model the two lipid structures quickly begin to merge (see Figure 5). The sebum lipids are full absorbed by the LM and all the lipids rearrange. The full absorption process takes less than 600 ns.

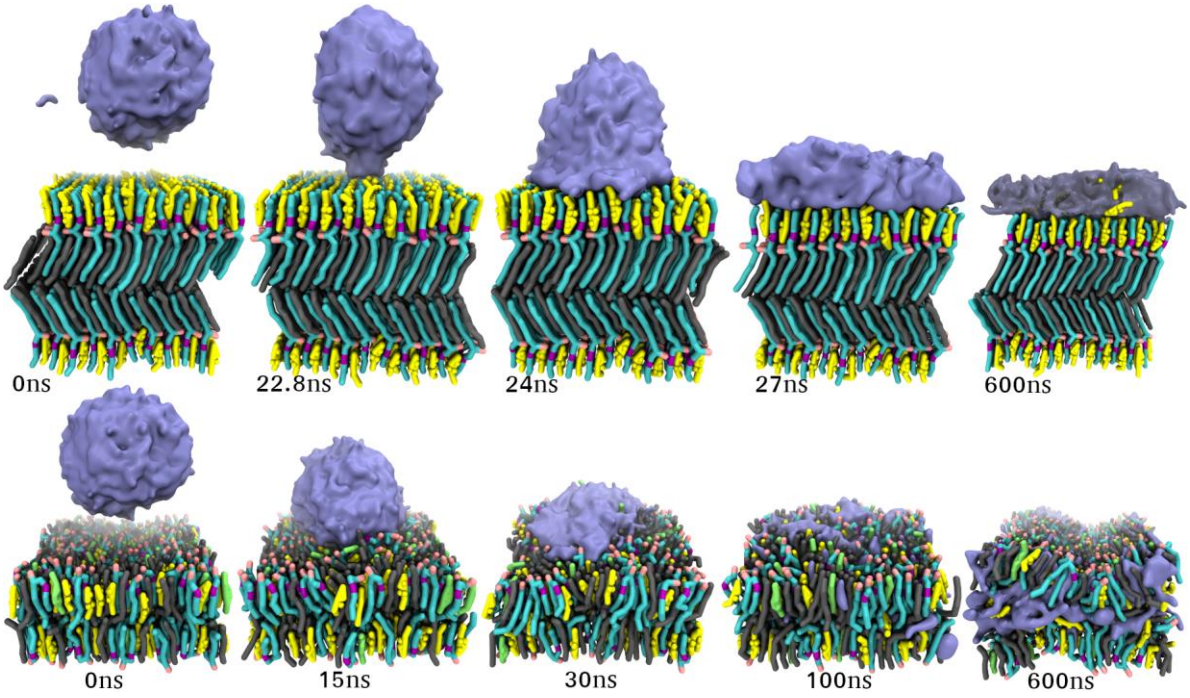

Figure 5: Time evolution snapshots of the interaction simulations between the sebum and the developed LM model **(top),** and old LM model **(bottom)**. The LM is represented as sticks and the sebum as surface. The sebum is translucid in the 600ns top snapshot to reveal the CHOL molecules drifted from the LM to the sebum interior (yellow sticks). The color code is the same from previous figures. The water is omitted.

The results of the sebum interaction with the two LM models clearly show that it is important to know the sebum properties and how it interacts with the other skin

components, since these strong interactions pointing to a significant role of sebum on the TD process that should be take into account in the developing of new drugs or strategies for the transdermal route.

Steered Simulations

Sampling some states in standard simulations can be hard or even impossible due to the existence of high free energy barriers or because these states may require very long simulation times. We applied steered MD simulations, in which molecules of NRD and water were forced to cross the lipid structures, increasing the sampling and allowing the calculation of the potential of mean force (PMF) in order to obtain insights about the permeation potential of the new LM model.

Unfortunately, we had problems on the steered simulation with the new LM model. All these simulations crashed before the full crossing of NRD or water molecules through the LM, more precisely when the molecules are trying to cross the CER head-group zone by the second time. Some artifacts also happen in some replica of steered simulations with the sebum model. We point out that these facts may be related with problems already known, concerning the calculation of free energies, enthalpies and entropies with MARTINI and other coarse-grained force-fields, and is always suggested some caution in the analysis of this kind simulations with coarse-grained resolution.[25] The information provided is however valuable, and we focus on the qualitative analysis of these results.

Some snapshots of the developed LM model steered simulations, with one NRD molecule, are shown in the Figure 6 (see the Figures 10 and 11 in Chapter IV attachments for the steered simulations with old LM and sebum models). The calculated PMF for the replicas with intermediate values are also presented on the Figure 6 (see the PMF of all replicas in Graph 5, 6 and 7 in Chapter IV attachments). The visual inspection of the steered simulations with NRD crossing the new LM model pointed some difficulty of this molecule to insert into the middle of CER and CHOL lipids, and later to cross the zone with the CER and FFA polar groups. The PMF variation confirm these observations, it begins with a big increase in energy followed by a smaller decrease that correspond to the NRD molecule insertion process into first CHOL and CER zone. Then a pronounced increase emerges, that seems be caused by the more compactness of the CER head-group

zone. After that, the PMF continues to increase but at lower rate until the global maximum that reflects the crossing of the LM along the FFA zone. Later there is a decrease in energy reaching one local minimum near to the middle of the layer that is almost composed only by FFA and seems to be one zone more fluid. After this zone, the remaining PMF values are, as expected, almost symmetrical but the premature end of these simulations resulted in one final abrupt decrease of the PMF values.

We expected a very different profile for the PMF variation of the water crossing the new LM model, as well with significantly higher values comparing with the NRD profile, since the NRD is a hydrophobic molecule. Surprisingly the PMF profile for the water molecule crossing this model was very similar to the NRD and presented lightly inferior values of energy. This is one more evidence of a high compactness of the lipids in the developed model, since the chemical properties such as the hydrophobicity and polarity have small impact in the computed energies, because are overcome by the physical resistance of the lipids to the crossing of the molecules. The smaller values of PMF for the water molecule should result of its smaller size (one coarse-grained bead for water against eleven for NRD).

The PMF variation for the systems with NRD crossing the older LM model and the sebum model presented more expectable profiles (see Figure 6), namely the decrease of free energy when the NRD inserts into the lipid interior, with posterior increase when the molecule leaves the lipids in the opposite side. The energy values were smaller for the systems with the sebum, which should be the result of more fluidity of this lipid aggregate comparing with the old LM model. These results agree with the previous observations that the NRD molecules were able to insert with no difficulty in these models, and also pointed that the unusual PMF profile presented for systems with new LM model arise from the way how the lipids are packed in that structure.

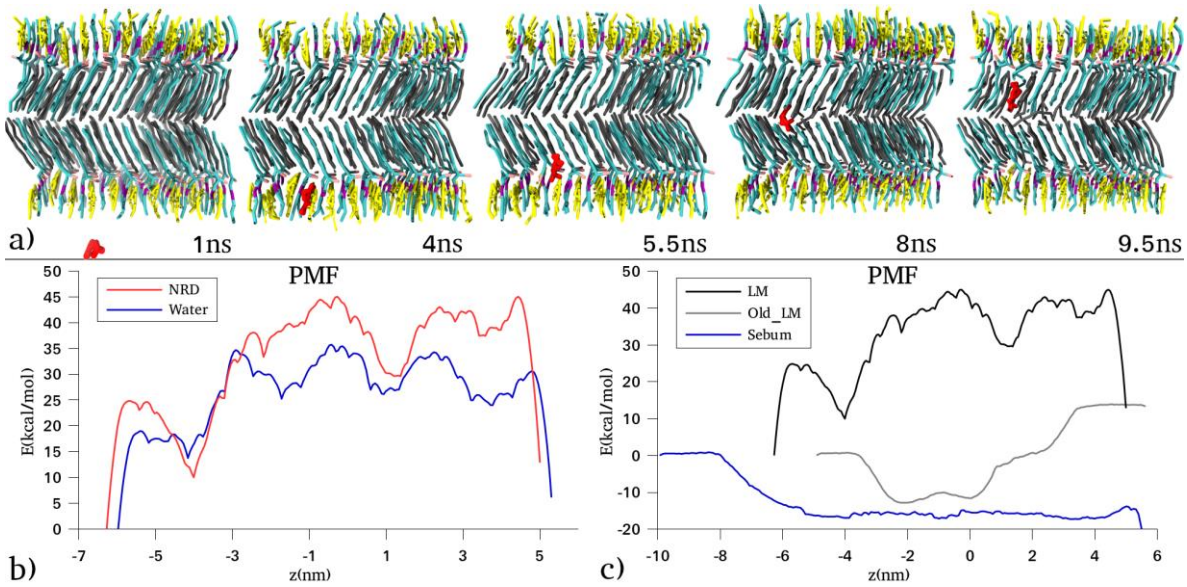

Figure 6: **(a)** Snapshots of steered simulation evolution with one NRD pulled through the LM model. The same representation type of the previous figures was used. **(b)** Calculated PMF variation for the steered simulation of NRD (red line) and water (blue line) crossing the LM model. **(c)** Calculated PMF variation for NRD pulling simulations through the LM model (black line), the old LM model (gray line) and the sebum model (blue line).

Conclusions

In this work new MD models of LM and sebum were developed and their interaction with some compounds was tested. From our knowledge is the first time that one MD model of sebum is developed, and the first time that one coarse-grained LM model with full splayed is developed.

Our results show that the skin lipid conformation suggested by Iwai is possible to occur. The simulations shown that this packing is very stable, promotes a big compactness, have low interaction potential with other compounds and low permeability. Magnus Lundborg and collaborators published recently two extensive works in which they also developed an LM model based on Iwai work, although the final lipid composition and configuration were changed. [51,52] Their model also presented stability with the splayed CER and some tilt in the zone where the FFA are located, observations that are also

presented in one recent work of neutron diffraction of skin lipids.[53] These results agree with the performed tests in this work, however the PMF profiles in the Lundborg work were different, which could be a result of more precise calculations, since the model was not coarse-grained, or due to less compactness in the LM model. It should be noted that some authors propose models of lipid packing in which there are zones with different phases, co-existing gel/crystalline phases with fluid/liquid phases.[11,54] The lipid packing configuration proposed by Iwai and studied here can correspond to more crystalline and impermeable zones. This aspect of LM variability should be a target of more intense research to allow the improvement of computational or even *in vitro* and *ex vivo* models of skin SC models.

The sebum role in the TD should not be underestimated. Our simulations showed strong interaction with the LM models, meaning that the sebum may have significant impact in the TD of many compounds. In addition, the sebum model can allow the study of how the drugs can behave at follicular ducts that are filled with this oil.

The two developed models showed stability and robustness, however some improvement can be made in the future, mainly in the LM model to overcome the possible overestimation of its lipids packing compactness, or even developing new parameterizations for MARTINI, that make possible to better differentiate the lipids and the beads. The MD simulations have huge potential to provide unique and valuable information about the molecular mechanisms that lead to the translocation of drugs through the skin components. However, the MD models should correctly represent the study targets and we expect that the models developed in this work are strong enough in that task and allow the improvement of TD research area.

Acknowledgments

We want to thank the access of Minho University “SeARCH” ("Services and Advanced Research Computing with HTC/HPC clusters") cluster. We also thank the Portuguese Foundation for Science and Technology (FCT) for providing the grant for part of Egipto Antunes PhD studies (scholarship SFRH/BD/122952/2016), and to Tarsila Castro for its advices and text revision.

References

[1]. Feingold KR. Thematic review series: Skin Lipids . The role of epidermal lipids in cutaneous permeability barrier homeostasis, *J Lipid Res.*, 2007, 48, 2531–2546.

[2]. Freinkel, R. K.; Woodley, D. T. *The Biology of the Skin*, CRC Press: London, 2001.

[3]. Menton DN. A minimum-surface mechanism to account for the organization of cells into columns in the mammalian epidermis, *Am J Anat.*, 1976, 145, 1–22.

[4]. Wertz PW, van den Bergh B. The physical, chemical and functional properties of lipids in the skin and other biological barriers, *Chem Phys Lipids*, 1998, 91, 85–96.

[5]. Norlén L, Nicander I, Lundh Rozell B, Ollmar S, Forslind B. Inter- and intra-individual differences in human stratum corneum lipid content related to physical parameters of skin barrier function in vivo, *J Invest Dermatol.*, 1999, 112, 72–7.

[6]. Weerheim A, Ponec M. Determination of stratum corneum lipid profile by tape stripping in combination with high-performance thin-layer chromatography, *Arch Dermatol Res.*, 2001, 293, 191–9.

[7]. Philip, W.; Lars, N. *Skin, Hair, and Nails: Structure and Function*, CRC Press: New York, 2003.

[8]. Rabionet M, Gorgas K, Sandhoff R. Ceramide synthesis in the epidermis, *Biochim Biophys Acta*, 2014, 1841, 422–34.

[9]. Farwanah H, Raith K, Neubert RHH, Wohlrab J. Ceramide profiles of the uninvolved skin in atopic dermatitis and psoriasis are comparable to those of healthy skin, *Arch Dermatol Res.*, 2005, 296, 514–21.

[10]. Norlén L, Nicander I, Lundsjö A, Cronholm T, Forslind B. A new HPLC-based method for the quantitative analysis of inner stratum corneum lipids with special reference to the free fatty acid fraction, *Arch Dermatol Res.*, 1998, 290, 508–16.

[11]. Bouwstra JA, Dubbelaar FE, Gooris GS, Ponec M. The lipid organisation in the skin barrier, *Acta Derm Venereol Suppl (Stockh),* 2000, 208, 23–30.

[12]. Norlén L. Skin Barrier Structure and Function: The Single Gel Phase Model, *J Invest Dermatol.*, 2001, 117, 830–836.

[13]. Al-Amoudi A, Dubochet J, Norlén L. Nanostructure of the epidermal extracellular space as observed by cryo-electron microscopy of vitreous sections of human skin, *J Invest Dermatol.*, 2005, 124, 764–777.

[14]. Mojumdar EH, Groen D, Gooris GS, Barlow DJ, Lawrence MJ, Deme B, et al. Localization of cholesterol and fatty acid in a model lipid membrane: A neutron diffraction approach, *Biophys J. Biophysical Society*, 2013, 105, 911–918.

[15]. Iwai I, Han H, Hollander L Den, Svensson S, Öfverstedt L-G, Anwar J, et al. The Human Skin Barrier Is Organized as Stacked Bilayers of Fully Extended Ceramides with Cholesterol Molecules Associated with the Ceramide Sphingoid Moiety, *J Invest Dermatol.*, 2012, 132, 2215–2225.

[16]. Grams YY, Whitehead L, Cornwell P, Bouwstra JA. Time and depth resolved visualisation of the diffusion of a lipophilic dye into the hair follicle of fresh unfixed human scalp skin, *J Control Release*, 2004, 98, 367–78.

[17]. Lademann J, Otberg N, Richter H, Weigmann HJ, Lindemann U, Schaefer H, et al. Investigation of follicular penetration of topically applied substances, *Skin Pharmacol Appl Skin Physiol*, 2001, 14 Suppl 1, 17–22.

[18]. Essa EA, Bonner MC, Barry BW. Human skin sandwich for assessing shunt route penetration during passive and

iontophoretic drug and liposome delivery, *J Pharm Pharmacol.*, 2002, 54, 1481–1490.

[19]. Nikkari T. Comparative chemistry of sebum, *J Invest Dermatol.*, 1974, 62, 257–67.

[20]. Smith KR, Thiboutot DM. Thematic review series: Skin Lipids. Sebaceous gland lipids: friend or foe?, *J Lipid Res.*, 2008, 49, 271–281.

[21]. Stefaniak AB, Harvey CJ. Dissolution of materials in artificial skin surface film liquids, *Toxicol Vitr.*, 2006, 20, 1265–1283.

[22]. Antunes E, Cavaco-Paulo A. Skin barrier molecular dynamics studies, *In submission process*, 2018.

[23] Hess B, Kutzner C, van der Spoel D, Lindahl E. GROMACS 4: Algorithms for Highly Efficient, Load-Balanced, and Scalable Molecular Simulation, *J Chem Theory Comput.*, 2008, 4, 435–447.

[24]. Marrink SJ, Risselada HJ, Yefimov S, Tieleman DP, de Vries AH. The MARTINI force field: coarse grained model for biomolecular simulations, *J Phys Chem B.*, 2007, 111, 7812–24.

[25]. Marrink SJ, Tieleman DP. Perspective on the Martini model, *Chem Soc Rev.* 2013, 42, 6801–6822.

[26]. Ingólfsson HI, Lopez C a., Uusitalo JJ, de Jong DH, Gopal SM, Periole X, et al. The power of coarse graining in biomolecular simulations, *Wiley Interdiscip Rev Comput Mol Sci.* 2014, 4, 3, 225-248.

[27]. Hess B, Bekker H, Berendsen HJC, Fraaije JGEM. LINCS: A linear constraint solver for molecular simulations, *J Comput Chem.*, 1997, 18, 1463–1472.

[28]. Plasencia I, Norlén L, Bagatolli LA. Direct visualization of lipid domains in human skin stratum corneum's lipid membranes: effect of pH and temperature, *Biophys J.*, 2007, 93, 3142–55.

[29]. Berendsen HJC, Postma JPM, van Gunsteren WF, DiNola A, Haak JR. Molecular dynamics with coupling to an external bath, *J Chem Phys.*, 1984, 81, 3684.

[30]. Roux B. The calculation of the potential of mean force using computer simulations, *Comput Phys Commun.*, 1995, 91, 275–282.

[31]. Hub JS, de Groot BL, van der Spoel D. g_wham—A Free Weighted Histogram Analysis Implementation Including Robust Error and Autocorrelation Estimates, *J Chem Theory Comput.*, 2010, 6, 3713–3720.

[32]. Wassenaar TA, Ingólfsson HI, Böckmann RA, Tieleman DP, Marrink SJ. Computational Lipidomics with insane : A Versatile Tool for Generating Custom Membranes for Molecular Simulations, *J Chem Theory Comput.*, 2015, 11, 2144–2155.

[33]. Ingólfsson HI, Melo MN, van Eerden FJ, Arnarez C, Lopez C a, Wassenaar T a, et al. Lipid organization of the plasma membrane, *J Am Chem Soc.*, 2014, 136, 14554–9.

[34]. Vuorela T, Catte A, Niemelä PS, Hall A, Hyvönen MT, Marrink SJ, et al. Role of Lipids in Spheroidal High Density Lipoproteins, *PLoS Comput Biol.*, 2010, 6, e1000964.

[35]. Malde AK, Zuo L, Breeze M, Stroet M, Poger D, Nair PC, et al. An Automated Force Field Topology Builder (ATB) and Repository: Version 1.0, *J Chem Theory Comput.*, 2011, 7, 4026–37.

[36]. Schmid N, Eichenberger AP, Choutko A, Riniker S, Winger M, Mark AE, et al. Definition and testing of the GROMOS force-field versions 54A7 and 54B7, *Eur Biophys J.,* 2011, 40, 843–56.

[37]. Lee H, De Vries AH, Marrink SJ, Pastor RW. A coarse-grained model for polyethylene oxide and polyethylene glycol: Conformation and hydrodynamics, *J Phys Chem B.* 2009, 113, 13186–13194.

[38]. Lee H, Pastor RW. Coarse-grained model for pegylated lipids: Effect of pegylation on the size and shape of self-assembled structures, *J Phys Chem B.*, 2011, 115, 7830–7837.

[39]. Hezaveh S, Samanta S, De Nicola A, Milano G, Roccatano D. Understanding the interaction of block copolymers with DMPC lipid bilayer using coarse-grained molecular dynamics simulations, *J Phys Chem B.*, 2012, 116, 14333–14345.

[40]. Martins M, Azoia NG, Ribeiro A, Shimanovich U, Silva C, Cavaco-Paulo A. In vitro and computational studies of transdermal perfusion of nanoformulations containing a large molecular weight protein, *Colloids Surfaces B Biointerfaces*, 2013, 108, 271–278.

[41]. Pappas A, Johnsen S, Liu J-C, Eisinger M. Sebum analysis of individuals with and without acne, *Dermatoendocrinol*., 2009, 1, 157–161.

[42]. Picardo M, Ottaviani M, Camera E, Mastrofrancesco A. Sebaceous gland lipids, *Dermatoendocrinol.*, 2009, 1, 68–71.

[43]. Robosky LC, Wade K, Woolson D, Baker JD, Manning ML, Gage D a, et al. Quantitative evaluation of sebum lipid components with nuclear magnetic resonance, *J Lipid Res.*, 2008, 49, 686–692.

[44]. Lu GW, Valiveti S, Spence J, Zhuang C, Robosky L, Wade K, et al. Comparison of artificial sebum with human and hamster sebum samples, *Int J Pharm.*, 2009, 367, 37–43.

[45]. Stefaniak AB, Harvey CJ, Wertz PW. Formulation and stability of a novel artificial sebum under conditions of storage and use, *Int J Cosmet Sci.* 2010, 32, 347–355.

[46]. Nordstrom KM, Labows JN, McGinley KJ, Leyden JJ. Characterization of wax esters, triglycerides, and free fatty acids of follicular casts, *The Journal of investigative dermatology.*, 1986, 700–705.

[47]. Das C, Noro MG, Olmsted PD. Lamellar and inverse micellar structures of skin lipids: Effect of templating, *Phys Rev Lett.*, 2013, 111, 1–5.

[48]. Greenspan P, Fowler SD. Spectrofluorometric studies of the lipid probe, nile red, *J Lipid Res.*, 1985, 26, 781–9.

[49]. Stuart MC a., van de Pas JC, Engberts JBFN. The use of Nile Red to monitor the aggregation behavior in ternary surfactant-water-organic solvent systems, *J Phys Org Chem.*, 2005, 18, 929–934.

[50]. Fernandes B, Silva R, Ribeiro A, Matamá T, Gomes AC, Cavaco-Paulo AM. Improved Poly (D,L-lactide) nanoparticles-based formulation for hair follicle targeting, *Int J Cosmet Sci.*, 2015, 37, 282–290.

[51]. Lundborg M, Narangifard A, Wennberg CL, Lindahl E, Daneholt B, Norlén L. Human skin barrier structure and function analyzed by cryo-EM and molecular dynamics simulation, *J Struct Biol.*, 2018, 203, 2, 149-161.

[52]. Lundborg M, Wennberg CL, Narangifard A, Lindahl E, Norlén L. Predicting drug permeability through skin using molecular dynamics simulation, *J Control Release.*, 2018, 283, 269-279.

[53]. Schroeter A, Stahlberg S, Školová B, Sonnenberger S, Eichner A, Huster D, et al. Phase separation in ceramide[NP] containing lipid model membranes: neutron diffraction and solid-state NMR, *Soft Matter.*, 2017, 13, 2107–2119.

[54]. Forslind B. A domain mosaic model of the skin barrier, *Acta Derm Venereol.*, 1994, 74, 1–6.

Chapter IV Attachments

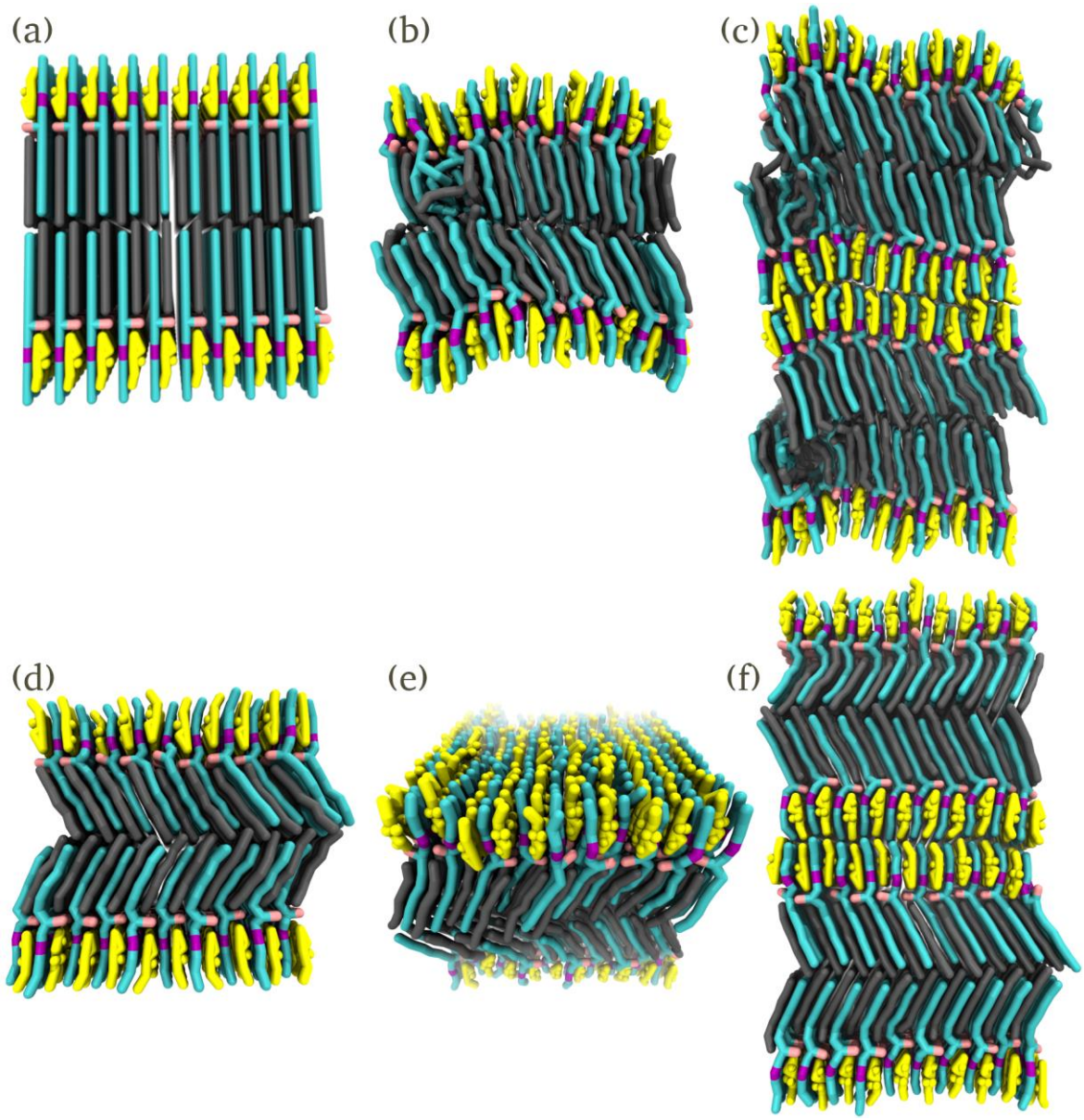

Figure 7: Snapshots of the computational LM models at different stages. **(a)** The LM coarse-grained model with two layers (DOUB model) before simulations. The DOUB **(b)** and BIDOUB **(c)** models presented some disorganization after the first simulation tests (600ns at 306K). Simulations at low temperature (100K) presented more organized structures **(d)**. We applied an heating protocol to obtain the final models **(e)** and **(f)**, used on the work. The lipids are represented as wide sticks, with the CER at cyan (with its polar groups at pink), the CHOL at yellow and the FFA at gray.

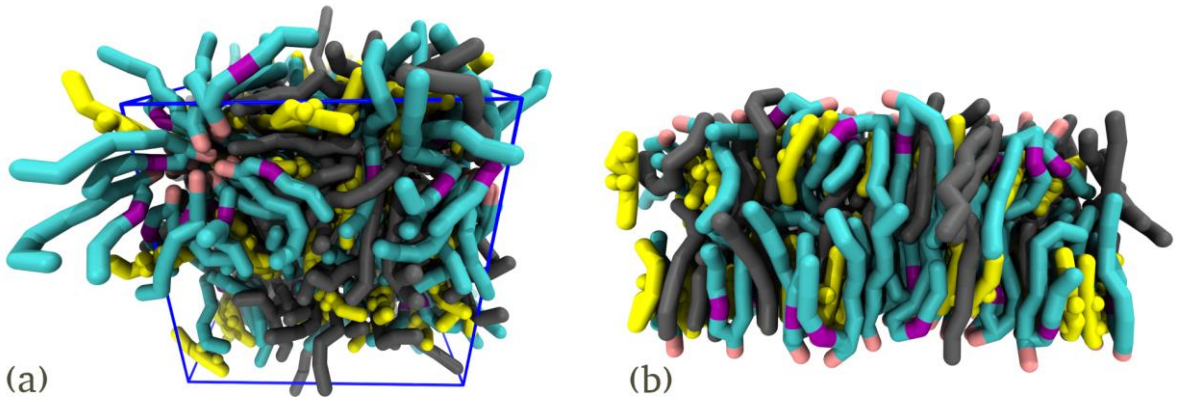

Figure 8: LM final configurations after 600ns of self-assembling simulations without **(a)** and with **(b)** water. The water molecules were omitted in the **(b)** system for clarity.

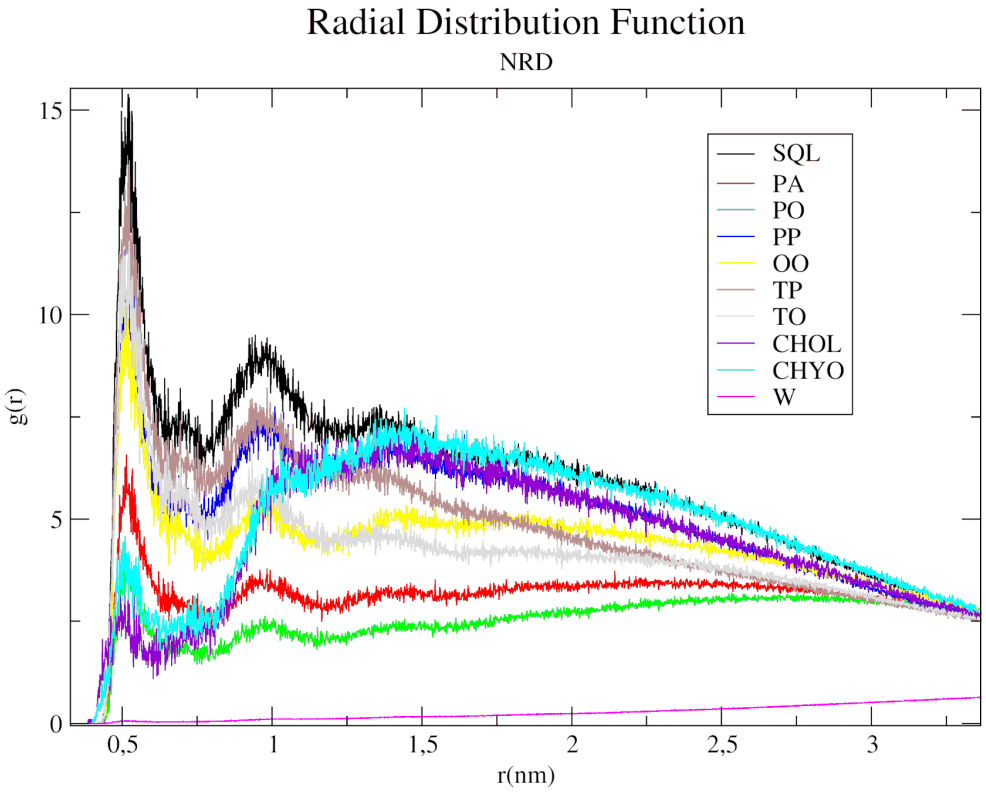

Graph 3: Radial Distribution Function (RDF) of sebum lipids and water over NRD, in the NRD – sebum interaction simulations. The RDF was calculated over the final nanosecond of sebum sphere interaction simulation with 5 NRD molecules. It is noticeable the greater

probability of squalene (SQL) and lipids with oleic chains (except the palmitoleic acid (PO)) to be found near to the NRD molecules.

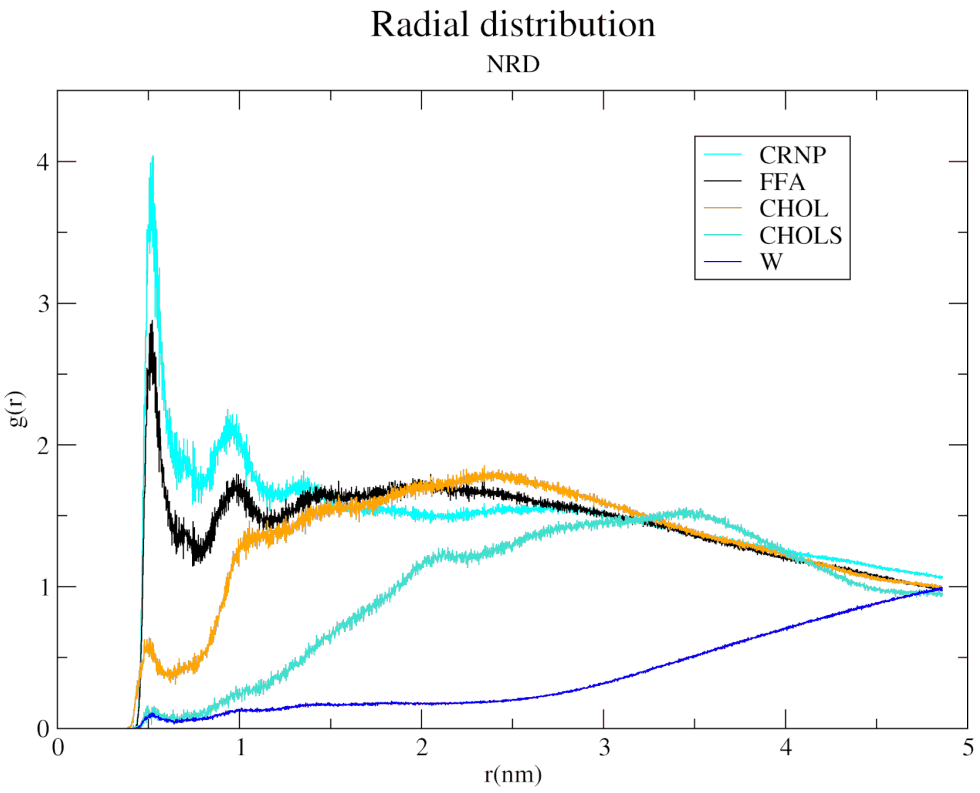

Graph 4: RDF of old LM model lipids and water over NRD. The RDF was calculated over the final nanosecond of old LM interaction simulation with 5 NRD molecules. The curves indicate the propensity of NRD to be located near to ceramides NP (CRNP) and to the free fatty-acids (FFA).

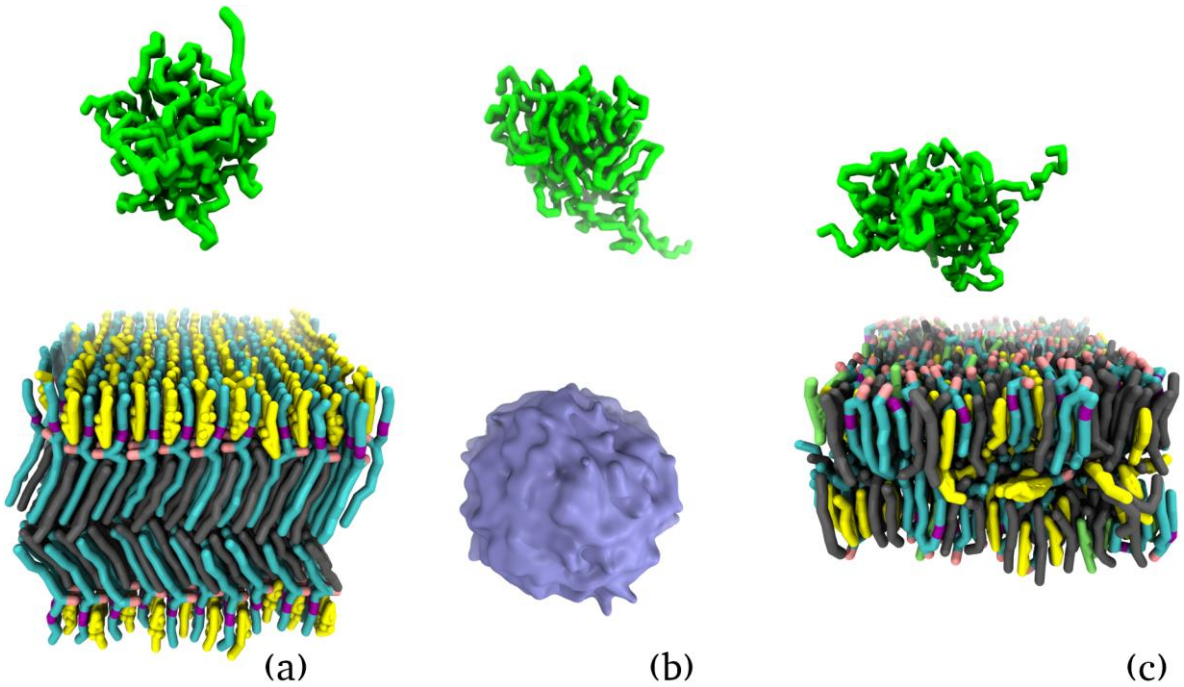

Figure 9: Snapshots of the PLA – lipidic structures interaction simulations after 600ns. Aqueous systems composed of 5 PLA with the developed LM model **(a)**, the sebum model **(b)** and the old LM model **(c)** were built to study the interaction between these molecules. The PLA polymers aggregate and do not interact with the lipidic structures. The LM models are represented by wide sticks, with CER at cyan (with polar groups at pink), CHOL at yellow, CHOLS at lime (only presented in the old LM model) and FFA at gray. The PLA polymers are green and the sebum model is represented as ice blue surface. The water molecules were omitted for clarity.

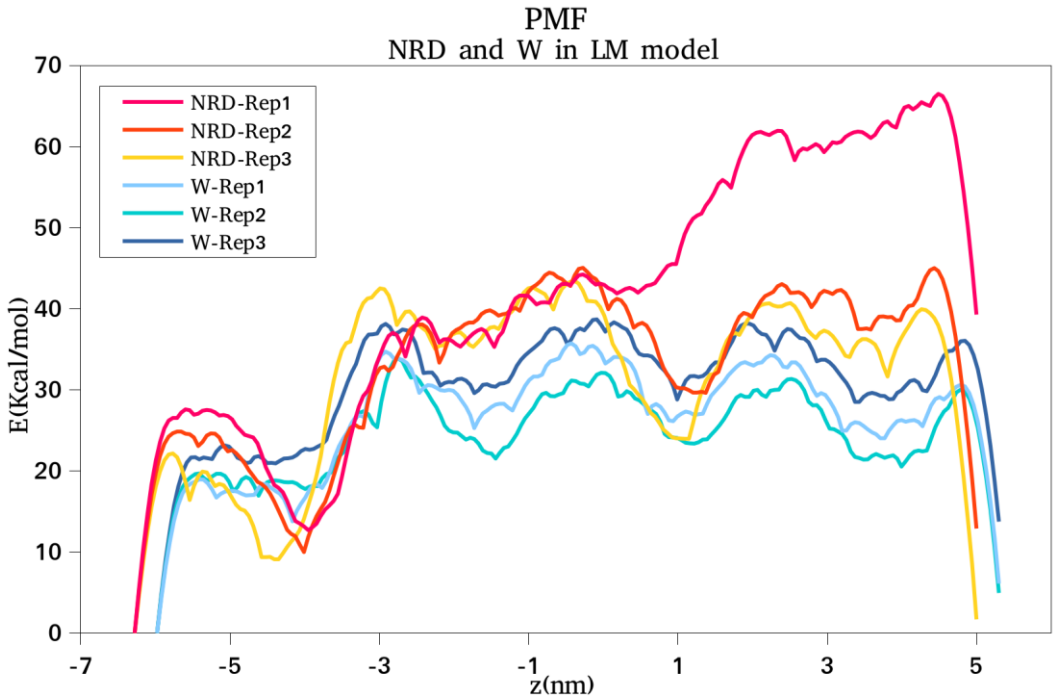

Graph 5: Calculated PMF variation of steered simulations with NRD and water pulled through the LM model. The final abrupt decrease result of the crash of the simulations before the NRD or water molecules be able to completely cross the lipidic structure.

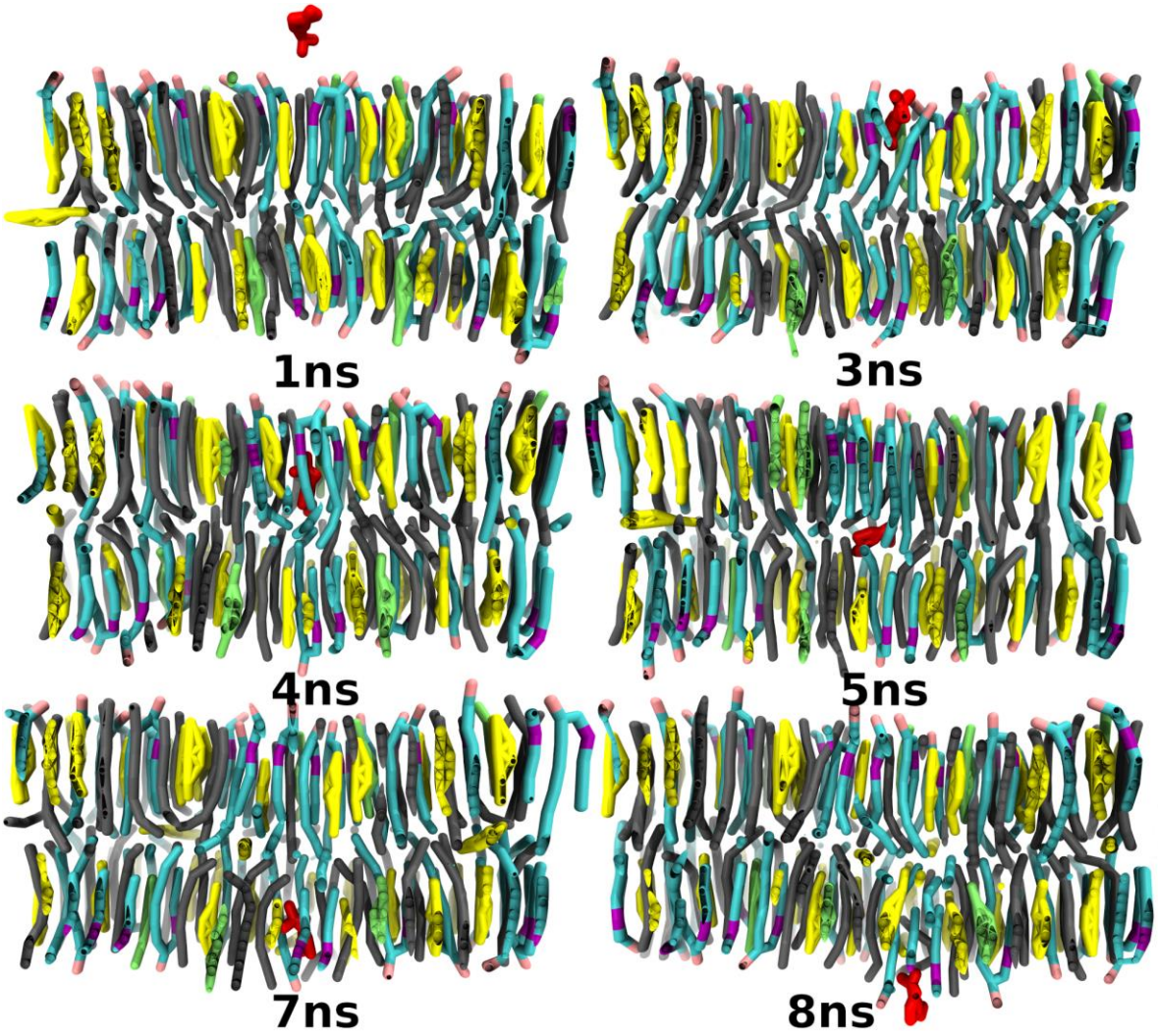

Figure 10: Snapshots of steered simulation evolution with one NRD (at red) pulled through the old LM model.

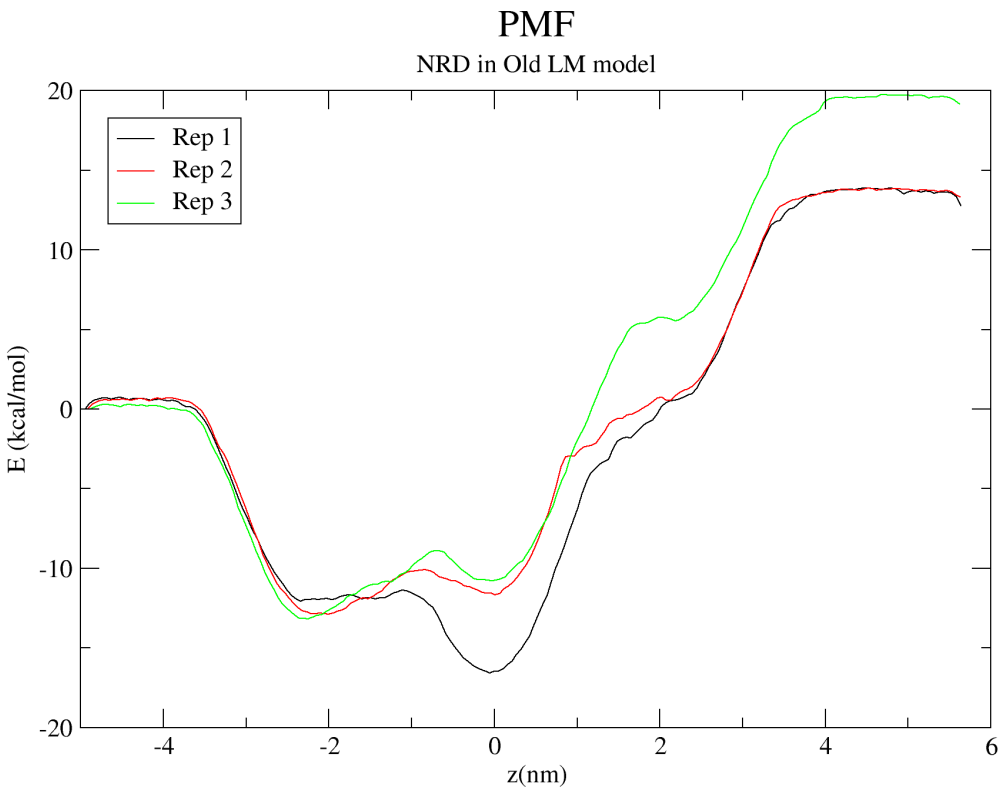

Graph 6: Calculated PMF variation of steered simulations with NRD pulled through the old LM model.

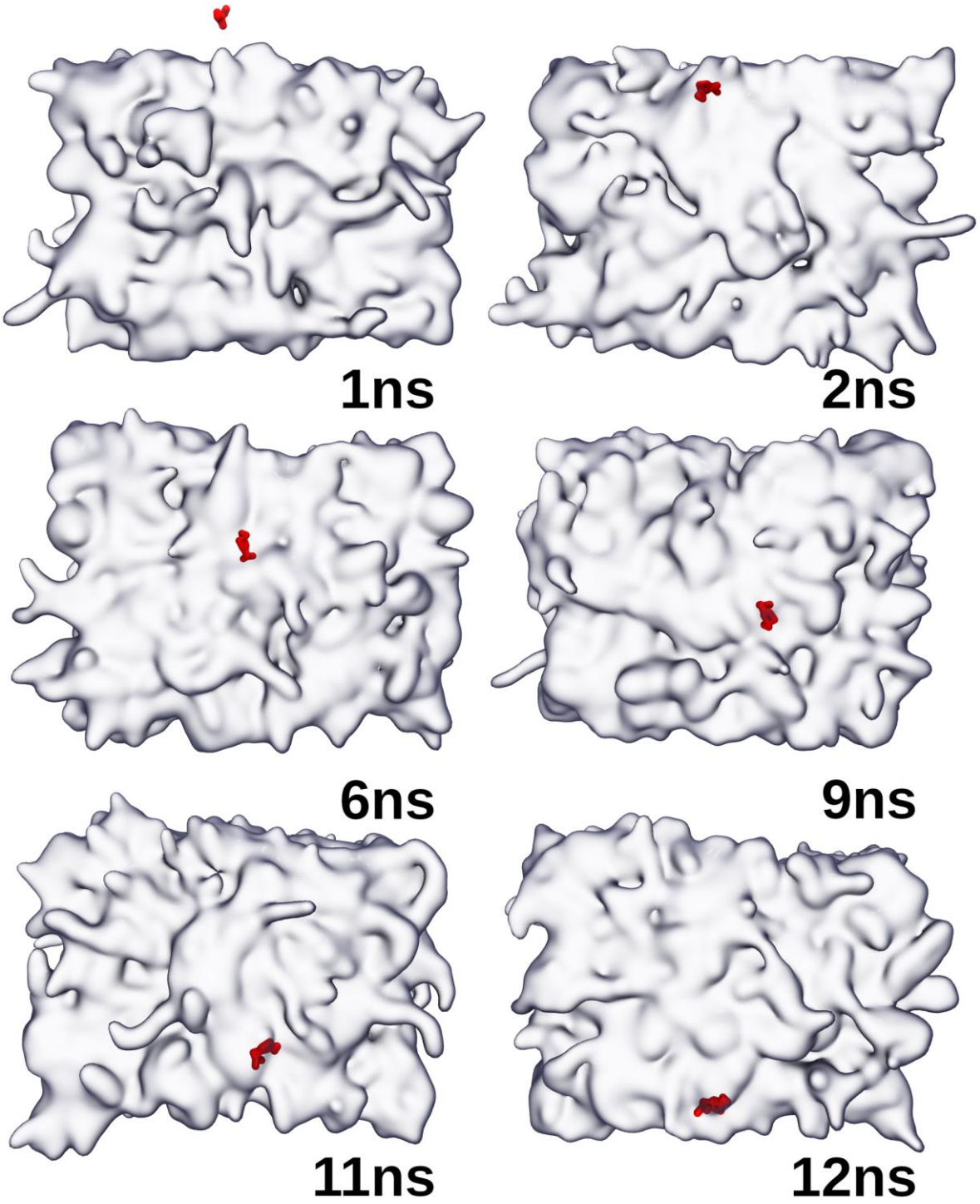

Figure 11: Snapshots of steered simulation evolution with one NRD (at red) pulled through the sebum model (ice blue translucid surface).

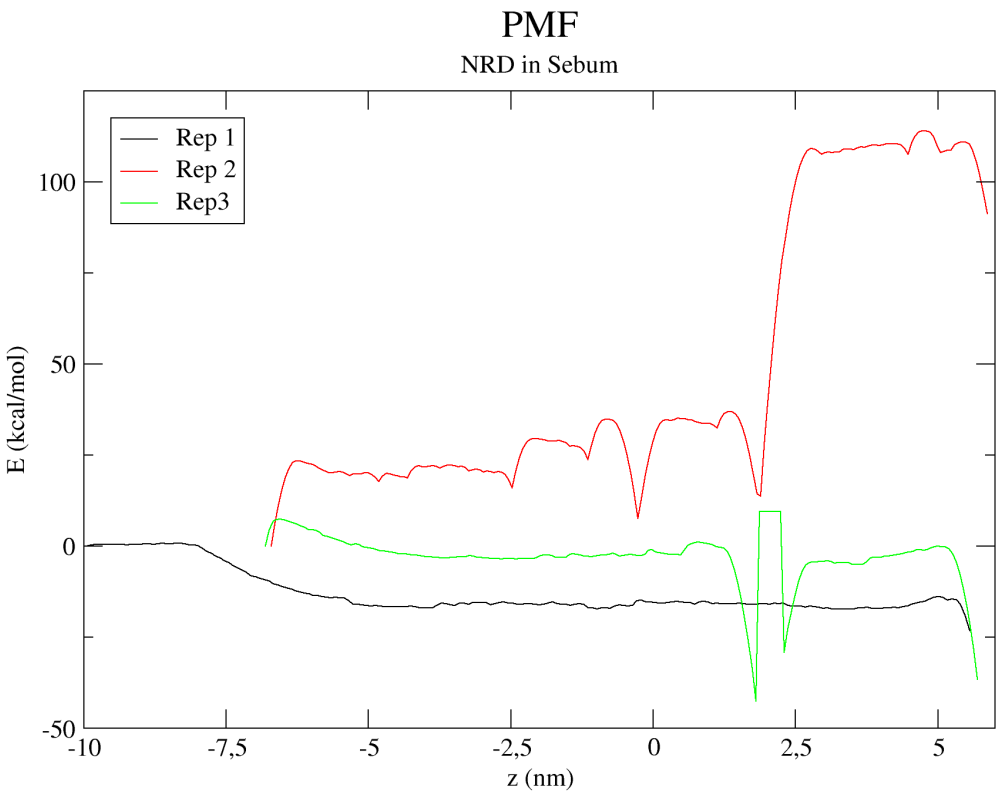

Graph 7: Calculated PMF variation of steered simulations with NRD pulled through the sebum model. The big jumps in the replica 2 and 3 should be a result of numerical calculation artifacts.

Final Remarks

The initial main goal of this thesis was the development, or optimization of systems, formulations or process for hair modulation and for transdermal delivery based on molecular dynamics simulation data. Now, at the end of this journey, it seems clear that this goal although feasible is very ambitious.

To obtain strong and reliable data from the simulations we needed computational models of the hair and skin structures that correctly mimic the behavior of these structures in reality. Most of the effort of this thesis was applied in the development of these models, which resulted in four main models built. Two of the models are representative of hair keratin protofibril structure, one of the stratum corneum lipid matrix and one of the sebum. The simulations results with these models shown that they are able to correctly predict properties or phenomena in the hair or explain the effectiveness of the skin as a barrier to external compounds. It can be concluded that the development of reliable models was achieved with success.

The output of this thesis, relatively to the hair modulation and the transdermal delivery improvement, was however modest. We demonstrated the potential of formulations with benzyl alcohol to increase the uptake of peptides by the hair, as well the improvement of hair mechanical properties by one peptide. We also point that the shape of molecules and how they interact with sebum can significantly impact on their potential to cross the stratum corneum lipid matrix. These results although modest, prove that the use of molecular dynamics studies is a valid strategy to achieve the initial main goal of this thesis.

The developed models can also improve fundamental research on the fields of hair keratin and stratum corneum, providing unique molecular and dynamic data. Other researchers can even use the models, or build similar models, to test other properties or phenomena that we did not even think.

Much more work would be needed to pass from the obtained knowledge to reach potential final products able to significantly modulate the hair as desired or to penetrate the skin. However we demonstrate the great potential of molecular dynamics simulations to improve that quest, and the developed models can be very useful on the way.

We think that this thesis can be see it as a first, but strong, step on the persecution of that ambitious objectives and also a step in the very long way to achieve the excellence in science research.